AFML-TR-67.116

Development Of Columbium Base Alloys

R. T. Begley, J. A. Cornie, and R. C. Goodspeed

Westinghouse Astronuclear Laboratory

Technical Report AFML-TR-67-116

November, 1967

Air Force Materials Laboratory
Research and Technology Division
Air Force Systems Command
Wright-Patterson Air Force Base, Ohio

NOTICES

When Government drawings, specifications, or other data are used for any purpose other than in connection with a definitely related Government procurement operation, the United States Government thereby incurs no responsibility nor any obligation whatsoever; and the fact that the Government may have formulated, furnished, or in any way supplied the said drawings, specifications, or other data, is not to be regarded by implication or otherwise as in any manner licensing the holder or any other person or corporation, or conveying any rights or permission to manufacture, use, or sell any patented invention that may in any way be related thereto.

Copies of this report should not be returned to the Research and Technology Division unless return is required by security considerations, contractual obligations, or notice on a specific document.

AFML-TR-67-116

DEVELOPMENT OF COLUMBIUM BASE ALLOYS

R. T. Begley, J. Cornie, and R. Goodspeed
Westinghouse Astronuclear Laboratory

TECHNICAL REPORT AFML-TR-67-116

November 1967

Air Force Materials Laboratory
Research and Technology Division
Air Force Systems Command
Wright-Patterson Air Force Base, Ohio

FOREWORD

The work described in this report was carried out by personnel of the Westinghouse Astronuclear Laboratory under USAF Contract AF 33(615)-1728, BPSN Nr. 64-6899-7351-735101. The contract was initiated under Project No. 7351, "Metallic Materials", Task No. 735101, "Refractory Metals". The work was administered under the direction of the Air Force Materials Laboratory, Research and Technology Division, Air Force Systems Command, Wright-Patterson Air Force Base, Ohio, with Mr. J. T. Gow and Mr. R. G. Ault as Project Engineers.

This report describes the results of research conducted during the period 1 July 1965 to 31 December 1966. The manuscript was released by the author in April 1967 for publication as a technical report.

The authors wish to acknowledge the assistance of A. Filippi (melting and extrusion), E. Vandergrift (creep-rupture testing), C. Schenone (x-ray analysis), and W. Harding (electron microscopy) in conducting this program.

This technical report has been reviewed and is approved.

I. PERLMUTTER
Chief, Metals Branch
Metals and Ceramics Division
Air Force Materials Laboratory

ABSTRACT

A high strength columbium base alloy, Cb-28W-2Hf-0.067C, developed for potential gas turbine blade applications was scaled-up to 3 inch diameter ingot size and processed to bar stock for mechanical property evaluation. Studies of recrystallization, grain growth, and response to thermal-mechanical processing were carried out to characterize the material. Detailed investigations of carbide phase identity, stability, and morphology were undertaken to correlate structure with mechanical properties. A metastable zeta carbide phase similar to the zeta phase found in the Ta-C system was observed to form in material after annealing at temperatures above 1700°C, which subsequently transformed to the cubic $(Cb,Hf)C_{1-x}$ phase on aging at intermediate temperatures. Phase boundaries were established for the columbium rich region of the Cb-W-Hf-C system.

Mechanical property studies were carried out on material in a number of structural conditions. The best combination of low temperature ductility and high temperature creep strength was exhibited by material annealed 1 hour at 1700°C following extrusion and warm swaging. Material in this condition had a 100 hour rupture strength at 1315°C (2400°F) of 25,500 psi, corresponding to a strength-density ratio of 68,500 inches. Room temperature elongation was 11%. Electron microscopy studies indicate that the carbide phase in this alloy may contribute considerable strengthening by the stabilization of dislocation networks.

A section of extruded bar stock was successfully precision forged into a turbine blade by another Air Force contractor.

A limited study of the substitution of 1 atomic % Zr for 1 atomic % Hf in carbide strengthened alloys showed essentially no difference in creep strength, although the hafnium containing alloy was more fabricable.

CONTENTS

CONTENTS (Continued)

LIST OF ILLUSTRATIONS

LIST OF ILLUSTRATIONS (Continued)

LIST OF ILLUSTRATIONS (Continued)

LIST OF ILLUSTRATIONS (Continued)

LIST OF ILLUSTRATIONS (Continued)

LIST OF TABLES

I. INTRODUCTION AND SUMMARY

This program was undertaken to develop a columbium base alloy suitable for application as a gas turbine bucket material. Mechanical property target values of a 100 hour rupture life at 2400°F of 70,000 inches (on a strength-density basis) and 5% (minimum) tensile elongation over the entire operating temperature range were selected. Further requirements were that the alloy be capable of being forged into a complex air foil shape, as well as having, ideally, resistance to shock and thermal cyclic loading, good fatigue characteristics, coatability, and tolerance for minor coating defects.

Nickel and cobalt base superalloys are being utilized in the high temperature sections of present and advanced gas turbine aircraft engines. The superalloys are limited to maximum blade or vane temperatures of approximately 1800°F although considerably higher inlet temperatures have been achieved by the use of cooled turbine designs. Refractory metal alloys in general and columbium base alloys in particular have long been considered as replacement materials for the high temperature sections of gas turbine engines. However, the potential of columbium base alloys has not been realized because of the poor reliability of present day coatings (or coating techniques) and suprisingly only a relatively moderate strength advantage of the current generation of columbium base alloys over existing superalloys in terms of resistance to creep deformation. This moderate strength advantage has been essentially eliminated with the recent advances in cooled turbine technology. The results of the current program, however, have demonstrated that very high strength columbium alloys, with adequate fabricability to permit precision forging of complex turbine buckets, can be considered for gas turbine applications. The alloy XB-88 (Cb-28W-2Hf-0.067C) developed during this program offers a 600 to 800°F temperature advantage over the best available superalloy and a 300 to 400°F advantage over the current generation of columbium base alloys (see Figure 1).

Coating reliability remains the number one obstacle to the use of refractory metals and therefore coating development is quite logically receiving continuing support from government and private sectors. Recently a fresh new approach to the coating reliability

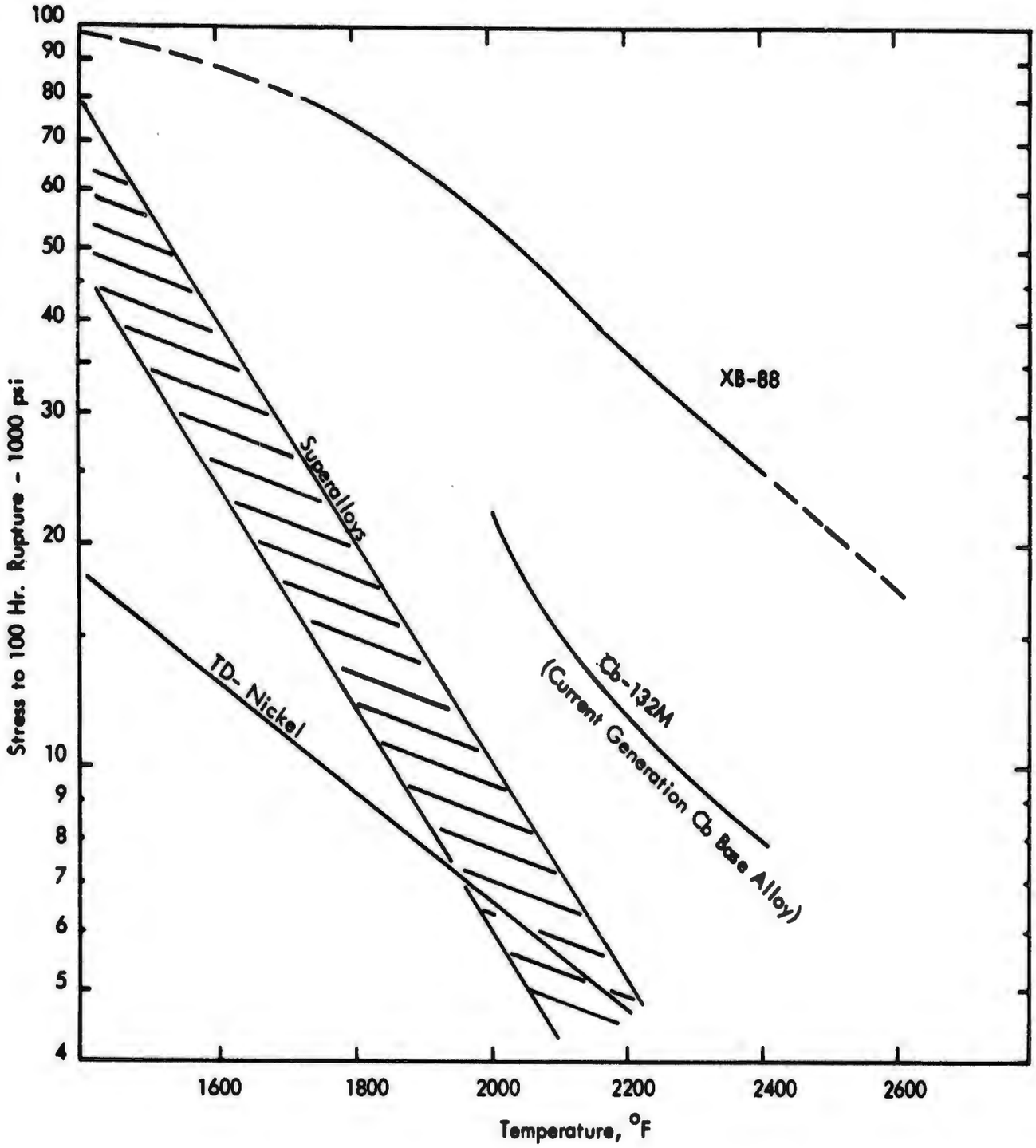

FIGURE 1 - 100 Hour Rupture Strength vs. Temperature for XB-88 and Other Gas Turbine Bucket Materials

problem has been initiated by the Air Force Materials Laboratory. A program is now underway to establish the feasibility of a duplex or composite turbine blade consisting of high strength columbium alloy core cladded with a ductile oxidation resistant columbium base alloy. The cladding alloy would then be coated to provide oxidation resistance. If a flaw develops in the coating, the clad alloy would have sufficient oxidation resistance to prevent catastrophic failure. The alloy XB-88 evaluated in this report would be a logical core alloy candidate.

During the first phase of this program, the Cb-W-Hf-C system was selected as the most promising system for achieving the mechanical property goals. The effects of compositional variables on mechanical properties were evaluated, and the results of this study led to the selection of a Cb-28W-2Hf-0.067C alloy (designated XB-88) for more detailed investigation. These initial studies are described in a previous report[1].

During the second phase of this investigation, described in this report, experimental work was concentrated on scale-up of XB-88 to 3 inch diameter ingots, and optimization of mechanical properties with respect to high temperature creep strength and low temperature ductility. Previous work in this program demonstrated the pronounced effect of structure on the creep properties of dispersed phase strengthened columbium-base alloys. High temperature annealed, essentially fully recrystallized structures provided significantly enhanced creep strength, both in terms of lower secondary creep rates and longer rupture lives, compared to wrought structures. The strength improvement resulting from high temperature annealing is associated, directly or indirectly with changes in carbide identity, morphology, and/or distribution. Consequently major emphasis was devoted to studies of dispersed phase identity, stability, morphology, and distribution in order to establish a correlation between structure and mechanical properties. Thus in this report, observations on phase relationships, recrystallization and grain growth, and microstructure are described in detail to provide a proper reference for evaluating and interpreting mechanical property data.

Studies of the effect of prior thermal-mechanical processing on the properties of XB-88 showed that material processed by extruding at 1930°C (3500°F), followed by swaging at 1300°C, with a final anneal of 1 hour at 1700°C, exhibited the best combination of high temperature creep resistance and low temperature ductility. The final anneal at 1700°C provided a structure which was almost fully recrystallized, with a relatively fine grain size. The room temperature tensile strength of the material annealed 1 hour at 1700°C was somewhat lower than that of specimens in the stress-relieved condition (i. e., material given a final anneal at temperatures below 1700°C) but room temperature ductility was superior. The extruded, swaged, plus annealed 1 hour at 1700°C condition was thus chosen as the reference condition for detailed evaluation of creep rupture and tensile properties.

The tensile properties of XB-88 in the reference condition were determined over the temperature range of -110°F (-80°C) to 2500°F (1370°C), and the data are plotted in Figure 2. The low temperature ductility values improve markedly slightly above room temperature, with reduction in area increasing from 8% at room temperature to 24% at 200°F (93°C). The plot of ultimate strength versus temperature showed typical strain aging response, with a strength maxima extending over the range from 760°C (1400°F) to 980°C (1800°F). High temperature tensile strength values were quite high, 86,000 psi at 1095°C (2000°F) and 46,800 psi at 1370°C (2500°F). The tensile strength values are quite comparable to those obtained initially on XB-88 processed from a 2 inch diameter ingot.[1] The elevated temperature tensile ductility was excellent.

Creep rupture properties were evaluated over the temperature range 980°C (1800°F) to 1315°C (2400°F). The rupture properties of XB-88 in the reference condition for the various test temperatures are given in the log stress versus log rupture time plot of Figure 3. Both rupture and 1% creep data are summarized in the Larsen-Miller plot of Figure 4. In addition to attractive creep-rupture properties, XB-88 in the reference condition had low secondary creep rates. The transition from second to third stage creep, however, occurred at low strain values, on the order of 2%.

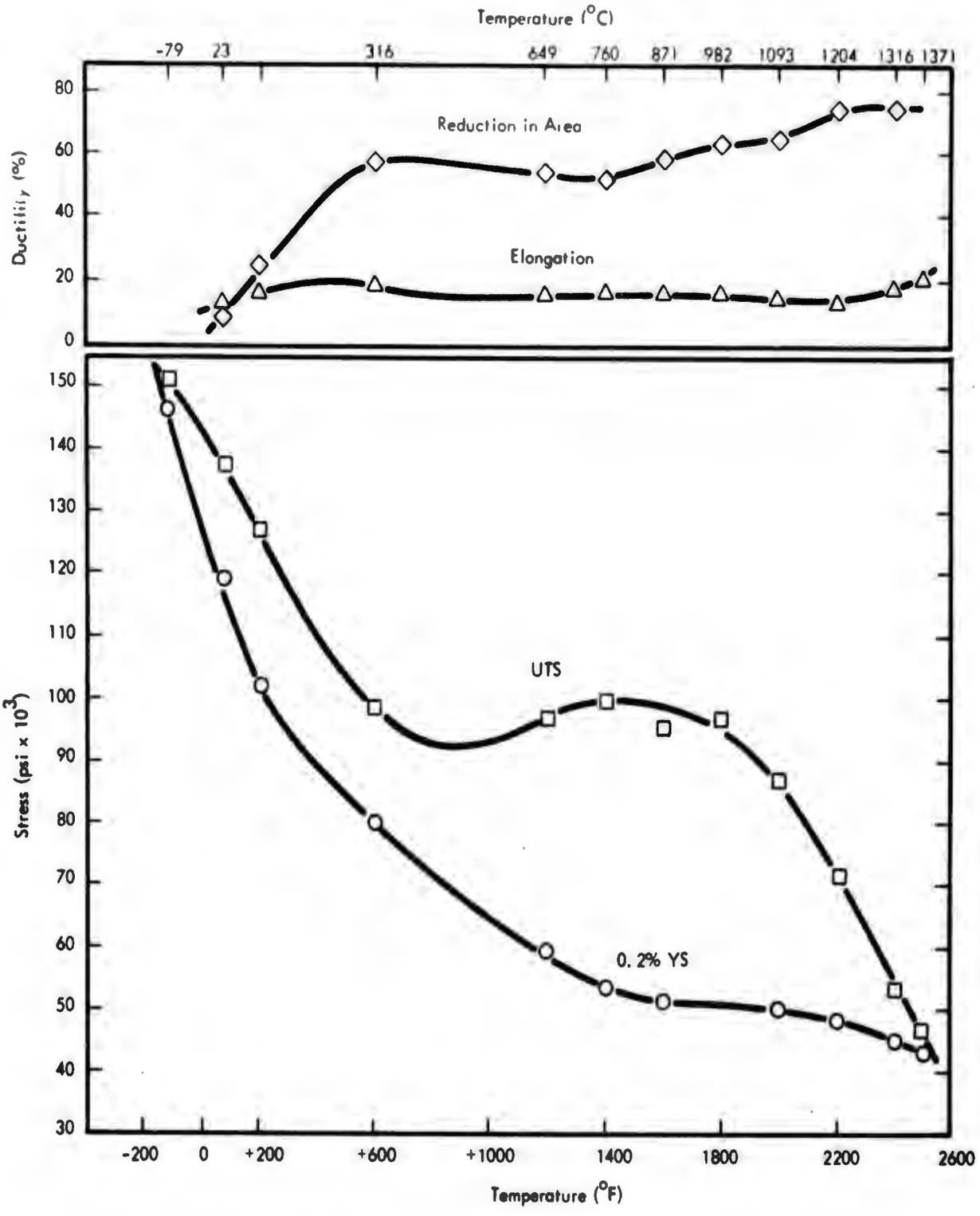

FIGURE 2 - Variation of Tensile Properties of XB-88 as a Function of Test Temperature (Reference Condition)

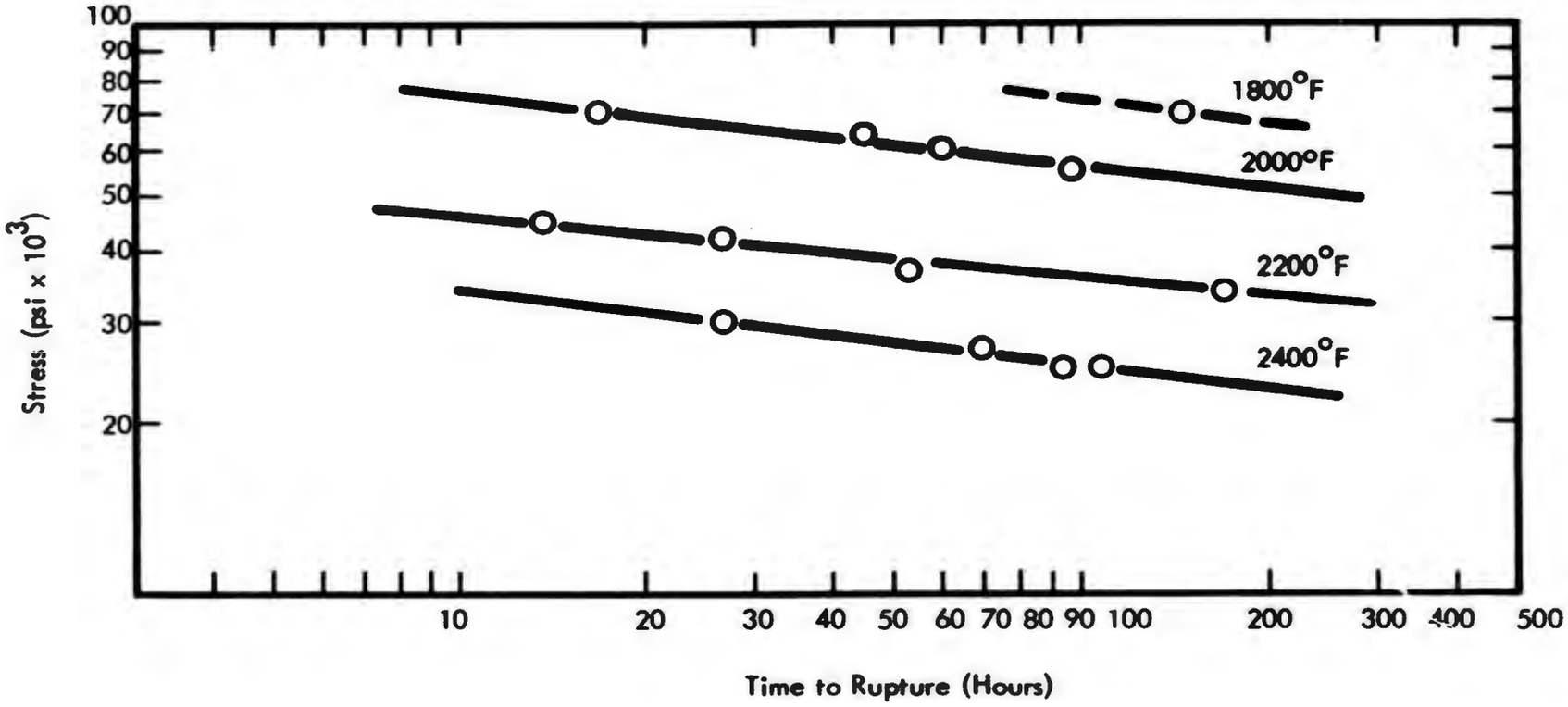

FIGURE 3 - Stress-Rupture Properties of XB-88 in the Reference Condition (Annealed 1 Hour at 1700°C).

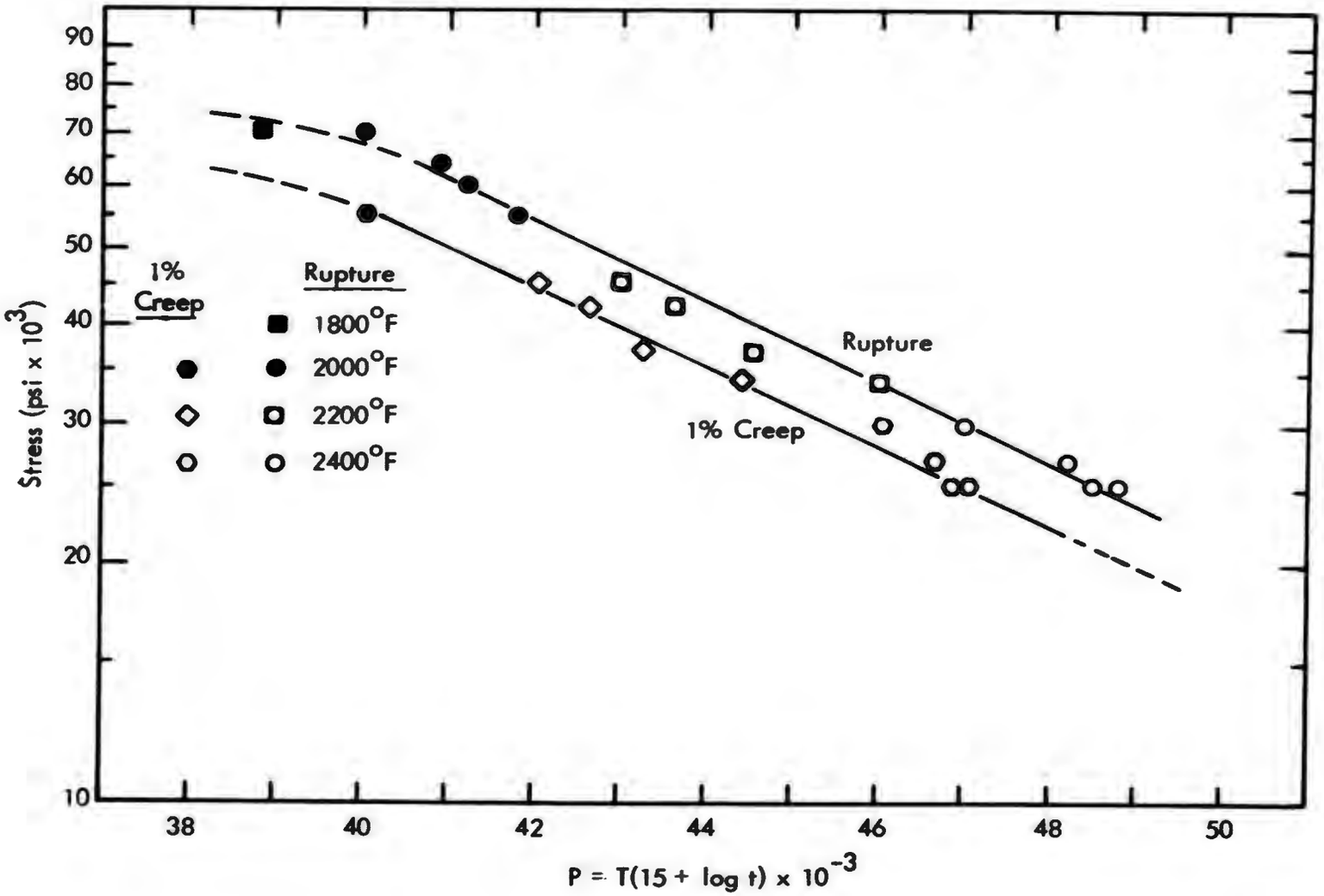

FIGURE 4 - Larsen-Miller Plot of Rupture and 1% Creep for XB-88, Reference Condition

The 100 hour rupture life of XB-88 in the reference condition as a function of test temperature is given below in Table 1.

TABLE 1 - 100 Hour Rupture Strength of XB-88 in Reference Condition

Temperature (°C/°F)	100 Hr. Rupture Life (psi)	Stress/Density* (in)
1315/2400	25,500	68,500
1215/2200	36,000	96,500
1095/2000	56,000	150,000
980/1800	74,000**	198,500

* Density = 0.373 lb/in^3

** Estimated value

The 100 hour rupture strength/density ratio of 68,500 inches at 1315°C (2400°F) is quite close to the target property of 70,000 inches. During the first phase of this program a value of 74,000 inches was obtained for XB-88 (heat VAM-80) in the high temperature (2000°C) annealed condition, although this material had no room temperature ductility. It was found in the current study that the 2000°C anneal provided poorer rupture properties than the reference condition. Microstructure and chemical analysis of the two heats of XB-88 were quite comparable, hence the difference in properties may be attributed to processing difference inherent in scaling up to larger ingot sizes.

II. GENERAL EXPERIMENTAL PROCEDURES

Alloy Preparation

Alloys were prepared in the form of 2.85 inch diameter ingots by consumable electrode AC vacuum arc melting. The electrodes were fabricated using the highest purity materials commercially available. The vendor's chemical analysis of the columbium base material is listed in Table 2. The source and form of the alloy additions are listed in Table 3.

First melt electrodes were prepared using the sandwich technique described by Ammon and Begley[13]. Starting materials were rolled to the appropriate thickness and sheared to size. Final weight adjustment was accomplished by etching to ±1% of the required value. The strips were assembled to provide the nominal composition and then welded together in a vacuum purged weld chamber under a high purity helium atmosphere to maintain the integrity of the composite during melting. Carbon, which was added as high purity graphite cloth, was wrapped in columbium foil and placed between the strips of material which comprised the electrode. The first melt electrodes, 0.95 inch by 0.88 inch by 43 inches long, weighing 10 pounds, were melted into a 2 inch diameter water cooled copper mold. The furnace chamber was evacuated to below 1×10^{-5} torr prior to melting and the chamber pressure did not exceed 5×10^{-4} torr during melting. The arc was struck on a starting pad of the same composition as the electrode. The first starting pad was an arc melted button of the XB-88 composition. Subsequent starting pads were taken from the top of the preceeding first melt ingots. Melting was accomplished at approximately 2400 amps and 30 volts, with the current being reduced to 1350-1500 amps to hot top the ingot. The average melting rate was approximately 2 pounds per minute. Because of the uniform electrode burnoff with AC melting, sound homogeneous ingots were produced by the first melt.

The first melt ingots were lathe conditioned on the ends, and then drilled, tapped, and studded together to form the second melt electrodes. The studs used were machined from XB-88 bar. After assembly circumferential welds were made to reinforce the electrode.

TABLE 2 - Chemical Analysis of Columbium Base Metal
(Vendor Ingot Analysis)

Element	Analysis (ppm)	
	Lot 89B1060	Lot 89B1061
C	30	30
N	35	20
O	60	50
H	4.3	2.4
Al	20	20
B	1	1
Cb	Bal.	Bal.
Cd	5	5
Co	10	10
Cr	20	20
Cu	40	40
Fe	50	50
Hf	80	80
Mg	20	20
Mn	20	20
Mo	20	25
Ni	20	20
Pb	20	20
Si	50	50
Sn	10	10
Ta	500	690
Ti	40	80
V	20	20
W	30	120
Zr	100	175

TABLE 3 - Source and Form of Alloy Additions

Alloy Element	Form	Source
Columbium	Plate	Fansteel Metallurgical Corp.
Tungsten	Sheet	Fansteel Metallurgical Corp.
Hafnium	Sheet	NUMEC
Carbon	Graphite Cloth	National Carbon

These electrodes were remelted using AC power at 2700 amps and 30 volts. The ingots were hot topped at 2100 amps. Five ingots of XB-88 were produced during the program. The first ingot (VAM-88-A1) was melted into a 3 inch diameter mold. Difficulties during extrusion, which will be discussed later in this report, necessitated the melting of the remaining ingots into a 2.85 inch diameter mold. An example of a final double arc melted ingot of XB-88 is shown in Figure 5. The chemical analyses of the ingots are listed in Table 3. The compositions are very close to nominal and show excellent reproducibility from ingot to ingot.

Extrusion. The first ingot, VAM-88-A2 was surface conditioned, cut in half, and machined with a 60 degree nose chamfer. The billets were then plasma sprayed with a 0.020 inch coating of molybdenum. The two billets were extruded at the Air Force Materials Laboratory at 1930°C (3500°F) and 2040°C (3700°F) respectively. The extrusion ratio was approximately 9:1. The resultant extrusions were of poor quality with numerous circumferential tears due to die friction. Approximately 0.25 inch was machined from the diameter before the cracks could be removed.

While plasma sprayed molybdenum coatings had previously been used successfully for lower temperature Dynapak extrusions,[1] conventional extrusion of the plasma molybdenum coated billets resulted in radial cracks and a poor extrusion surface. Based on this experience, thin wall molybdenum cans were used for subsequent extrusion billets. The remaining ingots were melted into 2.85 inch diameter molds, surface conditioned to 2.75 inch diameter, and extruded in a 0.125 inch thick molybdenum can. Ingots VAM-88-B1 and VAM-88-B2 were successfully extruded at 1930°C at an extrusion ratio of 5.5:1. The resultant extrusions are shown in Figure 6.

To evaluate the properties of material which had been hot extruded to final size, sections of extrusion VAM-88-A2 which had previously been extruded at 2040°C (3700°F) and a 9:1 extrusion ratio, were conditioned to 0.75 inch diameter and placed in a molybdenum

FIGURE 5 - Three Inch Diameter Ingot of XB-88 (Cb-28W-2Hf-0.067C)

TABLE 4 - Chemical Analysis Data for XB-88 (Cb-28W-2Hf-0.067C)

Heat No.	Ingot Location	Analysis (w/o)				
		W	Hf	C	O	N
VAM-88-A2	Top	27.6	1.89	0.066	0.0014	0.0041
	Bottom	27.8	1.82	0.068	0.0042	0.0041
VAM-88-B1	Top	27.4	1.88	0.066	0.0019	0.0043
	Bottom	28.0	1.80	0.066	0.0031	0.0048
VAM-88-B2	Top	27.0	1.85	0.068	0.0019	0.0057
	Bottom	27.4	1.88	0.066	0.0029	0.0050
VAM-88-C1	Top	27.2	1.84	0.068	0.0031	0.0033
	Bottom	27.2	1.88	0.070	---	0.0030
VAM-88-C2	Top	27.2	1.82	0.065	0.0021	0.0041
	Bottom	27.1	1.90	0.067	0.0027	0.0030

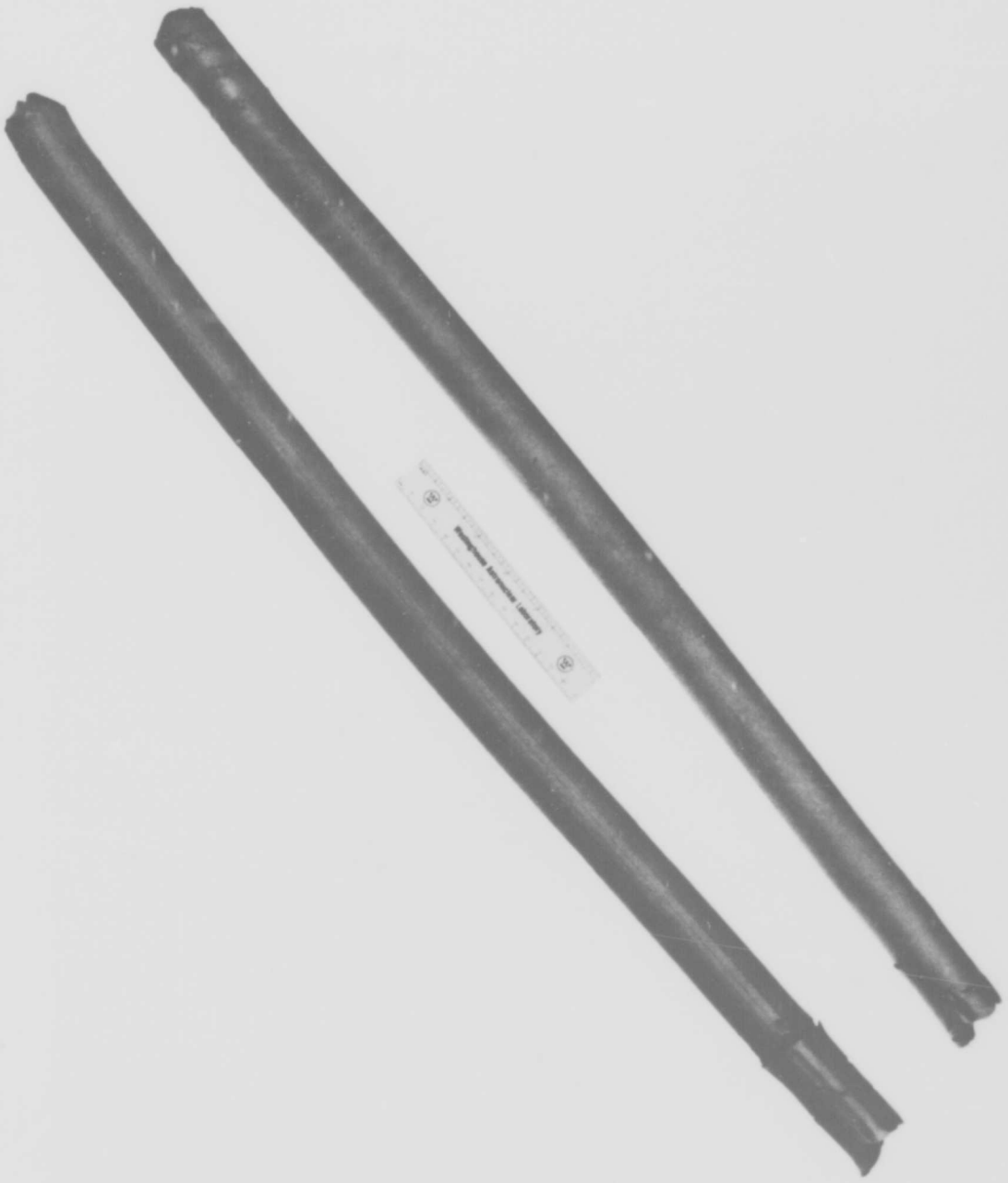

FIGURE 6 - As-Extruded XB-88. Extruded at 1930°C(3500°F) and 5.5:1 Extrusion Ratio

can as shown in Figure 7. This configuration was used to permit the extrusion of several short sections of material in one billet. The billet assembly was extruded at 2040°C (3700°F) at a reduction ratio of 2:1. The double extruded billet was pickled in aqua regia until the molybdenum was removed. The columbium alloy was not attacked by the pickling solution. The second extrusion provided excellent quality rod.

Swaging. All swaging operations were conducted at 1300°C. The material was reduced from single extruded material to 0.440 inch diameter bar stock without intermediate annealing. The extrusions from ingots VAM-88-B1 and VAM-88-B2 had a 0.050 inch residual co-extruded layer of molybdenum from the extrusion can. This coating provided protection from contamination during swaging. The remaining traces of molybdenum on the bar were removed during specimen machining. The total loss of material processed in this manner from conditioned billet to bar stock was only 9.8%. By contrast, ingot conditioning losses amounted to 23%. The total yield of bar stock from ingot was approximately 70%. Figure 8 shows the general flow diagram followed during the processing and evaluation of the material produced during the program.

Heat Treatment

Heat treatments were carried out in tantalum and tungsten element resistance heated vacuum furnaces. These cold wall furnaces are capable of maintaining pressures below 5×10^{-6} torr at temperature. Specimens for heat treatment were etched in a HNO_3-HF solution, rinsed, and wrapped in tantalum foil. Temperatures up to 1600°C were measured by Pt-Pt/Rh thermocouples. At higher temperatures a calibrated optical pyrometer was utilized for temperature measurement, with suitable corrections being applied for the sight port transmittance. To insure reliable and consistent environmental control, the furnace leak rate was checked before each annealing cycle. Any significant increase in the hardness of the check sample resulted in a complete examination of the furnace. When a more rapid cooling rate than that achieved by normal radiation cooling was desired, high purity helium was admitted to the furnace chamber at the termination of an annealing cycle. This provided

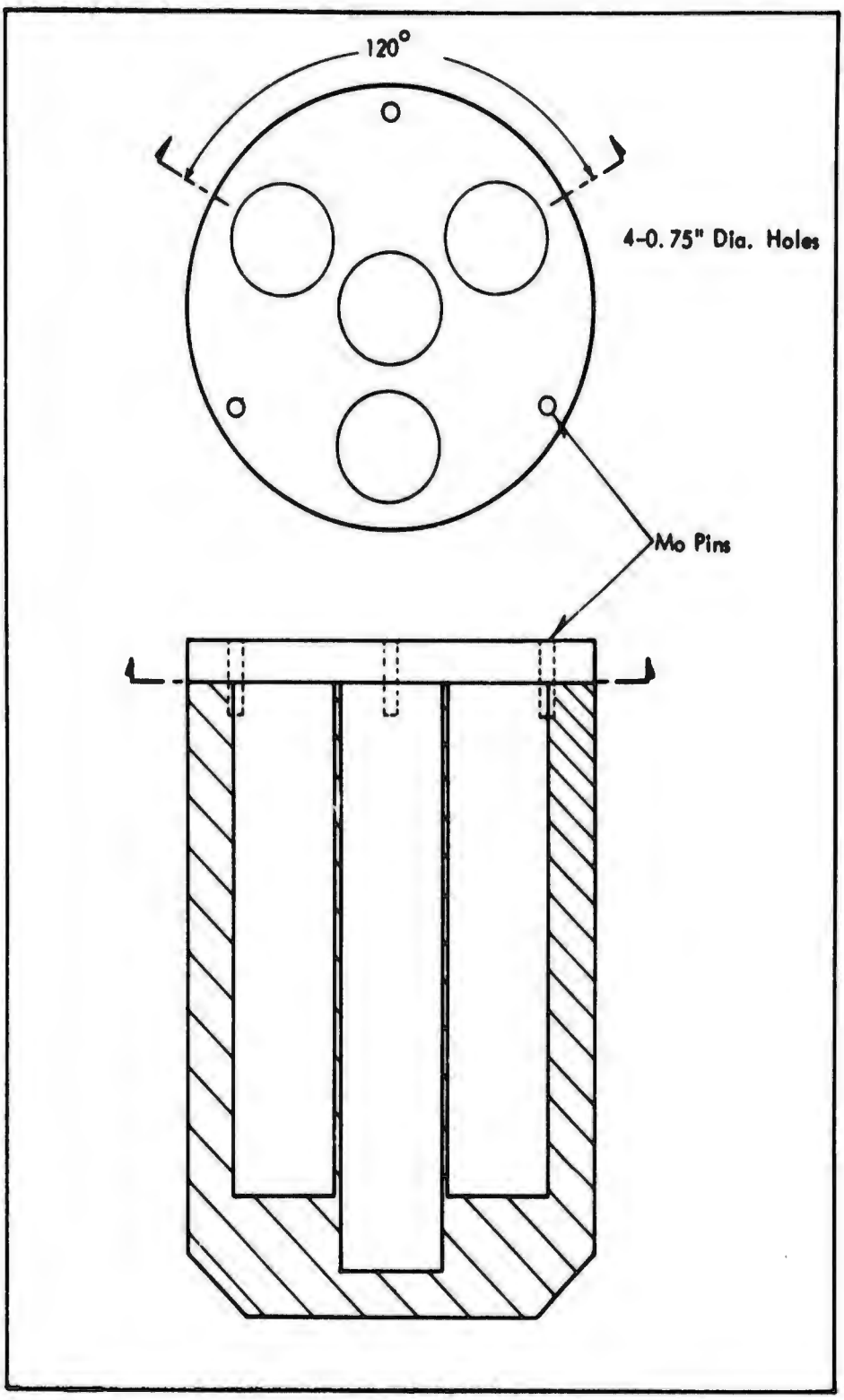

FIGURE 7 - Billet Configuration for Double Extrusion of XB-88 (VAM-88-A2)

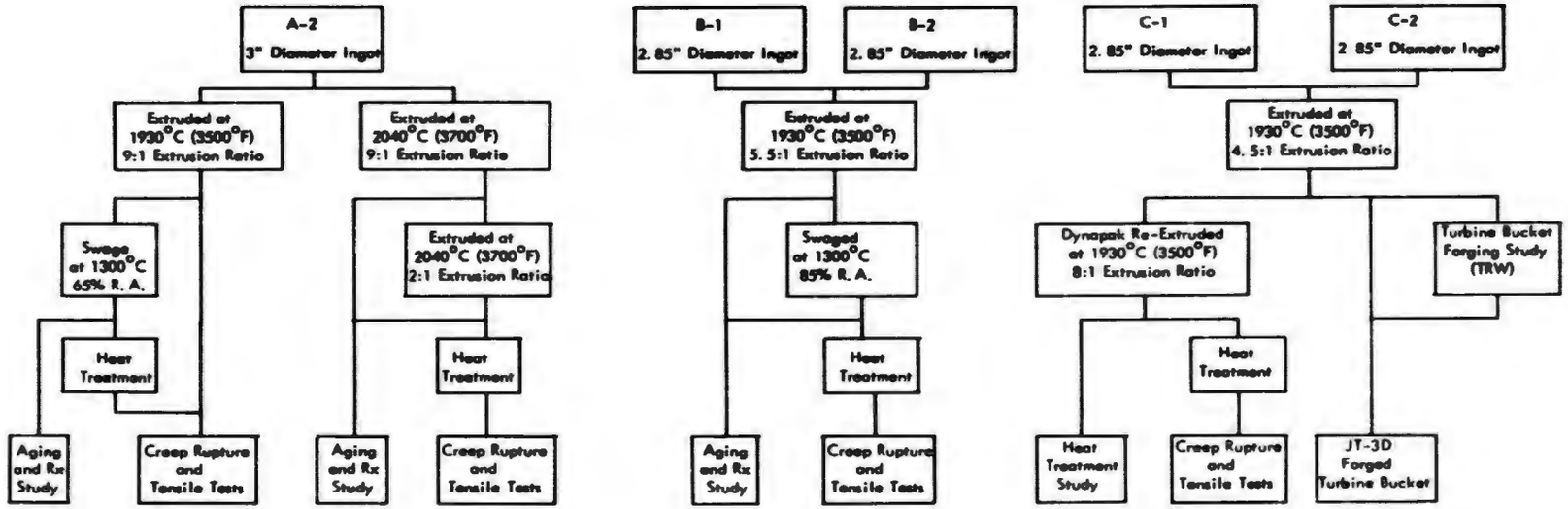

FIGURE 8 - XB-88 Processing and Evaluation Flow Chart

a cooling rate of approximately 400°C/min. as compared to approximately 60°C/min. for radiation cooling (to below black heat).

In a number of heat treatments the normal heat up rate or helium quenching rate was too slow for the short time recrystallization studies (flash heat treatments) or rapid quenching studies. In these cases a 10 KW R. F. induction furnace was used because of the short heating and cooling times. The heating time from room temperature to 2200°C was approximately 1 minute and the normal cooling rate from 2200°C to 1200°C (the temperature beyond which phase transition is extremely slow) was 2000°C/min. The short time induction anneals were carried out in a flowing argon atmosphere.

The normal cooling rate or helium "quenching" rate was found to be too slow for accurate interpretation of elevated temperature phase relationships. The problem was to devise a simple quenching system in which the quenching media would not contaminate either the vacuum system or the heating elements. The above problems were circumvented by encapsulating the specimens in quartz capsules, heating in an induction furnace, and quenching the specimen by dropping the capsule into a brine solution and breaking the glass. Contact between the specimen and the quartz capsule was prevented by suspending the specimen on a tungsten wire from a glass hook in the capsule as shown in Figure 9. The quartz capsules were repeatedly flushed with argon and then evacuated prior to closure. The temperature was measured by sighting into a black body hole in the specimen with a calibrated micro-optical pyrometer and applying the appropriate correction for the quartz capsule wall.

The specimens were cooled from the elevated annealing temperature (2000°C) to the cessation of brine boiling in 4 to 5 seconds, or a quenching rate of 400°C to 500°C per second. The contamination layer of 1-2 mils formed by the short exposure to the brine solution was removed by grinding and etching prior to metallography and x-ray diffraction analysis of the extracted phases.

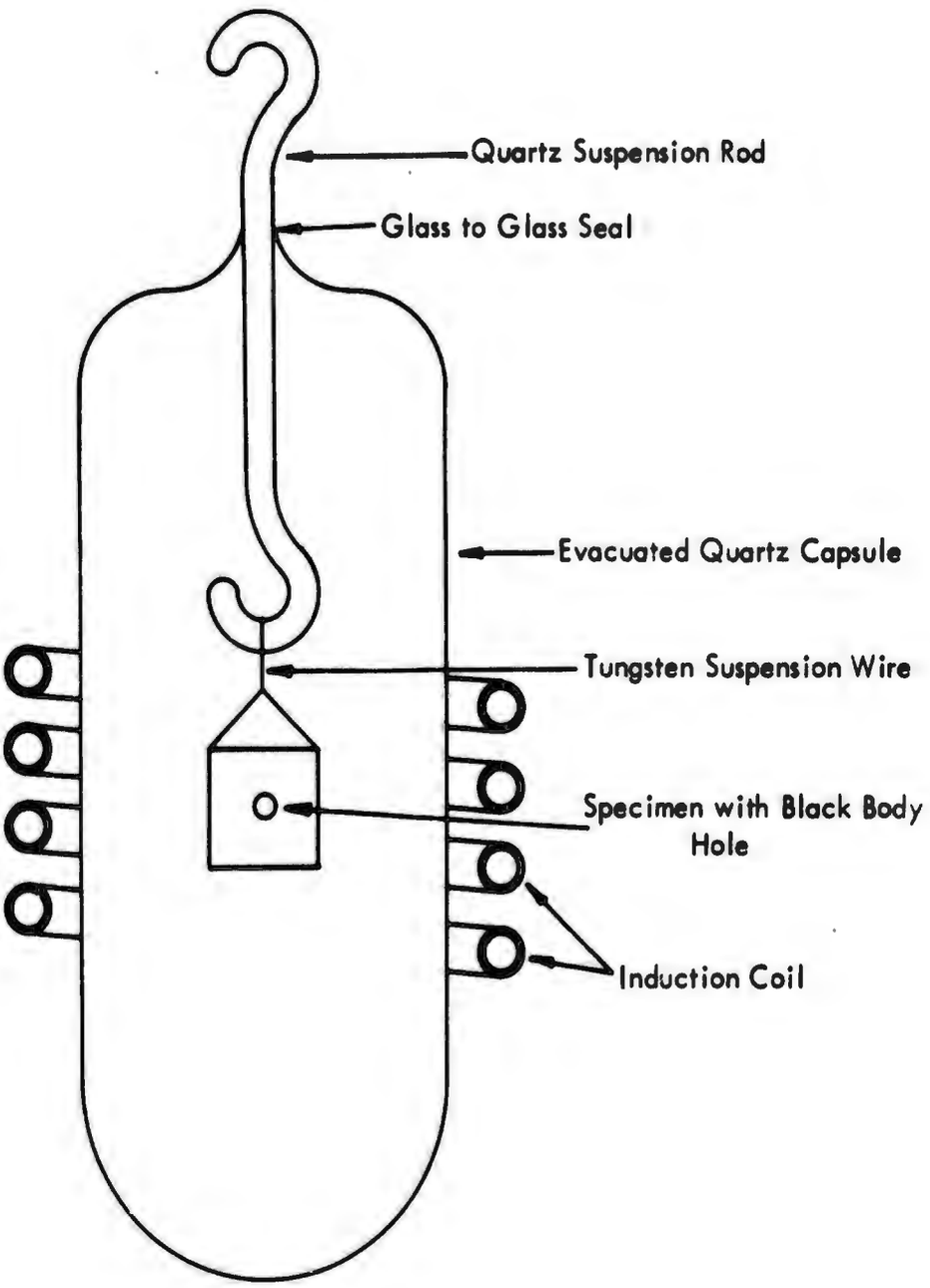

FIGURE 9 - Quartz Brine Quenching Capsule

Mechanical Property Testing

The mechanical properties of the alloys were evaluated by means of hardness, tensile, and creep-rupture tests.

Creep-Rupture Test Procedures. Creep-rupture tests were conducted in Satec Model VC-100 stress-rupture units. These are 5 to 1 lever machines with tantalum sheet heating elements capable of operation at temperatures up to 1650°C. The vacuum chamber is capable of pressures down to 5×10^{-7} torr. The pumping system incorporates a liquid nitrogen cold trap with automatic nitrogen level control. Leak rates of the systems are generally less than 1.7×10^{-5} cc atmosphere/sec or a pressure rise of less than 1 micron/hr. Pressures are measured with a CVC hot cathode ionization gage. The furnace is powered by a saturable core reactor and controlled with a Barber-Coleman MMC control unit to ± 2°C, with temperature being measured by Pt-Pt/Rh thermocouples. The temperature gradient over a 1-1/2 inch gage length is within ± 2°C. A Satec extensometer used in conjunction with a Wiedemann measuring system is used to measure deflections as low as 0.040 inch over a 10 inch recorder range. The stress-rupture specimens are shoulder loaded, having a 0.180 inch gage diameter, and a 1.5 inch gage length.

Tensile Testing. Low temperature tensile tests were conducted at a constant strain rate of 0.05 in/in/minute, using specimens having a 0.180 inch gage diameter and a 1.5 inch gage length. Elevated temperature tensile tests were carried out by Metcut Research Assoc., Inc., following the procedures outlined in MAB 192-M. Tests were conducted on a Baldwin B. T. E. 60,000 pound testing machine equipped with a 0-1200 pound scale. A stainless steel vacuum chamber with tantalum resistance element heaters provided protection from the environment. All testing was done at pressures below 5×10^{-6} torr. The tensile specimens were identical to the creep-rupture bars, and tests were carried out at a strain rate of 0.05 in./in/minute.

Metallography

Samples for metallographic examination were ground on 240, 400, and 600 grit silicon carbide papers, and then polished through 30, 15, and 6 micron diamond abrasive on a hard-finish cloth. The mechanical polish was continued on a short-pile cloth charged with a thick slurry of Linde B alumina in water. Finally, the specimens were acid polished by adding a solution of 25 parts of 10% chromic acid, 25 parts of concentrated sulphuric acid, and 10 parts of 48% hydrofluoric acid to the polishing cloth while still charged with Linde B. The specimens were then electropolished using as an electrolyte the same solution used for etch polishing. The electrolytic polishing was generally sufficient to clearly delineate precipitates. If additional definition of grain boundaries or other microstructural features was necessary, the sample was etched in a solution consisting of 1 part concentrated nitric acid, 1 part 48% hydrofluoric acid, and 2 parts glycerine.

Electron Metallography

Surface replicas for electron microscopy were prepared using a two stage parlodion-carbon technique. The replicas were shadowed with chromium and examined using a JEM-6A electron microscope. The following procedure was developed for preparing thin foils of XB-88 (Cb-28W-2Hf-0.067C) for examination by transmission electron microscopy. Approximately 40 mil thick slices were cut from the XB-88 specimen to be studied. These slices were then mechanically thinned by successively grinding on water cooled 120, 240, 320, and 400 grit silicon carbide papers and finally on a 600 grit paper lubricated with stick wax. Material was removed from both sides of the slices until they were 3 to 5 mils thick. One-eighth inch diameter discs, punched out of the thinned sections, were then electropolished to a thickness of less than 2000 $\mathring{A}$ in a G. E. M. dual-jet thinning apparatus. The electrolyte consists of 20 ml of concentrated sulphuric acid, 10 ml of hydrofluoric acid, and 370 ml of methyl alcohol. During electropolishing, which takes from 20 to 30 minutes, the electrolyte temperature was maintained at -94°F (-70°C) by using dry ice in ethyl alcohol, while the current was maintained at 5 to 10 milliamperes by periodically adjusting the voltage and/or electrolyte flow rate as thinning progressed. The voltage generally ranges between 20 and 40 volts and was never

allowed to go below 15 volts.* The resulting self-supporting foils were then inserted directly into the electron microscope for examination.

Phase Extraction

Two techniques were used in obtaining carbide phase residues suitable for x-ray and electron microscopic analysis: (1) the bromine-methanol-tartaric acid solution technique and; (2) the electrolytic extraction technique. In the former technique, the specimen was wrapped with platinum wire and immersed in the tartaric acid-bromine-methanol solution for approximately a week or until a substantial portion of the matrix had dissolved. The dispersed phase settled to the bottom of the container and was centrifuged, rinsed, and made ready for evaluation by electron microscope or x-ray diffraction techniques. The electrolytic technique is much faster. A residue may be obtained in a few hours. The specimen (anode) is suspended in a 7% HCl-Methanol solution. A 5 amp D. C. current flows through the specimen anode to a platinum cathode. The precipitates settled to the bottom of the container as the matrix of the specimen dissolved and were centrifuged, rinsed, and made ready for analysis.

Phase Identification

Material for x-ray diffraction studies was mounted in a glass fiber, and Debye-Scherrer diffraction patterns were obtained using nickel filtered CuK_{α} radiation. The material for electron diffraction studies was ultrasonically dispersed in amyl acetate, transferred on to a carbon film mounted on specimen grids, and dried.

X-Ray Fluorescence Analysis

X-ray fluorescence analysis was performed on the extracted residues using a vacuum-path spectrometer. A calibration curve was necessary to determine the relative amounts of Cb, W, and Hf present in each residue. Due to the availability of CbC and WC powders,

*Polishing is stopped at initial penetration and the foil is carefully washed.

these were used to determine the calibration curve. The curve was plotted as $\frac{I_{(WC\ L_\alpha)}}{I_{(WC\ L_\alpha)} + I_{(CbC\ K_\alpha)}}$ versus w/o W using 0.5 gram samples packed into holders. A similar curve using a very small sample volume (0.018 g) was determined and plotted. Both sets of samples gave similar intensity ratios resulting in the same calibration curve, thus it was felt that the small amount of sample obtained by extraction was sufficient to determine the composition.

Since the emitted radiation from the W and Hf are similar in wave length, their absorption characteristics in a columbium matrix are similar. For this reason the values of the intensity for WC and HfC may be used interchangeably on the calibration curve. When determining the composition of the unknown, the ratio of $\frac{I_{(WC\ L_\alpha + HfC\ L_\alpha)}}{I_{(WC\ L_\alpha + HfC\ L_\alpha + CbC\ K_\alpha)}}$ was used and the w/o WC is W/o WC+HfC. The chart intensities of the W L_α and Hf L_α lines are then direct percentages of the total WC and HfC with CbC found by difference. The small difference in the mass absorption coefficients of the emitted wave lengths of W and Hf in a Cb matrix results in accuracies of $\pm$2% for W+Cb compositions to $\pm$5% for Hf+Cb mixtures.

Chemical Analysis

Sections from the top and bottom of each ingot were analyzed for W, Hf, carbon, oxygen, and nitrogen. An x-ray fluorescence method was used to determine the metallics. Samples dissolved in an acid solution were compared to standard solutions. Oxygen, nitrogen, and carbon were determined by the vacuum fusion technique, the Kjeldahl technique, and the Leco low carbon analyzer respectively.

III. RESPONSE TO THERMAL MECHANICAL TREATMENT

Previous work in this program has demonstrated the dominant role of structure on mechanical properties of columbium base alloys. In order to establish a basis for selecting thermal-mechanical treatments which would provide the best combination of high temperature creep strength and low temperature ductility in XB-88, it was necessary to evaluate microstructure and thermal response as a function of processing history. Initial studies[1] of Cb-W-Hf-C alloys were carried out using material which had been Dynapak extruded at 1250-1350°C, and subsequently swaged to final size at 1300°C. However, limited experiments suggested that improvements in mechanical properties could be achieved by using high temperature extrusion for ingot breakdown. Results of previous studies indicated that the best combination of high temperature creep strength, rupture elongation, and low temperature ductility could be achieved with a fine grained recrystallized structure which was produced by working at temperatures high enough to permit carbide dissolution during working, and subsequent reprecipitation during cooling. Consequently, the structures developed during high temperature extrusion were investigated in detail.

As-Extruded Structure

Two billets of XB-88 were extruded at 1930°C (3500°F) at extrusion ratios of 9:1 and 5.5:1 respectively. The billet having the lower extrusion ratio yielded the wrought microstructure shown in Figure 10. Microstructure changed appreciably with higher reduction ratio during extrusion. The photomicrograph of Figure 11a shows that the billet having the 9:1 extrusion ratio was comprised of bands of recrystallized material in a matrix having an apparent wrought structure. The extrusion was approximately 60% recrystallized. The recrystallized areas were comprised of fine grains having a mean grain diameter of 0.007 mm (ASTM-12). The wrought appearing regions shown in Figure 11a are actually composed of well developed subgrains decorated with precipitates as revealed in the 1500X photomicrograph of Figure 11b.

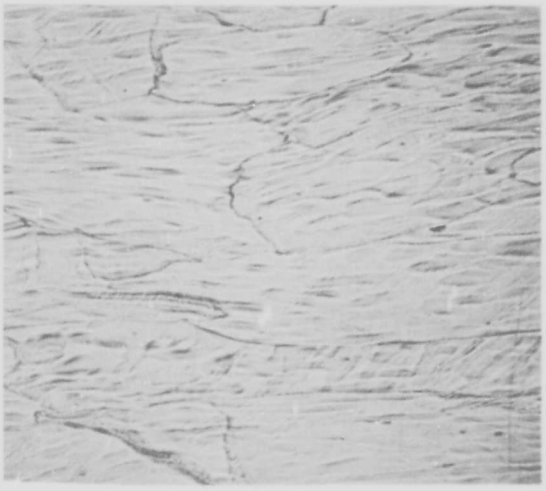

(a) Longitudinal Section

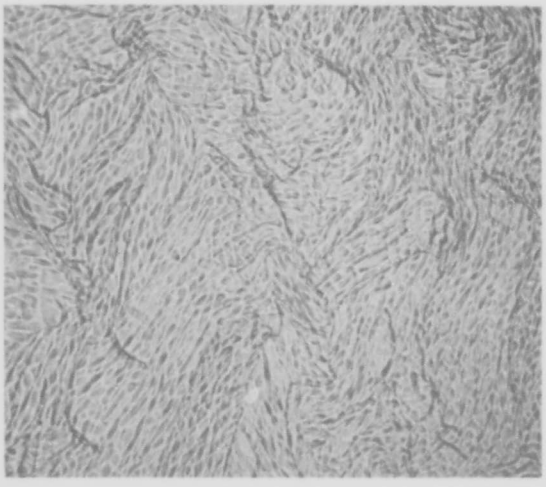

(b) Transverse Section

FIGURE 10- Microstructure of XB-88 Extruded at 5.5:1 Reduction Ratio at 1930°C (3500°F) 100X

(a) 100X

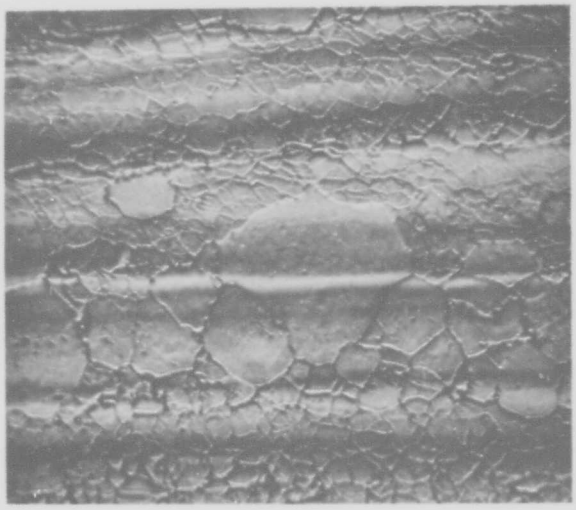

(b) 1500X

FIGURE 11- Microstructure of XB-88 Extruded at 1930°C(3500°F), 9:1 Extrusion Ratio

A structure similar to that shown in Figure 11 was obtained from material extruded at an 9:1 reduction ratio at 2040°C (3700°F) (Figure 12). This material, however, was coarser in texture, having a mean grain diameter of 0.014 mm (ASTM-10) in the recrystallized bands, and was approximately 90% recrystallized. The material obtained from the 2040°C extrusion was re-extruded at 2040°C. The extrusion ratio of 2:1 was the maximum permissible to obtain useful material for mechanical property testing since the first extrusion had to be machined to 0.75 inch diameter to remove deep cracks. The microstructure of the double extruded bar is illustrated in Figure 13. The microstructure, in contrast to the almost fully recrystallized single extruded bar, was wrought in appearance and showed no sign of recrystallization. The 1500X photomicrograph of Figure 13b shows a poorly defined substructure in the double extruded material. The difference in microstructure between single and double extruded material is attributed to the difference in reduction ratio, with the low ratio of the second extrusion resulting in an unrecrystallized microstructure.

The final hot worked condition studied was XB-88 conventionally extruded at 1930°C, 5 5:1 reduction ratio, and re-extruded in the Dynapak at 1930°C, 8:1 reduction ratio. The resulting structure shown in Figure 14 was approximately 40% recrystallized with a well defined substructure in the "wrought" appearing bands. The cellular substructure is well decorated with precipitates which form during cooling. The microstructure of Figure 14 also differs considerably from the microstructure of the material conventionally extruded at the same approximate temperature and reduction shown in Figure 11. The recrystallized grains of the Dynapak extruded material are more rectangular with the long grain boundaries perpendicular to the extrusion axis. The mean grain diameter is larger in the Dynapak extruded material, because of the temperature increase (estimated at 200 to 300°C) arising from adiabatic heating during high speed deformation.

(a) 100X

(b) 400X

FIGURE 12- Microstructure of XB-88 Extruded at 2040°C(3700°F) 9:1 Extrusion Ratio

(a) 100X

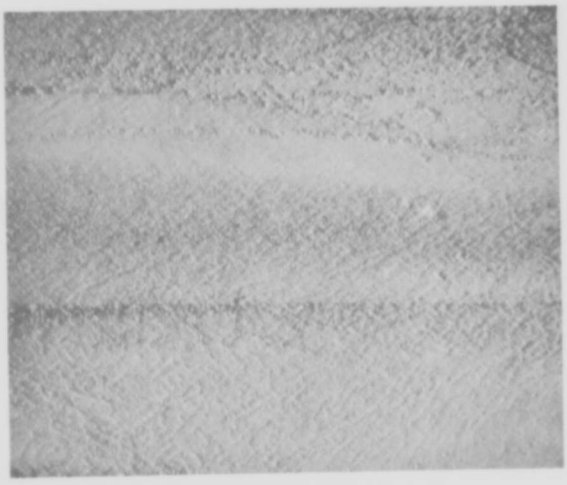

(b) 1500X

FIGURE 13- Microstructure of XB-88 Extruded at 2040°C, 9:1 Reduction Ratio, Re-extruded at 2040°C(3700°F) 2:1 Reduction Ratio, 89% Total Reduction

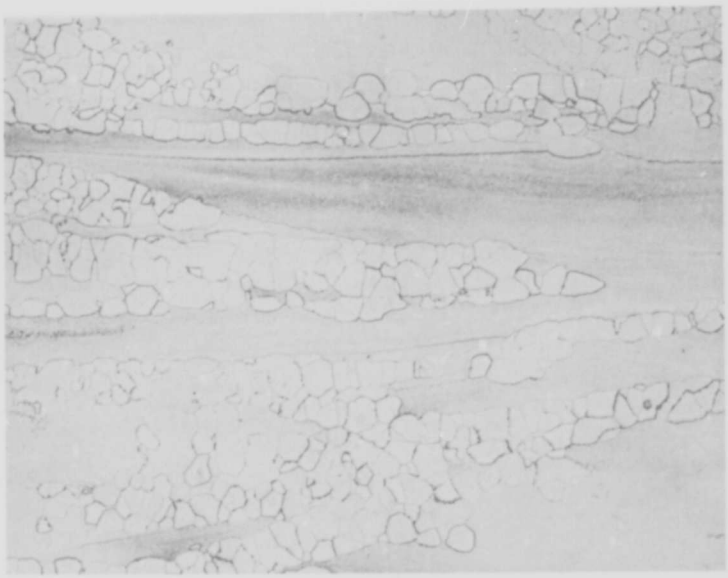

(a) 100X

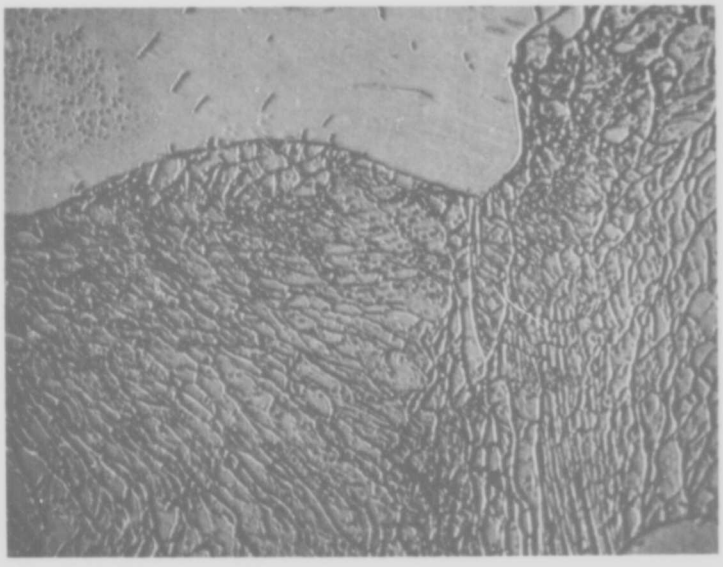

(b) 1500X

FIGURE 14 - Microstructure of XB-88 Double Extruded at 1930°C (3500°F). Conventional Extrusion at 5:1 Reduction Plus Dynapak Extrusion at 8:1 Reduction.

Aging Studies. Heat treatment studies were conducted on XB-88 in the following conditions:

1. Extruded at 1930°C (3500°F) 9:1 extrusion ratio (89% reduction)
2. Extruded at 2040°C (3700°F) 9:1 extrusion ratio (89% reduction)
3. Extruded as in (1) above, swaged at 1300°C(65% reduction during swaging)

Sections of bar representing each of the three conditions were annealed 2 hours at 2000°C, and then aged 1 hour at temperatures ranging from 1000 to 1900°C. Room temperature hardness data are shown as a function of aging temperature in Figure 15. The material in the three initial conditions, given the same solution and aging treatments, differ by only ±5 VHN. The data of Figure 15 support the premise that the high temperature annealing treatment erases the influences of prior processing variables on the microstructure and short time mechanical properties of this class of alloy. A very minor aging peak was noticed at 1200°C in the extruded plus swaged material similar to that observed for VAM-87 (Cb-22W-1Zr-0.13C) and VAM-78 (Cb-22W-2Zr-0.13C) presented in a later section of this report. A more significant peak with an amplitude of 20 VHN was observed at 1600°C.

The aging peak observed at 1600°C appears to be associated with the transformation of the high temperature complex phase(s) to the low temperature face centered cubic carbide $(Cb,Hf)C_{1-x}$. The photomicrographs of Figures 16 through 21 show the effects of the 2000°C anneal and subsequent aging treatments on the microstructure of high temperature extruded plus swaged material. The carbide phase(s) in material annealed above 1600°C occur as acicular precipitates at grain and subgrain boundaries, as well as on preferred crystallographic planes within the matrix (Figures 16 and 17). At 1600°C and below the carbides became more massive and precipitation is more extensive, particularly on sub-boundaries, Figures 18, 19 and 20.

The sample aged at 1200°C (Figure 21) does not appear to differ substantially from the high temperature annealed structure. The kinetics of the precipitation of the cubic carbide are sufficiently slow to prevent transformation during the 1 hour aging treatment at

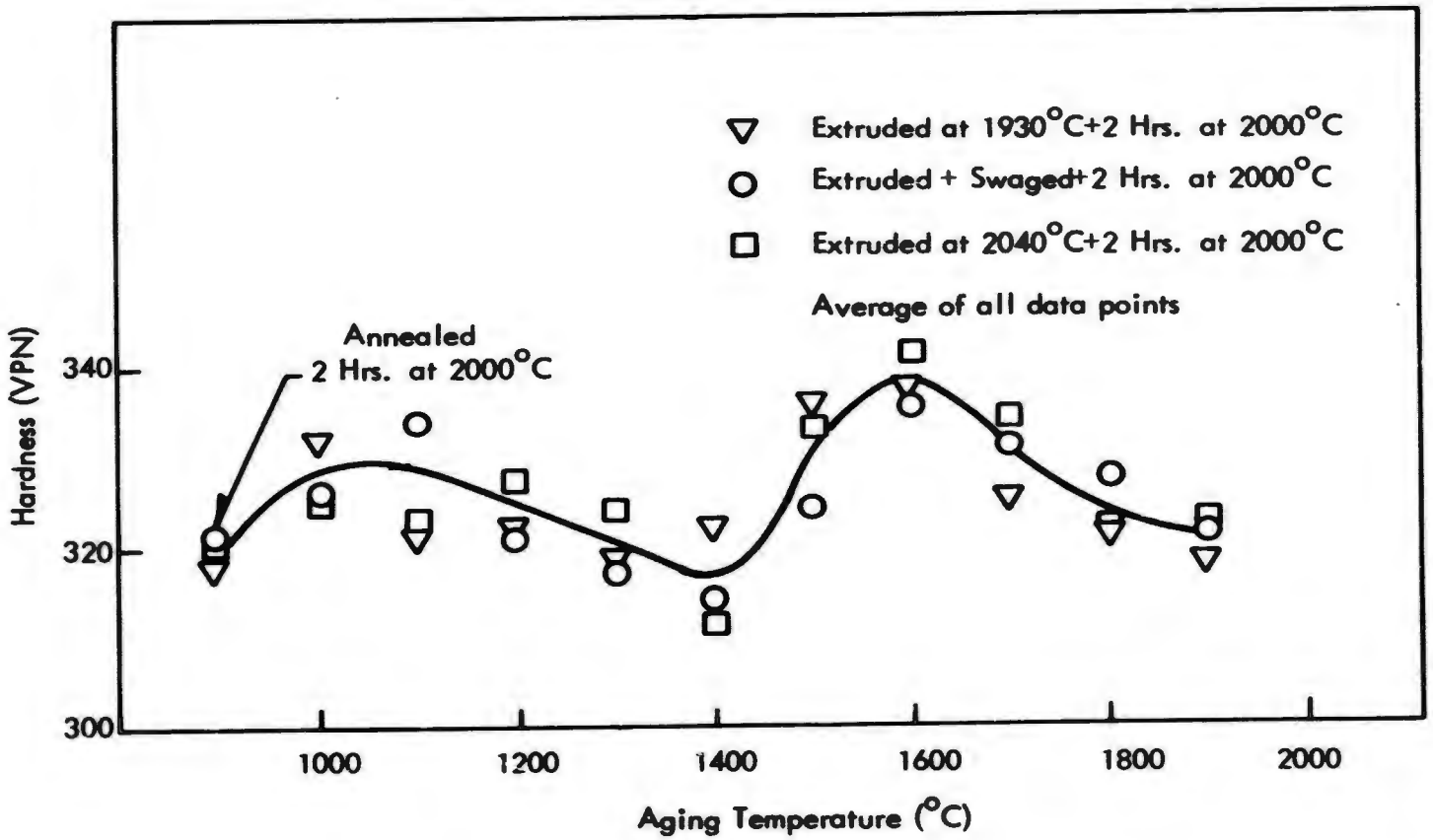

FIGURE 15 - Effect of Aging Temperature on the Hardness of XB-88(1 Hr. Anneals)

400X

FIGURE 16 - Microstructure of XB-88 Annealed 2 Hrs. at 2000°C

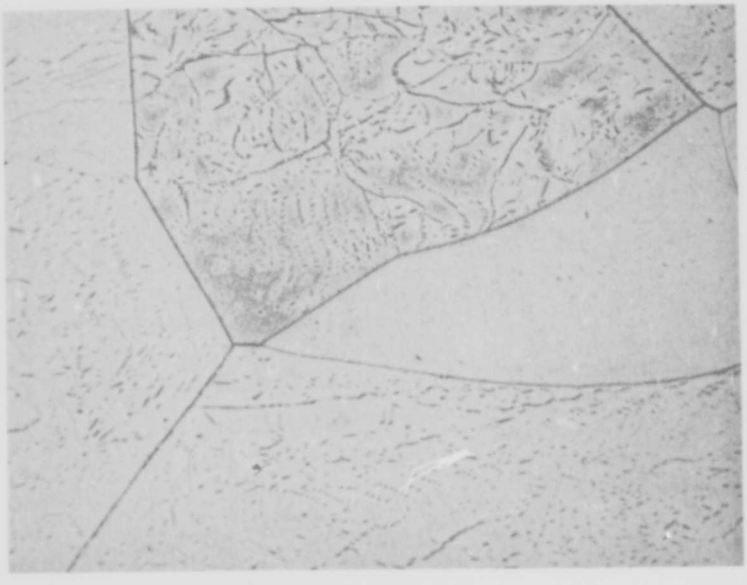

400X

FIGURE 17 - Microstructure of XB-88 Annealed 2 Hrs. at 2000°C Plus 1 Hr. at 1800°C

400X

FIGURE 18 - Microstructure of XB-88 Annealed 2 Hrs. at 2000°C Plus 1 Hr. at 1600°C

400X

FIGURE 19 - Microstructure of XB-88 Annealed 2 Hrs. at 2000°C Plus 1 Hr. at 1500°C

1200°C. The response to heat treatment of XB-88 is very similar to the behavior of the series of Cb-W-Hf-C alloys investigated during the first phase of this program.

Recrystallization and Grain Growth

The 1 hour recrystallization and grain growth behavior of XB-88 in the various conditions studied is summarized in Figure 22. As noted previously the 1930°C (3500°F) and 2040°C (3700°F) extrusions were partially recrystallized during hot working to a mean grain diameter of 0.007 mm and 0.013 mm (in the recrystallized regions) respectively. The 1930°C extrusion was approximately 60% recrystallized and the 2040°C material was 90% recrystallized. The hot extruded material was not completely recrystallized after annealing 1 hour at 1700°C, even though the average grain diameter in the recrystallized areas had increased to 0.019 mm. Above 1700°C recrystallization of both extruded conditions was complete and the grain growth characteristics were very similar.

The material double extruded at 2040°C was not recrystallized during processing as was the severely worked single extruded specimen (see Figure 13). With this material the slope of the grain size vs isochronal annealing temperature (Figure 22) was somewhat flatter than that of the other conditions studied.

The extruded plus swaged bar (extruded at 1930°C with a 5.5:1 reduction ratio, plus swaged 86% R.A. at 1300°C) recrystallized with a larger grain size than the as-extruded material. The recrystallization behavior of the extruded plus swaged material is illustrated by the photomicrographs of Figures 23 and 24, and the x-ray back reflection photographs of Figure 25. The high magnification photomicrographs (Figure 24) show the initiation of well defined subgrains after annealing 1 hour at 1400°C, becoming better developed as annealing temperature is progressively increased to 1700°C. After annealing at 1800°C a completely recrystallized structure is obtained. The x-ray back reflection photographs of Figure 25 confirm the microstructures illustrated in Figures 23 and 24. The reflections are poorly resolved at 1400°C to 1600°C becoming better resolved at 1700°C and completely defined at 1800°C.

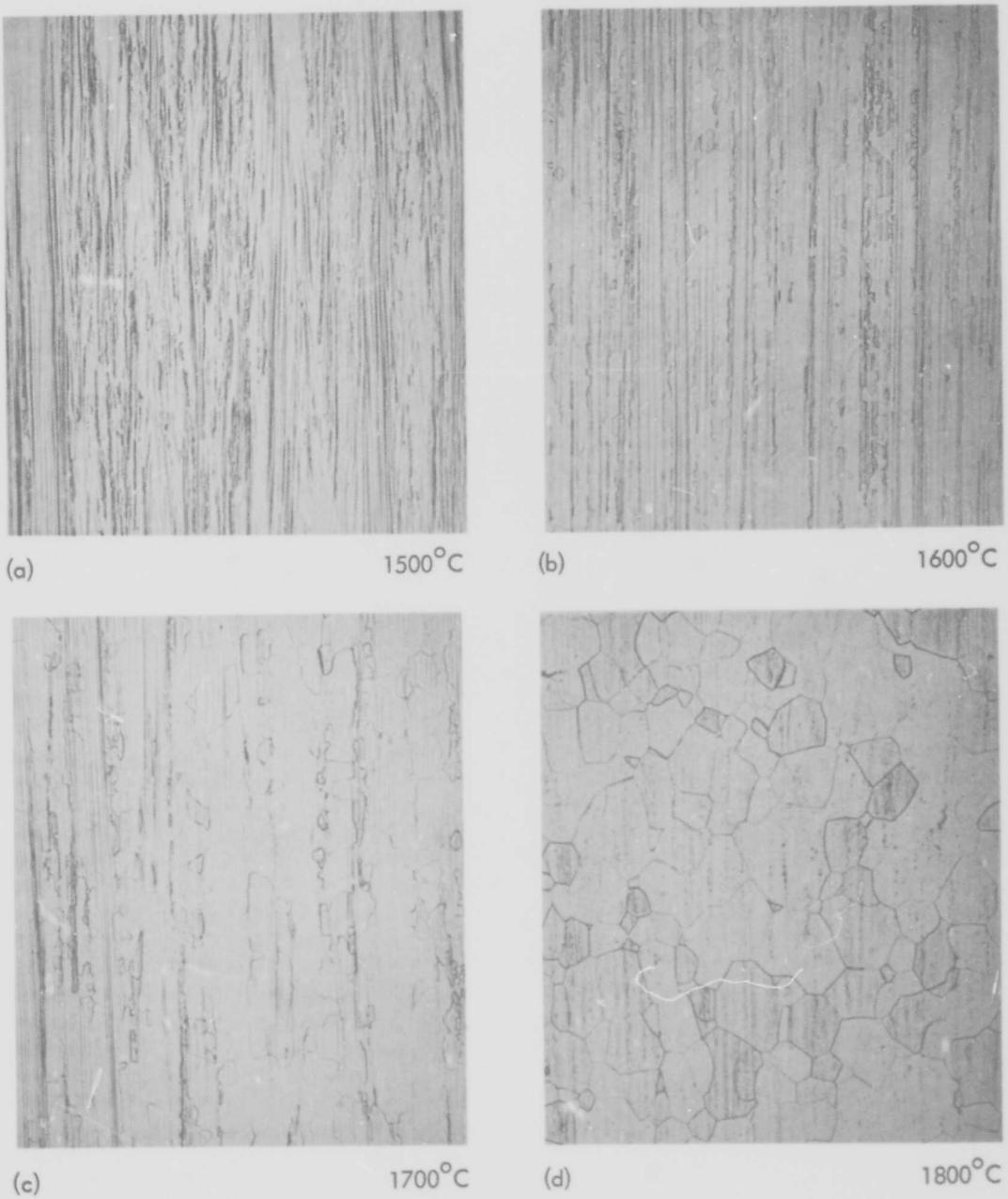

FIGURE 23 - Effect of Annealing on the Microstructure of Extruded Plus Swaged (92% R. A.) XB-88. 1 Hr. Anneals 100X

(a) 1400°C

(b) 1500°C

(c) 1600°C

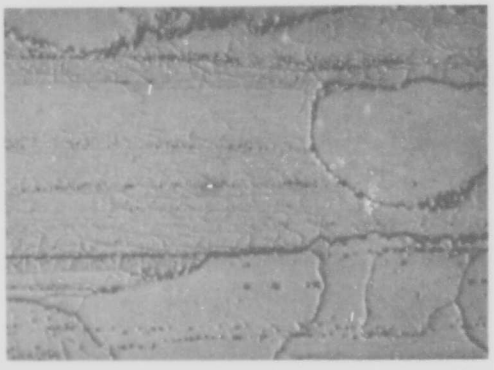

(d) 1700°C

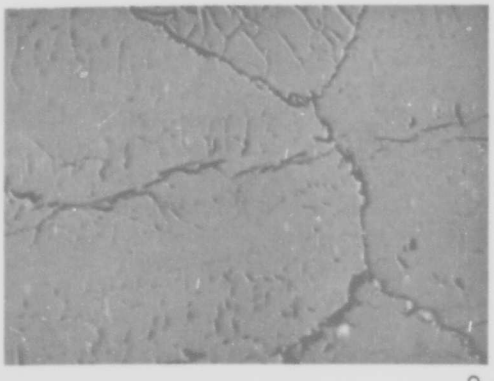

(e) 1800°C

FIGURE 24 - Effect of Annealing Temperature on Substructure Development in Extruded Plus Swaged (92% R. A.) XB-88. 1 Hr. Anneals 1500X

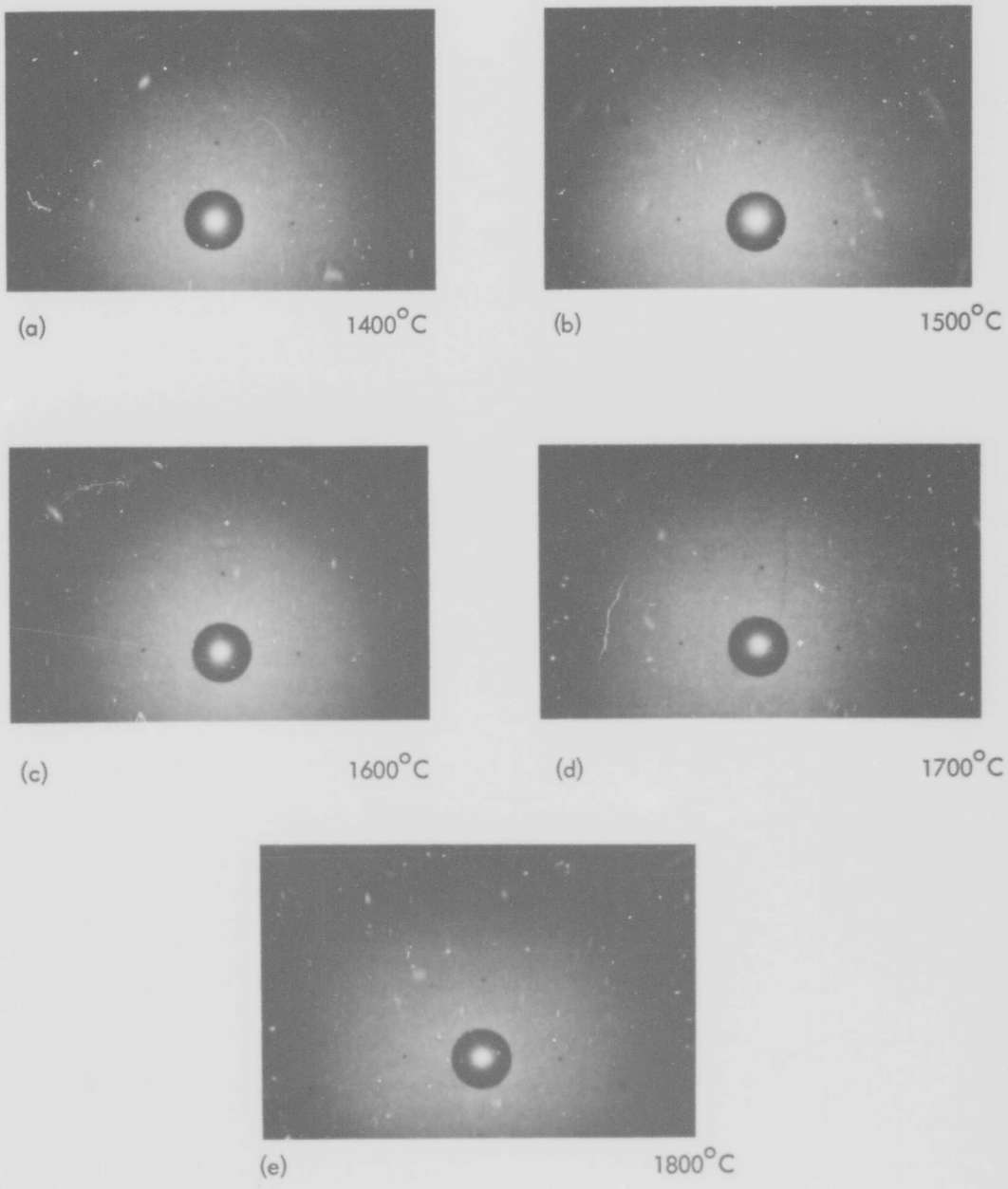

FIGURE 25 - Effect of 1 Hour Annealing Temperature on Recrystallization Behavior of Swaged XB-88. Back Reflection Photographs of (321) Planes.

Previous work in this program showed that high temperature annealed, fully recrystallized structures provided enhanced creep properties compared to wrought structures. The strength improvement resulting from high temperature annealing is associated with changes in carbide precipitate identity, morphology, and/or distribution. However, one problem encountered with the relatively large grained structures resulting from high temperature annealing is premature rupture in creep arising from grain broundary separation. It was apparent that the rupture life of XB-88 could be increased significantly if the tertiary creep strain could be extended by even a small amount. Such an improvement might result from reducing the grain size in the presence of the carbide precipitate identity and morphology achieved by high temperature annealing. Consequently a study of the recrystallization, grain growth, and phase transformation kinetics of XB-88 as a function of time at 1800°C and 2200°C was carried out.

Heat treatments were carried out at 1800°C on XB-88 in the extruded (1930°C) plus swaged (1300°C) and the double extruded (2040°C) conditions. The annealing times investigated ranged from 5 to 60 minutes. The effect of annealing time on mean grain diameter is shown in Figure 26. The mean grain diameter of the swaged material varied from 0.033 mm for the 5 minute anneal to 0.065 mm for the 60 minute anneal. The double extruded material recrystallized to somewhat smaller grain sizes, varying from 0.027 mm for the 5 minute anneal to 0.048 mm for the 40 minute treatment. Both materials apparently experience parabolic grain growth proportional to $t^{1/2}$ as shown in Figure 26, although there is some scatter of the data due to the uncertainty of grain growth during heating and cooling. The microstructures of swaged XB-88 heated for 5, 10, and 40 minutes are shown in Figure 27. It is believed that the bladelike precipitates are the complex zeta phase (to be discussed later in this report) which forms metastably during cooling. The small, more equiaxed, blockier precipitates are probably cubic carbides. The amount of the cubic phase can be seen to decrease as annealing time increased to 40 minutes. These metallographic observations are corroborated by x-ray diffraction results presented in the next section of this report.

Grain diameter versus annealing time for a similar series of annealing experiments at 2200°C is also shown in Figure 26. Representative photomicrographs for the 15 second and

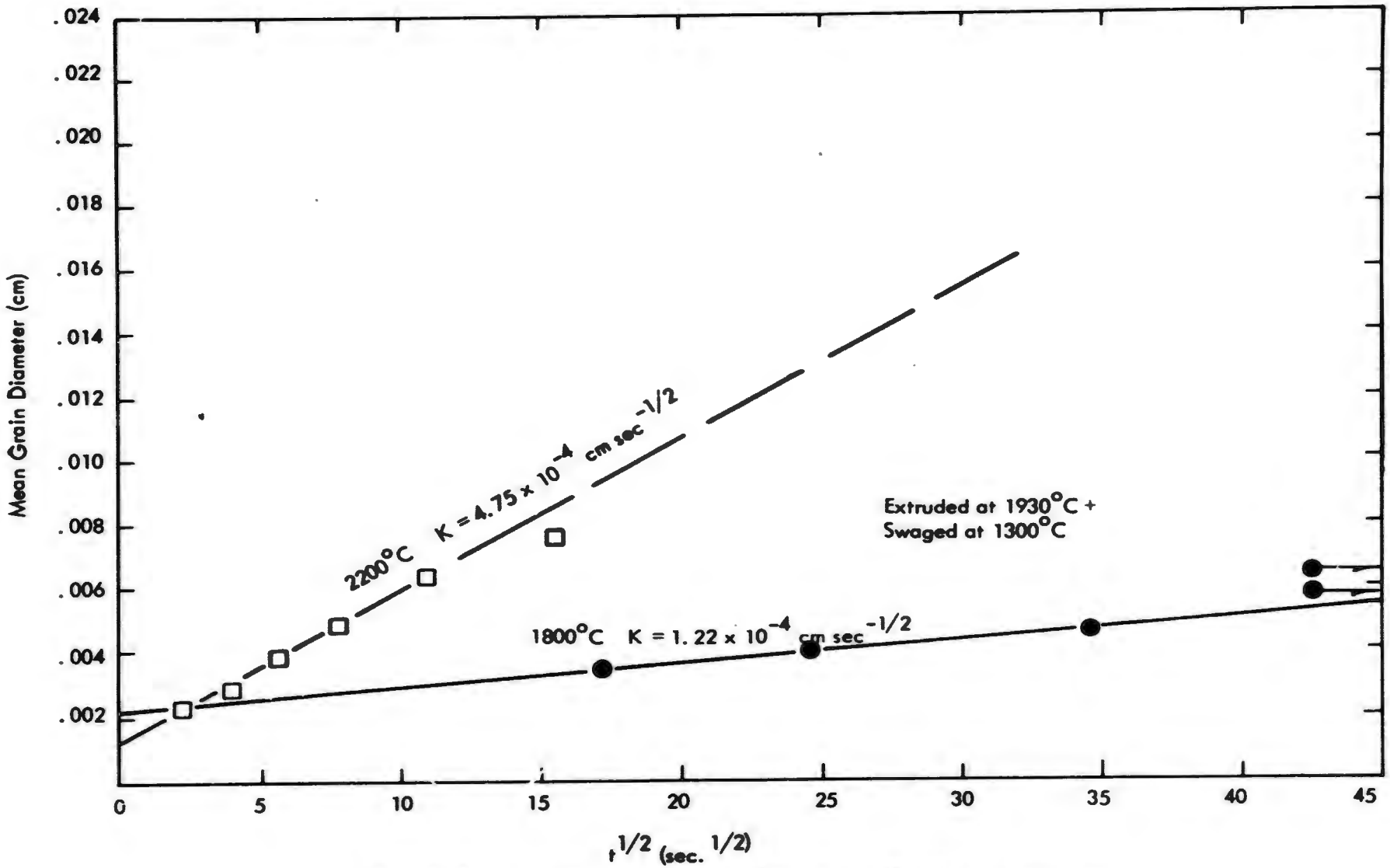

FIGURE 26 - Variation of Mean Grain Diameter of XB-88 with Annealing Time at 1800°C and 2200°C

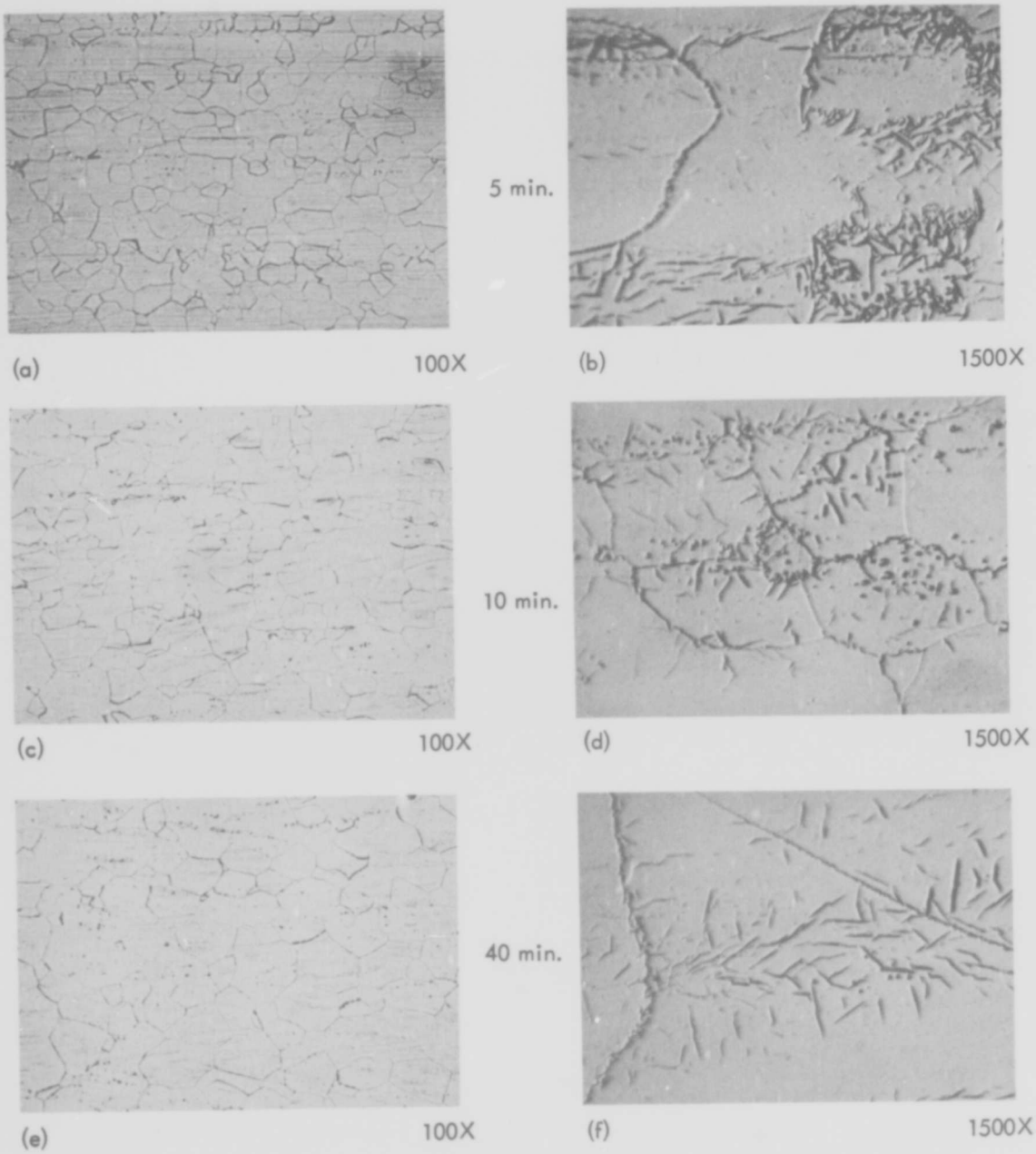

FIGURE 27 - Variation of Microstructure of Extruded Plus Swaged XB-88 as a Function of Annealing Time at 1800°C

240 second heat treatments are presented in Figure 28. The decorated sub-boundary networks shown in the high magnification photomicrographs resulting from the 15 second anneal at 2200°C are much less distinct after longer heat treatments. The few sub-cells remaining show an increase of size from approximately 1μ in the 15 second annealed material to about 7μ in the 240 second annealed material.

The data shown in Figure 26 are sufficient to calculate activation energy for grain growth and a rough approximation of the driving energy for grain growth, i.e., surface free energy. Christian[2] developed a grain growth theory from irreversible thermodynamic considerations. The velocity of an interface due to small driving forces may be represented by:

$$\frac{d\bar{D}_B}{dt} = \delta^B (\nu/k)(\gamma v A_v/T) \exp(-\Delta G^*/kT) \quad \ldots\ldots\ldots \quad (1)$$

where:

$\bar{D}_B$ = mean grain diameter

t = time, sec.

δ^B = jump distance across a grain boundary, 3×10^{-8} cm

ν = lattice vibration frequency $\simeq kT/h$

k = Boltzmann's constant

h = Planck's constant

T = temperature, °K

A_v = area of grain boundary interface per unit volume $= 3.35/D_B$

v = atomic volume, $\simeq 9.4 \times 10^{-24}$ cms

γ = grain boundary energy

ΔG^* = activation energy for grain growth

Integrating equation 1 from $D_B = D_o$ at $t = 0$, gives:

$$(\bar{D}_B)^2 - (\bar{D}_o)^2 = [3.35\gamma v \delta \nu/kT) \exp(-\Delta G^*/kT)]\, t \quad \ldots\ldots\ldots \quad (2)$$

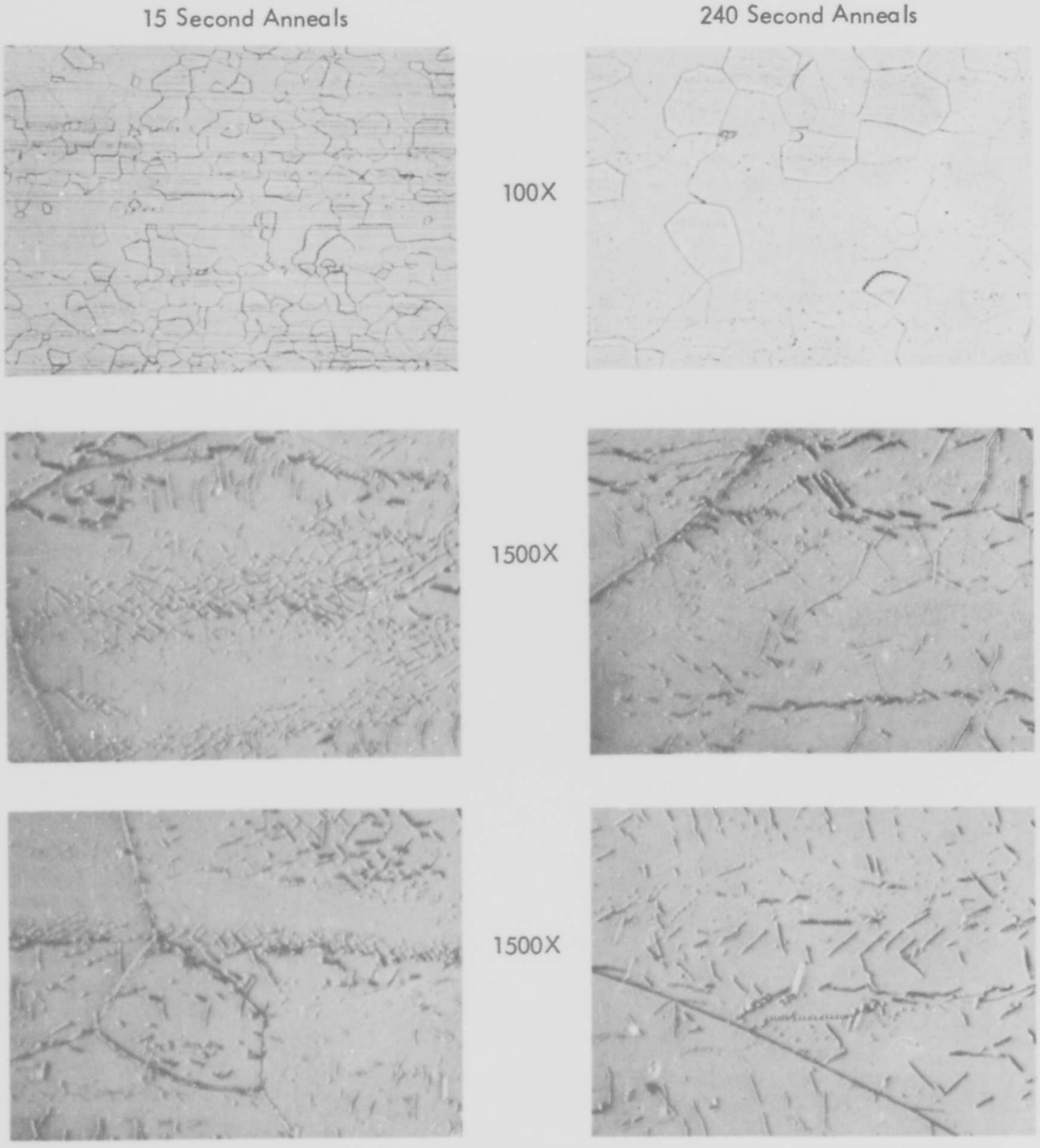

FIGURE 28 - Variation of Microstructure of Extruded Plus Swaged (92% R. A.) XB-88 with Annealing Time at 2200°C

It can be qualitatively shown that the positive intercepts of the extrapolations of the 1800°C and 2200°C $\bar{D}$ vs $t^{1/2}$ plots are due to recrystallization and grain growth during heating and cooling from test temperature. Therefore, D_o can be considered negligible in comparison to D_B. Equation 2 reduces to:

$$\bar{D}_B = K t^{1/2} \qquad \ldots\ldots\ldots \quad (3)$$

where $K = (3.35\gamma v \delta \nu t/k)^{1/2} \exp(-\Delta G^*/kT)^{1/2}$ $\ldots\ldots\ldots \quad (4)$

and is the slope of the D_B vs $t^{1/2}$ curves in Figure 26. The activation energy is now obtainable from equations 3 and 4 by plotting in K vs $\frac{1}{T}$ as shown in Figure 29 and setting the slope equal to $\frac{\Delta G^*}{2R}$. The activation energy was found to be 68,000 cal/mol. By assuming a vibration frequency of $\frac{kT}{h} = 5 \times 10^{13}$ sec^{-1} a value of 2600 ergs/cm^2 was obtained for the surface or driving energy. The activation energy obtained above appears in reasonable agreement with what would be expected for the activation energy for grain boundary diffusion. The best that can be said for the surface energy is that the number is reasonable and is within an order of magnitude of what one would expect. The assumption of jump distance, area of grain boundary per unit volume (tetrakaidecahedra grain shapes were assumed), and lattice vibration frequency which is known to an order of magnitude at best, precludes an accurate calculation of γ.

The model for grain growth developed above should be useful in predicting grain growth behavior. At or below the solubility limit for carbon the model breaks down because the carbide precipitation impedes grain boundary motion.

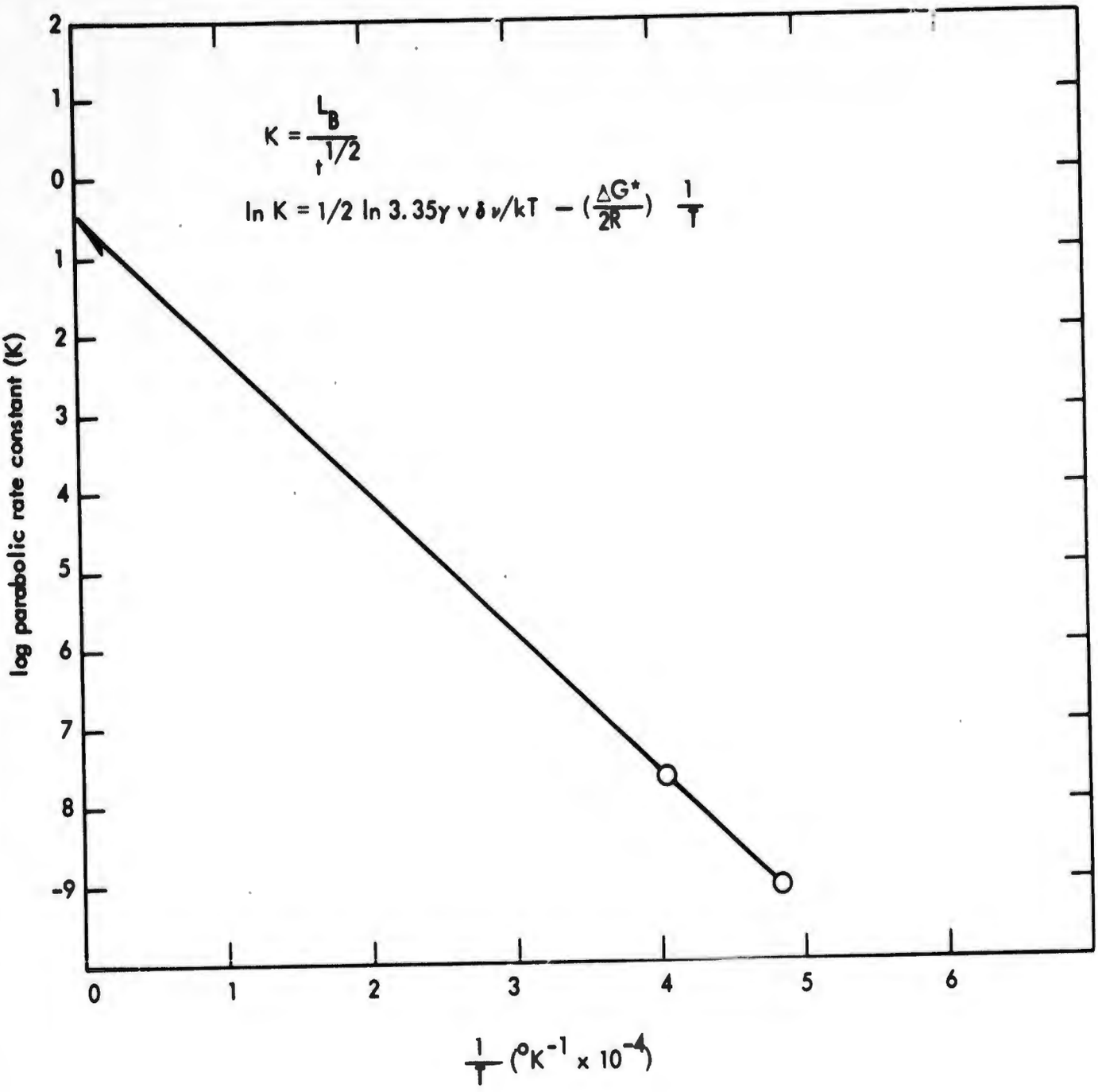

FIGURE 29 - Arrhenius Plot of Log Parabolic Rate Constant for Grain Growth vs. Reciprocal Temperature

IV. PHASE RELATIONSHIPS

Considerable effort was devoted to carbide phase relationship studies during the earlier phase of this program[1] in an attempt to obtain a better understanding of the relationship between precipitate identity, morphology, and mechanical properties. At that time the explanation and identification of complex phases from alloys annealed at higher temperature (>1700°C) and a more precise location of the phase diagram boundaries with respect to the alloy compositions under consideration were the major areas warranting further study.

Most of the continuing phase relationships effort has been on XB-88 (Cb-28W-2Hf-0.067C). However, alloys VAM-78 (Cb-22W-2Hf-0.13C), VAM-81 (Cb-22W-2Hf-0.167C), VAM-85 (Cb-22W-1Hf-0.067C) and VAM-87 (Cb-22W-1Zr-0.13C) were investigated to a limited extent to supplement the work done on the XB-88 composition.

Phase Identification

Two "complex" phases then designated "X-1" and "X-2", were observed in the Cb-W-Hf-C alloys during the previous phase relationships study[1]. The X-1 complex x-ray diffraction pattern was obtained from the lower carbon alloys annealed generally above 1700°C. This phase occurred most frequently in the 0.067 w/o C alloys VAM-80, now XB-88, VAM-85, and VAM-79. The X-1 complex was observed in alloys containing 0.13 w/o C and was sometimes associated with the hexagonal $(Cb,Hf,W)_2C$ phase and the X-2 phase. The X-2 phase appeared somewhat related in occurrence to the X-1 phase but always appeared in the higher carbon alloys (0.13 w/o and 0.167 w/o C).

Since alloy VAM-80 (Cb-28W-2Hf-0.067C) was selected for scale-up and the X-1 phase was always observed in this alloy, most of the study of these anomalous phases has been concerned with explaining the existence of the X-1 phase.

The "d" spacings and relative intensities obtained from the residue extracted from XB-88(extruded and swaged followed by annealing 1 hour at 1800°C and helium quenched) are given in column 2 of Table 5. This pattern is typical of a mixture of the X-1 phase and a fcc cubic phase observed after short anneals at high temperatures. This pattern is very similar to the x-ray data reported by Chang[3] on Cb-1 (Cb-30W-1Zr-0.06C-0.01O-0.04N) annealed 1 hour at 1930°C. This pattern is given in column 4, Table 5. Chang interpreted this phase to be the hexagonal phase. A comparison of Chang's phase to the hexagonal M_2C phase at the 0%Zr and 5%Zr limits of solid solution reported by Cornie et al[4] and repeated in column 7, Table 5 shows no similarity. Faunce and Peacock[5] have observed an almost identical pattern for extraction residues of the Cb-132M alloy in the recrystallized condition.

A remarkable similarity was noted between the x-ray patterns of the X-1 phase reported above and the zeta phase observed by Brizes and Tobin[6] in the Ta-C system. Their "d" spacings and intensities are repeated in column 3, Table 5. Brizes and Tobin grew a discrete layer of zeta between the hexagonal Ta_2C and the fcc TaC_{1-x} phase fields during a diffusion experiment. The zeta phase would appear to be an equilibrium phase. However, the literature on refractory metals shows numerous claims and counter claims as to the stability of the zeta phase. Zaplatynsky[7] also observed the zeta phase in the TaC system, occurring as Widmanstatten precipitates in Ta_2C and TaC_{1-x}. He also observed a shift in some x-ray diffraction lines and intensities after the specimen was comminuted as shown in columns 5 and 6 of Table 5. Zaplatynsky considered zeta in the Ta-C system to be a metastable phase formed on cooling, possibly due to a shear type transformation resulting from cooling stresses.

From the above discussion of the data in Table 5 it was concluded that the X-1 phase is isostructural with the zeta phase in the Ta-C system and hereafter will be designated as zeta. At present the structure of the refractory metal-carbon zeta phase has not been determined. The above identification of the zeta phase is supported by Nowotny and his co-workers[8] who have observed the zeta phase in the V-C and Cb-C systems isostructural with the zeta phase in the Ta-C system, giving essentially the same x-ray pattern reported here.

TABLE 5 - X-Ray Diffraction Data

1		2		3		4		5		6		7			
Extraction from VAM-81 (Cb-22W-2W-.167C) X-2 Phase		Extraction from XB-88 (Cb-20W-2W-.067C) (Zeta Phase) Swaged Plus Heat Treated 1 Hr at 1800°C		Reference 6 Zeta Phase, Ta-C System Microdrilled		Reference 5 Extraction from Cb-1 (Cb-30W-.83Zr-.06C-.010-.04N) 1 hour at 3500°C		Reference 7 Zeta Plus TaC_{1-x} in Situ		Reference 7 Zeta Plus TaC_{1-x} Comminuted Sample		Reference 4 Hexagonal M_2C Cb-6.05C	Cb4.9Zr-5.5C		
d	I	d	I	d	I	d	I	d	I	d	I	d	d	I	Hkl
						3.15	VW(111)ZrO_2								
						2.95	VW(111)ZrO_2FCC)								
						2.84	VW(111)ZrO_2								
				2.82	VW										
2.70	VW	2.68	M			2.69	MS	2.698	VW	2.690	VW				
								2.663	W						
				2.66	M					2.652	VW	2.646	2.696	M	10.0
2.58	S	2.57	M FCC(111)					2.556	S TaC (111)	2.546	VS TaC(111)				
								2.549	MS			2.473	2.479	M	00.2
2.48	M	2.48	S	2.48	S										
						2.47	S	2.468	VS	2.468	W				
		2.42	M	2.43	MS							2.336	2.372	VS	10.1
2.37	MS	2.37	VVW												
2.27	M	2.30	MS	2.28	S	2.30	S	2.292	W	2.281	W				
2.23	M	2.22	M FCC(200)					2.211	W TaC (200)	2.206	MS TaC(200)				
				2.02	VW							1.805	1.826	S	10.2
1.83	VW			1.88	VW										
						1.82	VW								
						1.72	VW								
				1.68	VW			1.684	VW						
										1.675	W				
1.58	MW	1.57	W FCC(220)												
1.56	M	1.555	M	1.56	M	1.56	S	1.563	VW TaC (220)	1.561	MS TaC(220)	1.549	1.561	S	11.0
				1.47	VW					1.482	VW				
1.410	VVW											1.401	1.432	S	10.3
														VW	20.0
1.350	M	1.365	VW	1.37	W	1.37	VW	1.368	VW	1.368	VW				
		1.340	W FCC(311)					1.331	VW TaC (311)	1.331	S TaC(311)				
1.320	M	1.320	MW	1.32	M	1.32	S	1.319	W			1.315	1.322	S	11.2
										1.300	VW				
								1.291	W						
1.290	VVW	1.290	W FCC(222)	1.29	W	1.290	W			1.288	VW	1.293	1.303	M	20.1
								1.276	VW TaC (222)	1.275	MS TaC(222)				
								1.266	VW	1.266	W				
1.250	VVW	1.245	VW	1.25	VVW			1.255	VW	1.254	VW				
						1.238	VW					1.233	1.241	M	00.4
1.120	VW							1.221	VW						
												1.101	1.108	M	20.2
										1.104	W TaC(400)	1.122	1.132	M	10.4
												1.041	1.048	S	20.3
1.028	W	1.025	VVW					1.027	VW			1.018	1.024	W	21.0
										1.014	MS TaC(331)				
1.002	VW	1.002	VVW			1.000	M	1.008	W						
												.9992	1.003	S	21.1
0.992	VVW	0.995	VVW	0.992	VW					0.989	MS TaC(420)				
0.975	VW			0.975	W			0.973	VW	0.978	W				
		0.970	VVW			0.969	M					.9689	.9745	S	11.4
								0.936	W			.9414	.9438	W	21.2
								0.924	W						
												.9294	.9344	S	10.5
0.915	VW							0.913	VW	0.911	VW				
												.9125	.9161	VW	20.4
								0.902	VW TaC(422)	0.903	MS TaC(422)				
						0.899	W					.9024	.8985	VW	30.0
								0.886	MS						
0.862	W														
						0.859	VW	0.859	S			.8641	.8716	S	21.3
								0.850	M TaC(333)	0.851	MS TaC(333)				
						0.844	W								
												.8409	.8482	M	30.2
												.8272	.8307	M	00.6
0.792	VVW											.7996	.8029	M	20.5
												.7917	.7965	M	10.6
												.7896	--	M	21.4
												.7835	--	M	22.0

Occurrence of the Zeta Phase in Cb-W-Hf-C Alloys

The identification of zeta in the metal-rich region of the Cb-W-Hf-C system is certainly an exception to existing phase diagrams. Zeta appears in several refractory metal-carbon binaries but was not observed in the Cb-Hf-C system[9,10], the Cb-W-C system[11], or the Ta-W-C system[12]. If zeta is a stable equilibrium phase in the carbon dilute alloys the phase diagrams must be reinterpreted as shown in Figure 30. The question of temperature and compositional range of zeta occurrence and the possible influence of cooling rates must be evaluated before postulating its stability or refuting the existing phase diagrams.

X-ray data obtained on extraction residues of XB-88 heated for a number of times and temperatures are shown in Table 6. The residue from as-swaged (at 1300°C) material (column 1, Table 6) gave a diffraction pattern of a fcc NaCl type carbide of $a_o = 4.55$. When this material was induction heated for 15 seconds, 240 seconds, and 30 minutes at 2200°C and helium quenched to room temperature (columns 2, 3, and 4) a zeta phase plus a fcc NaCl type phase of $a_o = 4.45$ Å were formed. The intensity of the cubic carbide phase decreased as annealing time increased. This was also noticed when comparing the 1 hour at 2000°C (column 6, Table 6), the 2 hour at 2000°C (column 5, Table 6), and 2 hours at 2000°C plus 1 hour at 1800°C (column 7, Table 6) heat treatments in which the cubic phase disappeared completely leaving only zeta in the extraction residue in the longer time 2000°C heat treatments. The variation of bulk extraction residue composition with heat treatment was studied by x-ray fluorescence analysis. The results are given in Table 7. The hafnium content of the extracted phases decreased with annealing time at 2200°C and therefore decreased with the disappearance of the cubic phase. The most likely explanation of this observation would be that the cubic phase is stabilized by local inhomogeneities of hafnium. The leveling of the Hf in the alloy requires a certain amount of diffusion time. Thus the more microsegregation of the hafnium in the original alloy, the more likely the formation of the cubic carbide either at temperature or upon cooling. The local hafnium inhomogeneities probably are residual from coring in the ingot.

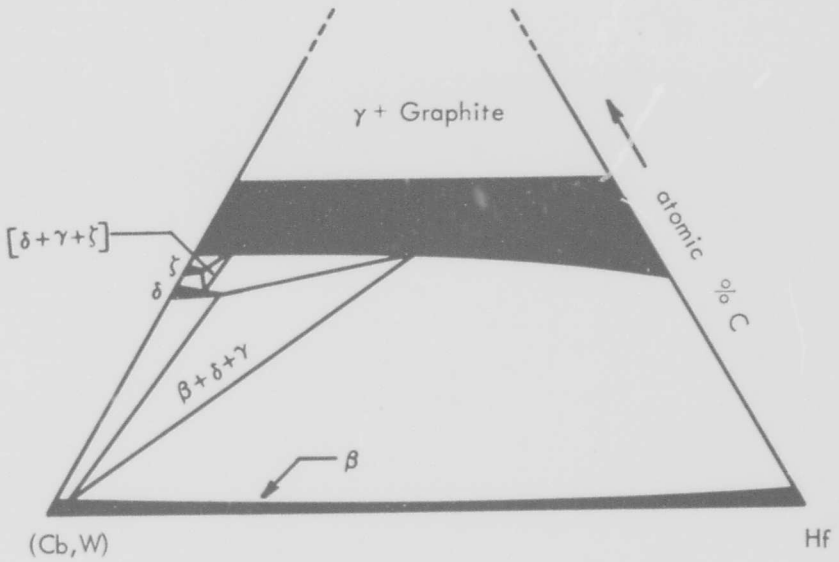

(a) Phase diagram of the (Cb,W)-Hf-C system based on the metastable existence of zeta in carbon dilute alloys.

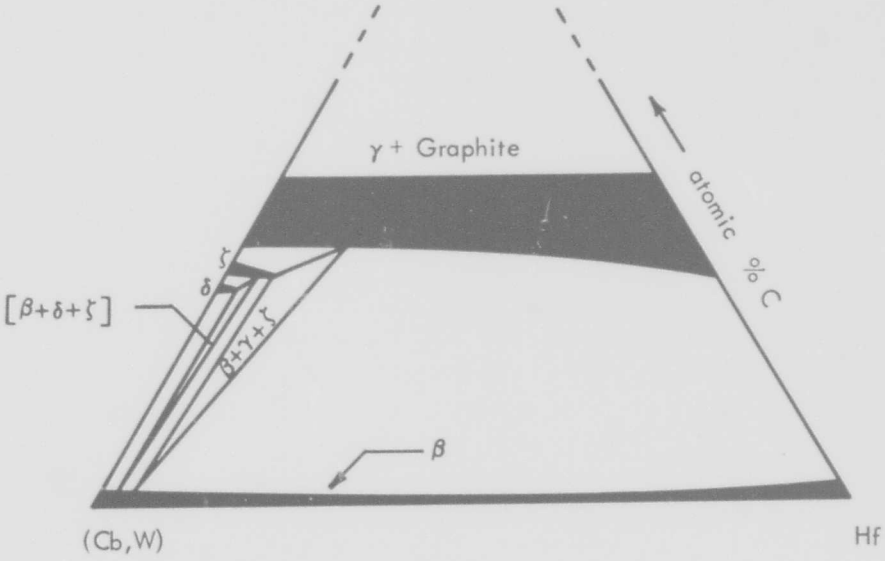

β = bcc matrix
δ = hcp M_2C
γ = fcc MC_{1-x}
ζ = zeta

(b) Required reinterpretation of (Cb,W)-Hf-C phase diagram if zeta is an equilibrium phase in carbon dilute alloys.

FIGURE 30 - Possible Interpretations of the (Cb,W)-Hf-C Phase Diagram as a Result of Observations of the Zeta Phase in Carbon Dilute Alloys

TABLE 6 - X-Ray Diffraction Data XB-88

1 As-Swaged at 1300°C		2 15 Seconds at 2200°C		3 240 Seconds at 2200°C		4 30 Minutes at 2200°C		5 2 Hours at 2000°C		6 1 Hour at 2000°C		7 2 Hrs. at 2000°C and 1 Hr. at 1800°C		8 1 Hour at 1800°C		9 1 Hour at 1750°C		10 1 Hour at 1700°C		11 1 Hour at 1650°C	
d	I	d	I	d	I	d	I	d	I	d	I	d	I	d	I	d	I	d	I	d	I
																3.15	VW HfO_2	3.15	VW HfO_2	3.15	VW HfO_2
																		2.82	VW HfO_2	2.82	VW HfO_2
		2.68	W (Z)**	2.68	W (Z)	2.68	W (Z)	2.67	MW (Z)	2.68	M (Z)	2.65	W (Z)	2.68	M (Z)	2.68	VVW (Z)				
2.62	S(111)*															2.61	S(111)*	2.62	VS(111)*	2.63	VS(111)*
		2.58	M(111)*	2.56	W(111)*	2.57	VW(111)*			2.56	VW(111)*	2.55	VW(111)*	2.57	M(111)*						
		2.47	S (Z)	2.47	S (Z)	2.47	S (Z)	2.47	S (Z)	2.48	S (Z)	2.48	MS (Z)	2.48	S (Z)					2.52	VVW HfO_2
		2.45	MW (Z)	2.43	M (Z)	2.42	M (Z)	2.42	M (Z)	2.42	M (Z)	2.42	Broad (Z)	2.42	M (Z)	2.45	MW (Z)	2.45	MW (Z)		
		2.38	VW (Z)											2.37	VVW (Z)						
2.46	M(200)*	2.30	S (Z)	2.29	S (Z)	2.30	S (Z)	2.30	S (Z)	2.30	MS (Z)	2.28	M (Z)	2.30	MS (Z)	2.30	W (Z)	2.30	W (Z)		
		2.23	M(200)*	2.23	W(200)*	2.23	VVW(200)*			2.22	VW(200)*			2.22	M(200)*	2.25		2.27	S(200)*	2.27	S(200)*
		1.83	VVW (Z)																		
		1.73	VVW (Z)	1.72	VW (Z)	1.72	VVVW(Z)														
1.60	M(220)*															1.595	MS(220)*	1.595	MS(220)*	1.60	MS(220)*
		1.575	M(220)*	1.57	VVW(220)*	1.57	VVVW(220)*			1.57	VVW(220)*			1.57	W(220)*	1.570	W (Z)				
		1.56	M (Z)	1.555	MS (Z)	1.555	MS (Z)	1.555	MS (Z)	1.555	MS (Z)	1.555	M (Z)	1.555	M (Z)	1.55	W (Z)	1.555	W (Z)		
						1.47	VW (Z)														
1.37	M(311)*									1.37	VVVW(Z)	1.365	VVW(Z)	1.365	VW (Z)	1.362	M(311)*	1.362	MS(311)*	1.367	MS(311)*
		1.365	VVW(Z)	1.365	VVW (Z)	1.365	VW (Z)	1.365	VW (Z)												
		1.340	W(331)*	1.34	VW(331)*	1.34	VW(331)*							1.340	W(311)*	1.34	VW (Z)				
1.315	W(220)*	1.32	MW (Z)	1.315	MS (Z)	1.315	MS (Z)	1.315	M (Z)	1.32	M (Z)	1.315	MW (Z)	1.32	MW (Z)	1.32	W (Z)	1.32	VW (Z)		
																1.305	W(222)*	1.305	MW(222)*	1.31	MW(222)*
		1.29	W(222)*	1.29	W(222)*	1.29	MW(222)*	1.285	VW(222)*	1.29	W (Z)	1.290	VVW(Z)	1.29	W(222)*						
		1.245	VW (Z)	1.24	W (Z)	1.24	VW (Z)	1.24	VVW (Z)	1.245	VW(Z)	1.240	VVW(Z)	1.245	VW (Z)	1.240	VVW(Z)				
1.40	VW(400)*																				
																1.130	W(400)*	1.132	W(400)*	1.35	W(400)*
1.042	W(331)*																			1.040	M(331)*
																1.036	MW(331)*	1.038	MW(331)*		
														1.025	VVW(Z)						
1.015	W(420)*	1.025	W(331)*																		
		1.00	W (Z)			1.005	W (Z)	1.00	VVW (Z)	1.005	VVW(Z)			1.002	VVW(Z)	1.010	M(420)*	1.010	MW(420)*	1.015	M(420)*
		0.995	W(420)*			0.992	W (Z)	0.990	VW(420)*	0.995	VVW(Z)			0.995	VVW(Z)	0.995	VW(Z)				
		0.973	W (Z)																		
						0.970	W (Z)	0.968	VW (Z)	0.970	VVW(Z)			0.970	VVW(Z)	0.970	VW(Z)				
0.928	VW(422)*																				
																0.922	W(422)*	0.924	M(422)*	0.925	M(422)*
		0.910	W(422)*			0.910	VW(422)*	0.910	VVW(422)*	0.910	VVW(Z)										
		0.900	W (Z)			0.848	VW (Z)	0.895	VVW (Z)	0.900	VVW(Z)										
																0.870	MW $^{(511)}_{(333)}$	0.870	M $^{(511)}_{(333)}$	0.872	W $^{(511)}_{(333)}$
		0.867	W (Z)			0.865	VW (Z)			0.865	VVW(Z)										
		0.857	W(333)*			0.858	VW(333)*														
						0.844	VW (Z)														
																		0.800	W(440)		
*FCC MC $_{o}$ =4.55 $_{1-x}$		*FCC a_o =4.45 **Z = Zero phase		*FCC a_o =4.45		*FCC a_o =4.45		*FCC a_o =4.45		*FCC a_o =4.43		*FCC		*FCC a_o =4.45		*FCC a_o =4.52		*FCC a_o =4.51		*FCC a_o =4.53	

TABLE 7 - Composition of Extracted Phases

Alloy	Heat Treatment	Phases Present in Extraction Residue	Bulk Extraction Composition w/o		
			W	Hf	C
XB-88	2 Hrs. at 2000°C+ 1 Hr. at 1400°C+H. Q.	$\gamma(S)^{*}, a_o = 4.52$	<1	60	---
XB-88	15 Secs. at 2200°C	Zeta(S)+γ(M) $a_o = 4.46$	30	10	---
XB-88	60 Secs. at 2200°C	Zeta(S)+γ(W) $a_o = 4.45$	30	<10	---
XB-88	240 Secs. at 2200°C	Zeta(S)+γ(W) $a_o = 4.45$	~37	<10	---
XB-88	30 Min at 2200°C	Zeta(S)+γ(VVW) $a_o = 4.45$	40	~5	6.8
XB-88	87 Hrs. at 2000°C	Zeta(slightly lower "d" spacings than in shorter time anneals)	45	7	---
VAM-81	87 Hrs. at 2000°C	X-2 phase+HCP(VW)+ Zeta(VVW)	13	22	---

* S - Strong
M - Moderate
W - Weak
VW - Very Weak

It was postulated that zeta might be stabilized by tungsten, i. e., have its origin within the Cb-W-Hf-C quaternary system. In order to test this hypothesis an alloy consisting of Cb-2Hf-0.067C was prepared as the tungsten free analog of XB-88. The alloy was heated 1 hour at 2000°C and helium quenched to room temperature. The resulting x-ray diffraction pattern of the extraction residue is compared to zeta in XB-88 below. The pattern was identified as the zeta phase with slightly higher "d" spacings. Thus, zeta is not stabilized by tungsten since it can form in the tungsten free analog.

Cb-2Hf-0.067C Extracted Phase		Cb-28W-2Hf-0.067C Zeta Phase	
"d"	I	"d"	I
2.70	S		
		2.67	MW
2.49	S	2.47	S
2.42	MW	2.42	M
2.33	S(broad)	2.30	S
1.565	M	1.555	MS
1.350	W	1.365	VW
1.295	W	1.315	M
		1.285	VW
1.245	W	1.240	VW

Brine quenching experiments were conducted on a number of Cb-W-Hf-C alloys. Alloys XB-88, VAM-78, and VAM-81 (0.067 w/o, 0.13 w/o, and 0.167 w/o C levels respectively) were brine quenched from 1500°C to 2100°C. The specimens were quenched to room temperature in approximately 4 to 6 seconds. The resultant x-ray diffraction data from extraction residues are given in Table 8. The zeta phase did not appear to the same extent that it did after the slower cooled vacuum heat treatments. If zeta occurred at all it was as a much weaker phase than in the conventionally cooled heat treatments. It is thus apparent that zeta does indeed form upon cooling after the conventional anneals and does

TABLE 8 – Summary of Phase Identification Data

Alloy	Annealed at 2000°C + H.Q.*				Annealed at 2000°C + Age at T + Brine Quench							1 Hr at 2200°C	1 Hr at 2300°C	2 Hrs at 2000°C + 1 Hr at T + H.Q.					As-Swaged at 1300°C
	87 Hrs	24 Hrs	6 Hrs	2 Hrs	1 Hr at 1600°C	1 Hr at 1650°C	1 Hr at 1700°C	1 Hr at 1750°C	1 Hr at 1800°C	1 Hr at 1900°C	2/2000°C Brine Quench			1200°C	1400°C	1600°C	1700°C	1800°C	
VAM 85 (Cb-22W-1Hf-0.06TC)				Zeta								Zeta	Zeta		HCP				
VAM 79 (Cb-22W-2Hf-0.06TC)		Zeta	Zeta	FCC											FCC	Zeta (W) FCC (S)		Zeta	
XB-88 (Cb-28W-2Hf-0.06TC)	Zeta		Zeta	Zeta	FCC	FCC	Unidentified Phases	Unidentified Phases	Zeta			Zeta (S) FCC (W)	Zeta (S) FCC (W)	FCC (S)	FCC (S)	FCC (S)	FCC (S) Zeta (VW)	Zeta	FCC
VAM 87 (Cb-22W-1Zr-0.13C)				FCC (M) Zeta (S) HCP (M)								Zeta (S) FCC (W) HCP (S)	Zeta (S) HCP (S)						
VAM 78 (Cb-22W-2Hf-0.13C)		Zeta	HCP (M) FCC (W) X-2 (S)	HCP (M) FCC (S)			FCC (S) X-2 (M)		FCC (S) HCP (VVW)	FCC (S) Zeta(W)					HCP (S) FCC (?) X-2 (S)	HCP (M) FCC (?) X-2 (S)		FCC(S) X-2 (S)	HCP (M) FCC (S)
VAM 81 (Cb-22W-2Hf-0.16TC)	Zeta (W) X-2 (S) HCP (M)	HCP (M) FCC (M) X-2 (?)	HCP (W) FCC (?) X-2 (S)	HCP (M) FCC (M) X-2 (M)					FCC (S) Zeta(VVW)		FCC (S) Zeta (VVW)								

*All alloys reported were initially swaged at 1900°C to 1300°C

not exist in equilibrium in the carbon dilute regions of the Cb-W-Hf-C quaternary system. Zeta and other metastable phases probably form near but below the solvus temperature. Its formation is probably controlled by carbon diffusion.

Morphology of the Zeta Phase

The zeta phase, in the form of extracted and redispersed residue from an alloy heated 2 hours at 2000°C plus 1 hour at 1800°C, was studied by transmission electron microscopy and selected area electron diffraction analysis of extracted residues. Its crystallographic structure, which has not been successfully determined by x-ray diffraction analyses, could not be determined by electron diffraction, although electron diffraction patterns were obtained on individual platelets of the zeta phase. Several typical zeta platelets and selected area diffraction patterns are shown in Figure 31. An internal structure within the platelets is very apparent, especially at a magnification of 50,000X. This internal structure is invariably in the form of mutually perpendicular sets of striations, indicative of the cubic or tetragonal systems. The diffraction patterns prove the platelets to be heavily faulted, again in mutually perpendicular directions, as indicated by the streaking. Thus, the striations are apparently either stacking faults or microtwins.

Phase Equilibria Studies

The x-ray diffraction data obtained during the present and past years phase of this program are summarized in Table 8. These data include x-ray diffraction of extractions obtained from brine quenching experiments, recrystallization and grain size experiments, aging studies, and long time creep rupture tests.

Figure 32 shows the 1800°C isotherm of the Cb-Hf-C system as determined by Stecher et al[9]. The variation of lattice parameter of the γ [fcc $(Cb\text{-}Hf)C_{1-x}$] phase with Hf content is given in Figure 33. By comparing lattice parameters obtained during this study to Figure 33, the variation of composition of the γ corner of the three phase equili-

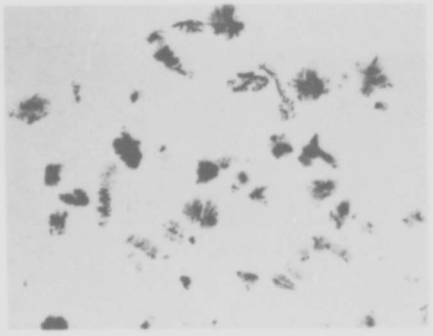

(a) 3200X

(b) 8000X

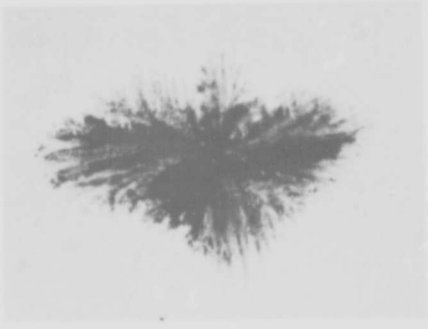

(c) 20,000X

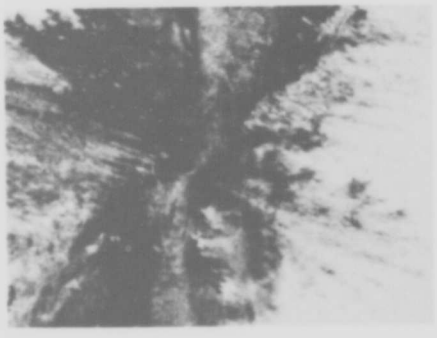

(d) 50,000X

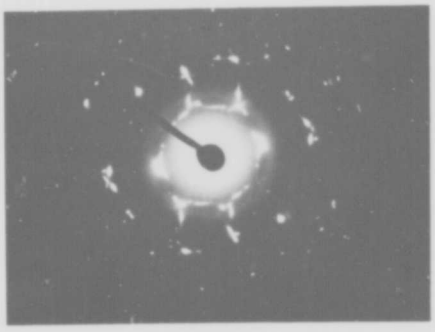

(e) SAED

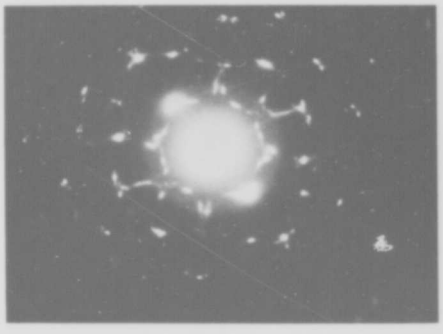

(f) SAED

FIGURE 31 - Electron Micrographs and Selected Area Electron Diffraction Patterns of Extracted and Redispersed Zeta Phase (Specimen Heat Treatment: 2 Hours at 2000°C Plus 1 Hour at 1800°C)

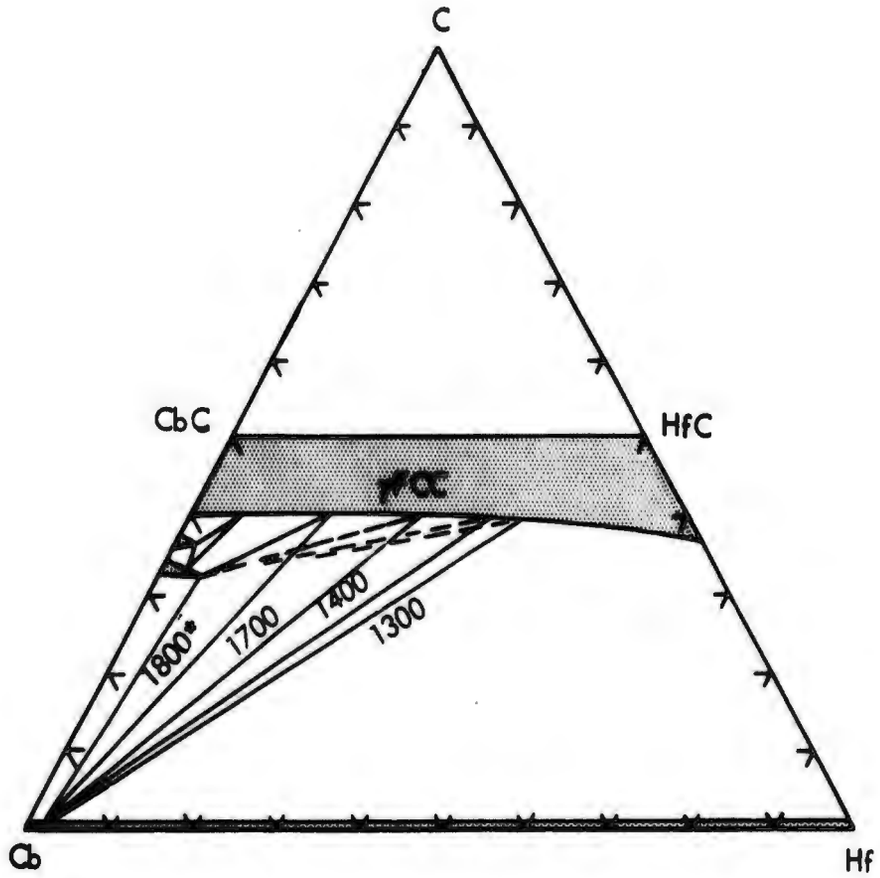

*From Stecher and Nowotny (Ref. 9)

FIGURE 32 - Variation of γ Rich Corner of (Cb,W)-Hf-C System with Temperature

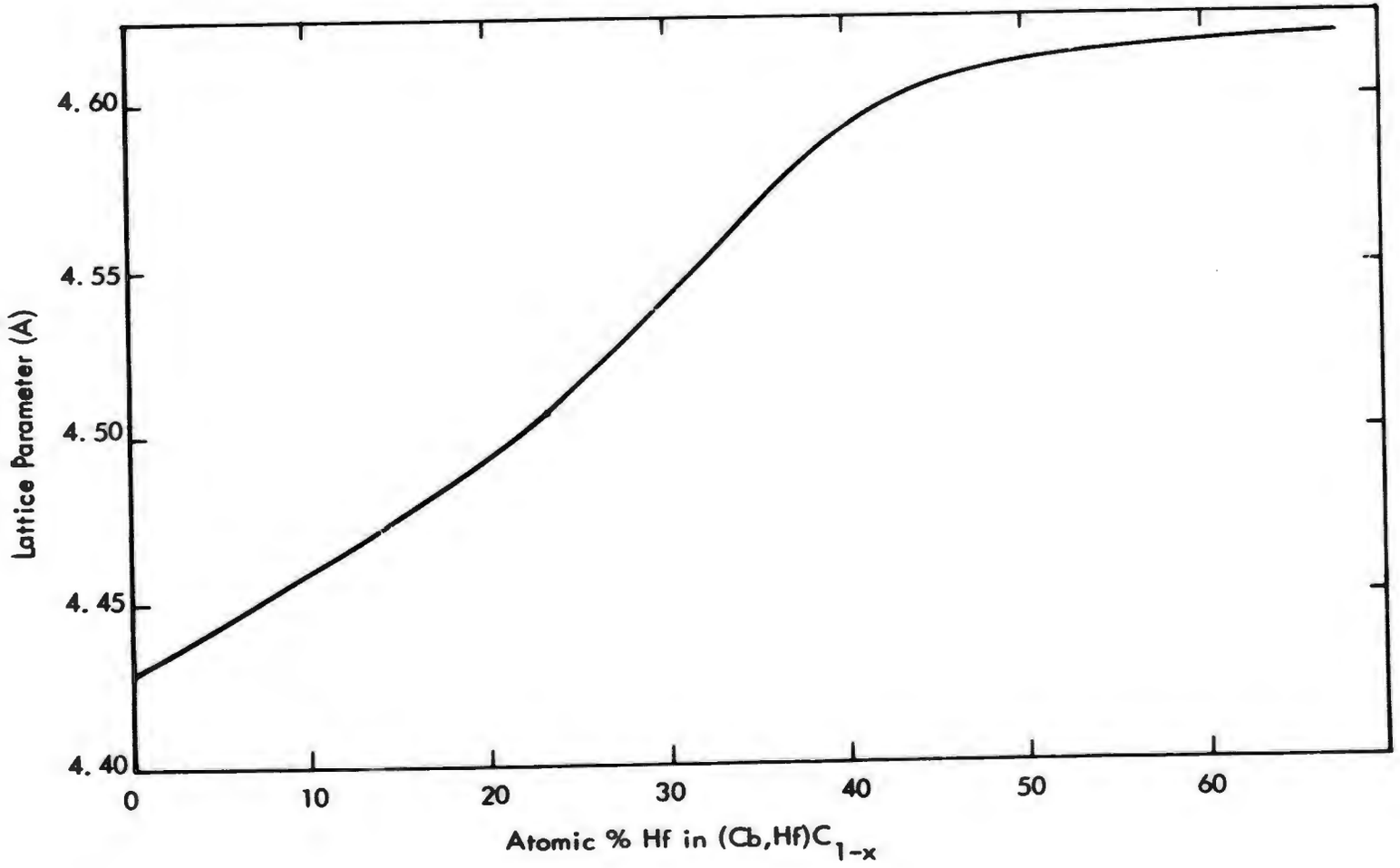

FIGURE 33 - Variation of Lattice Parameter of $(Cb,Hf)C_{1-x}$ as a Function of Hafnium Content (Ref. 9)

brium region with temperature could be approximated. We qualify this statement with the word "approximated" because:

1. Not all alloys studied contained the $\beta + \delta + \gamma$ phases. However none of the alloys were far enough away from the three phase region for this error to be significant.

2. The alloys investigated were taken from a variety of different studies, i. e. , grain size, heat treatment effects, grain growth, and creep rupture tests. In most cases these alloys were not homogenized sufficiently above the solvus temperature or aged long enough for complete equilibration.

The x-ray patterns obtained were generally broad and diffuse indicating some range of composition. The accuracy of lattice parameter measurement was $\pm$0. 005 Å. Figure 34 shows the variation of the composition of the γ corner of the $\beta + \delta + \gamma$ region with final annealing temperature. The scatter of data in Figure 34 indicates deviation from equilibrium in most of the alloys in this study. The function curve was drawn through the highest hafnium content data points because as explained previously, these alloys are only approaching equilibrium and those residues with the highest hafnium content for a given heat treatment (below the solvus temperature) will be the most nearly equilibrated.

The data obtained from Figure 34 are superimposed on the 1800°C isotherm of the Cb-Hf-C phase diagram determined by Stecher et al[9] in Figure 32. The variation of the composition of the γ rich corner of the three phase region may be significant when discussing reactions taking place during a long time creep test, especially when the substructure is stabilized by carbides that have an initial composition controlled by the final annealing treatment.

The alloy XB-88 displays a discontinuity in property trends at 1700°C. Approximately 1700°C is the temperature beyond which complete equiaxed recrystallization takes

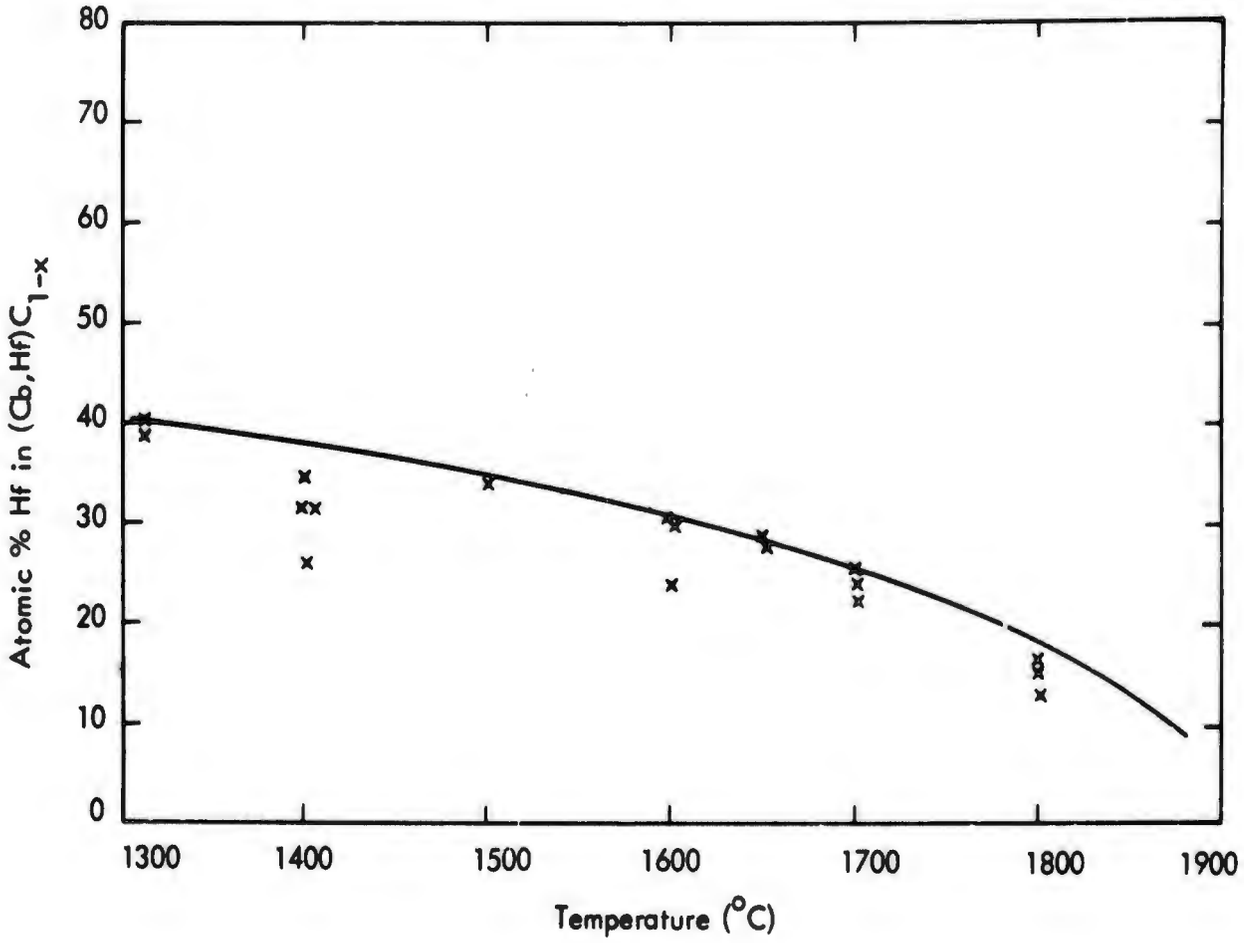

FIGURE 34 - Variation of Composition of $(Cb,Hf)C_{1-x}$ with Temperature as Determined by Lattice Parameter Measurements

place. Creep-rupture properties are degraded when the alloy is annealed below 1700°C. These anomalies suggest that the carbon solvus may be near 1700°C. A series of brine quenching experiments were designed to determine the carbon solvus in XB-88 and other similar alloys. Small pieces of XB-88 (Cb-28W-2Hf-0.067C), VAM-78 (Cb-22W-2Hf-0.13C) and VAM-81 (Cb-22W-2Hf-0.167C) were suspended in quartz capsules and evacuated. The alloys were annealed 2 hours at 2000°C and aged in an induction furnace for 1 hour at lower temperatures and brine quenched. The alloys were cooled from the aging temperature to room temperature in 4 to 6 seconds. The resulting microstructure from XB-88, VAM-78, and VAM-81 representing the 0.067, 0.13, and 0.167 carbon levels are shown in Figures 35, 36, and 37 respectively.

The metallography of the higher carbon brine quenched alloys (VAM-78 and VAM-81) is not as clear or definitive as the lower carbon XB-88. VAM-78 appears to be two phase at 1700°C and single phase above 1900°C (the platelets shown in Figure 36 were precipitated during quenching). The 1800°C quenched specimen appears to have had a grain boundary phase present at temperature but this cannot be definitely ascertained from metallography alone.

The highest carbon alloy studied, VAM-81, displayed metallographic structures more difficult to evaluate. Since this alloy was obtained from lower temperature Dynapak extruded material, the hafnium resulting from coring in the original ingot did not have sufficient annealing time for complete homogenization. This would be the explanation of the stringers of carbides shown in Figure 37 in both the 1800°C and 2000°C conditions. The massive phases have been identified as the fcc carbides. The matrix Widmanstatten platelets are probably the X-2 phase. The cubic carbides appear to be non-equilibrium in this case because of the hafnium inhomogeneity.

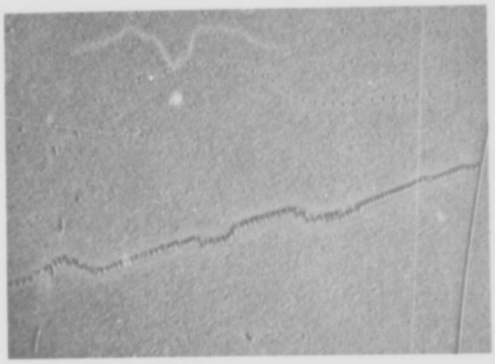

(a) 1750°C

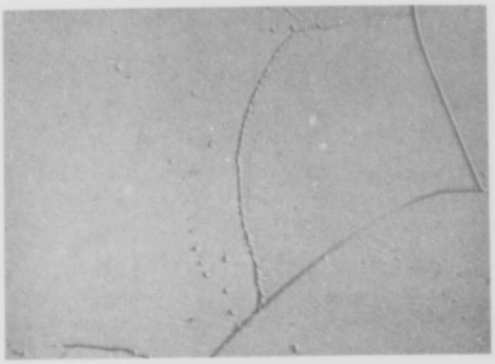

(b) 1700°C

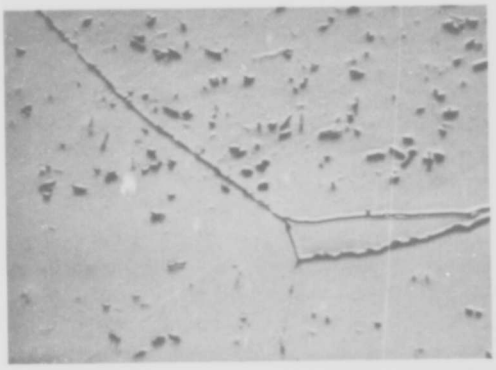

(c) 1650°C

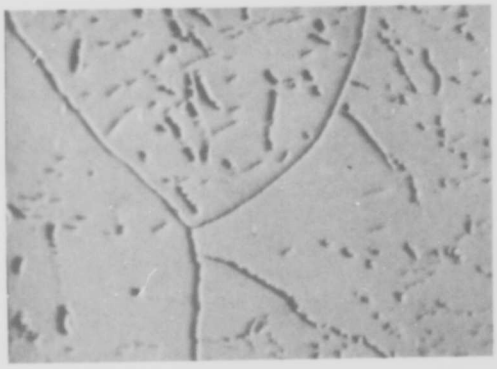

(d) 1600°C

(e) 1500°C

FIGURE 35 - Microstructures of XB-88 Annealed 2 Hrs. at 2000°C Plus 1 Hr. at Indicated Temperatures and Brine Quenched 1500X

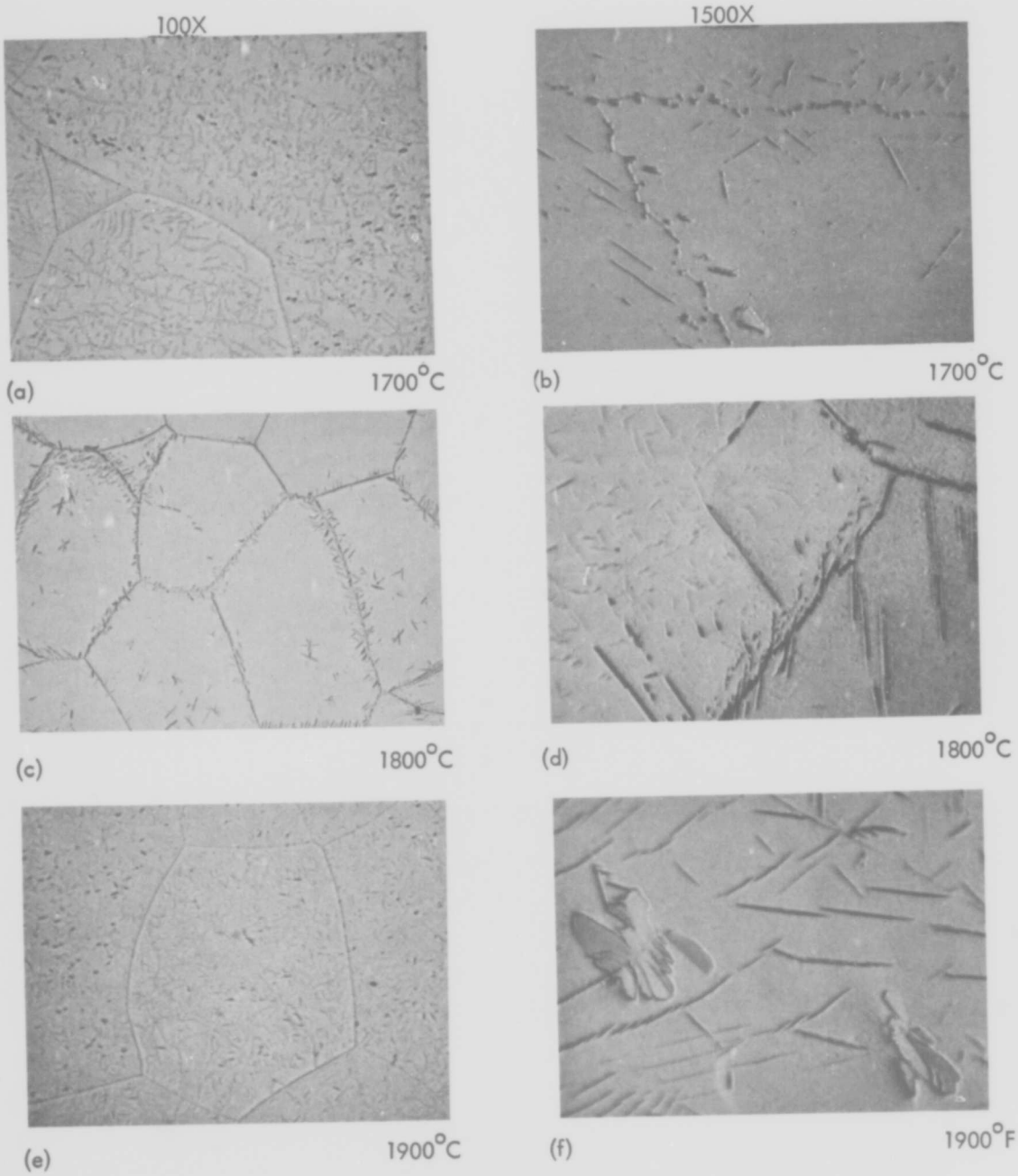

FIGURE 36 - Microstructures of VAM-78 (Cb-22W-2Hf-0.13C) Annealed 2 Hrs. at 2000°C Plus 1 Hr. at Indicated Temperature and Brine Quenched

100X

1500X

(a) Annealed 2 hrs. at 2000°C plus 1 hr. at 1800°C and Brine Quenched

(b) Annealed 2 hrs. at 2000°C and Brine Quenched

FIGURE 37 - Microstructures of VAM-81 (Cb-22W-2Hf-0.167C)

The x-ray phase identification data from the brine quenching studies are summarized in Table 8. From these data and the metallography the β solvus was determined as shown in Figure 38. The solvus temperature for XB-88 (0.067 w/oC level) was determined as accurately as the aging interval would permit (1675°C $\pm$25C°). However, there is much more uncertainty in the location of the solvus in the higher carbon alloys. This uncertainty is indicated in Figure 38.

A summary of the x-ray data determined during this program on Cb-W-Hf-C alloys is also given in Table 8. From these data and the approximate β solvus (Figure 38) the semi-quantitative representation of the (Cb,W)-Hf-C equilibrium system was constructed as shown in Figure 39. This figure along with Figures 34 and 38 almost completely defines the meaningful equilibrium phase relationships in the region of useful engineering alloys of the Cb-W-Hf-C system.

Discussion

The observation of apparent anomalous phases such as the zeta phase in XB-88 and alloys of very similar composition poses questions concerning the mechanism of its formation, since as noted previously, observation of this phase in the metal-rich region of the Cb-W-Hf-C system would not be predicted on the basis of available phase diagrams. The results of this study show that the zeta phase occurs in alloys heated above their carbon solvus, suggesting that the zeta phase is metastable. X-ray fluorescence analysis shows the zeta phase in XB-88 to contain 40 w/o W and 5 w/o Hf. The carbon content, determined by conductometric analysis of extracted residues, is 6.8 w/o C. If the zeta phase is assumed to have a psuedo unit cell of approximately the same volume as the low lattice parameter fcc carbide phase, the following comparison can be made between the matrix and the zeta phase.

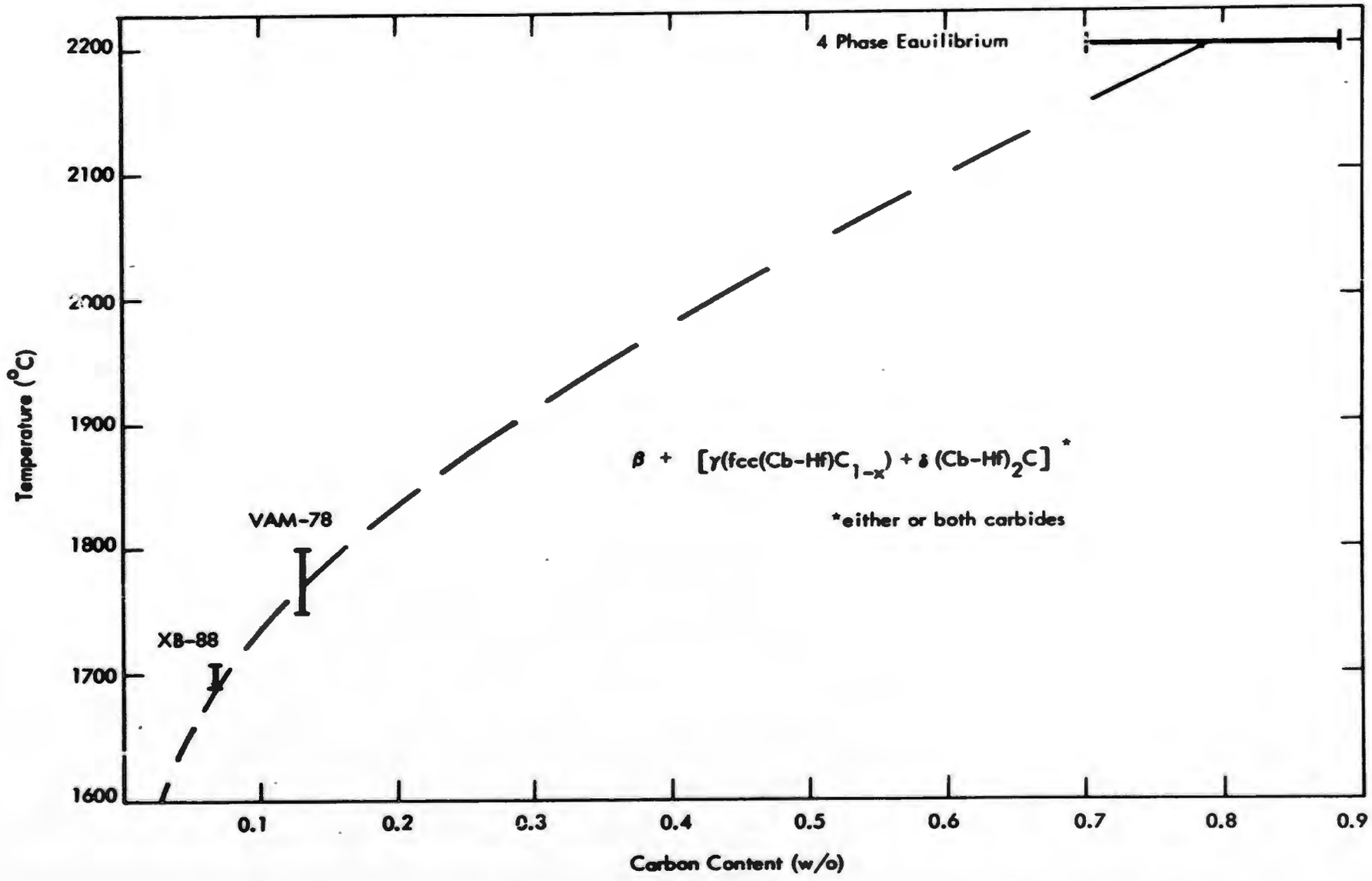

FIGURE 38 - Approximate Carbon Solvus in 22-28 w/o W - 2 w/o Hf Region of Cb-W-Hf-C System

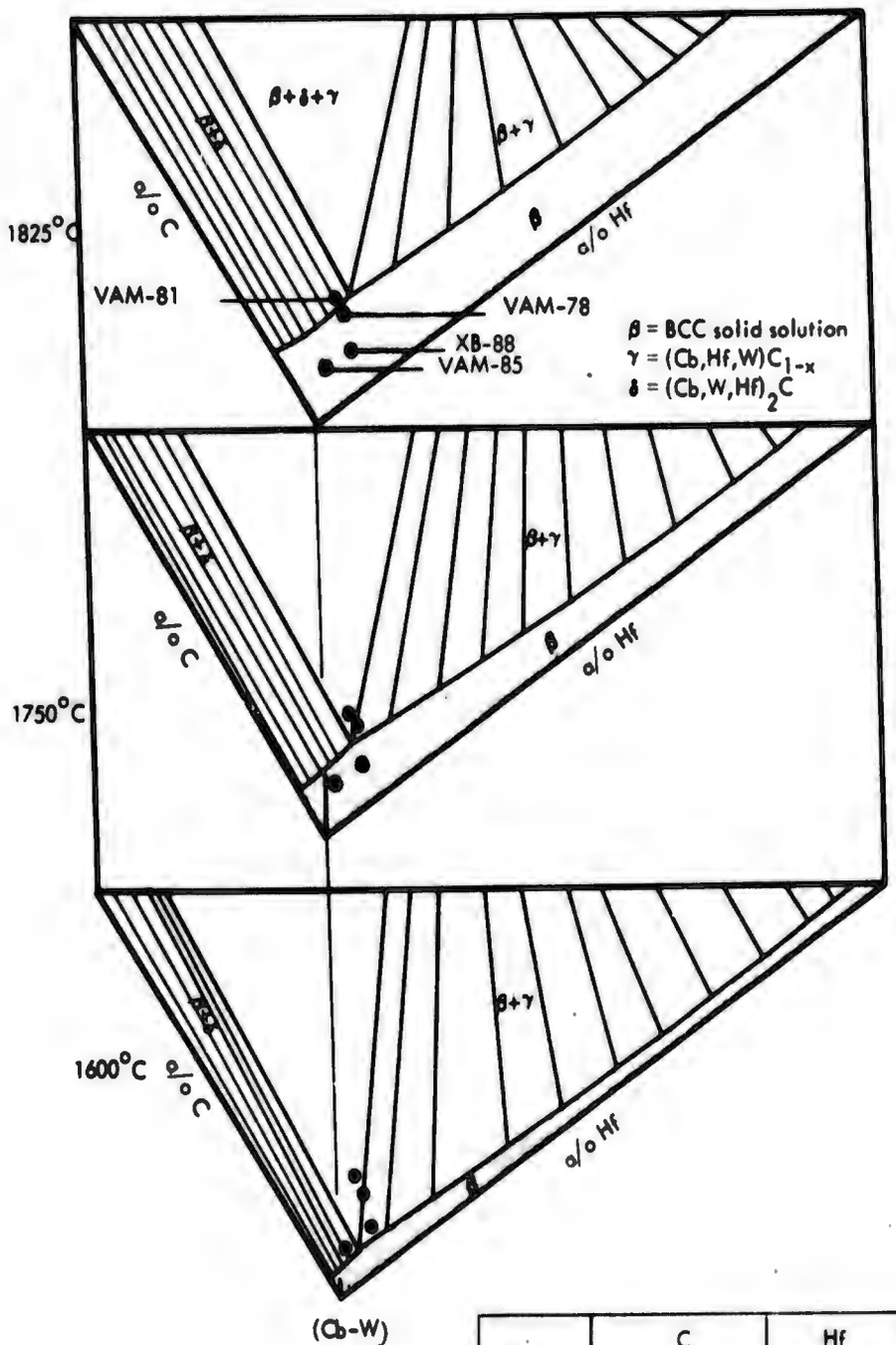

Alloy	C		Hf		W	
	w/o	a/o	w/o	a/o	w/o	a/o
XB-88	0.067	0.63	2.0	1.2	28	16.5
VAM-78	0.13	1.27	2.0	1.4	22	14.1
VAM-81	0.167	1.62	2.0	1.4	22	14.0
VAM-85	0.067	0.63	1.0	0.7	22	14.0

FIGURE 39 - Schematic Representation of (Cb,W)-Hf-C Psuedo Ternary System

β Matrix	Zeta Carbide
Cb - 0.078 moles/cc	0.039 moles/cc
W - 0.016 moles/cc	0.016 moles/cc
Hf - 0.0015 moles/cc	0.0019 moles/cc
C - 0.0006 moles/cc	0.038 moles/cc

The above molarities show that very little diffusion of the metallic elements is required to form the zeta carbide. Tungsten, for example, need not even be present as shown by the data from the tungsten free analog of XB-88. A certain decrease of Cb content occurs. However, this may be aided by the β-zeta volume change. On the other hand, an increase of carbon of 63:1 is required to form zeta. The above observation would suggest that zeta could form during cooling providing that the mobility of carbon is sufficient and is biased by the appropriate chemical potential. Since the observed zeta platelets are quite thin (~1000 Å) one would expect the zeta phase to form during normal radiation cooling from the solution anneal. A simple calculation based on the effective carbon diffusion distance $(Dt)^{1/2}$ at 1700°C shows that a sufficient volume of the β matrix may be depleted of carbon to form the zeta platelets in approximately 4 seconds. However, more rapid cooling rates i. e., less than 4 seconds, would not allow sufficient time for zeta precipitation. This is borne out by the brine quenching experiments, which did not reveal the presence of the zeta phase in the quenched samples. However, there was precipitation of another complex metastable phase in the quenched material. (Figure 35).

The chemical potential for the formation of carbide type phases is very large. The activation barrier is relatively low (probably no greater than the activation energy of carbon diffusion in columbium). If sufficient time is available the equilibrium phase will form, i.e., that phase having the lowest free energy. However there may be requirements for long range diffusion of hafnium as required in the fcc carbide. Since hafnium migration to nucleation sites to form the equilibrium phase may require more time than that available, a metastable carbide such as zeta phase would be formed. The metastable phase would then be resolutioned or transformed in-situ to the equilibrium phase during aging at a lower temperature.

Transformations to the equilibrium phase during aging are not limited to decomposition of the metastable zeta phase. The equilibrium cubic phase formed during the reference heat treatment has a hafnium content of 25 atomic percent. The equilibrium fcc monocarbide phase at 1315°C, contains approximately 40 atomic percent Hf. Thus a considerable diffusion of Hf may take place during long time service exposure or during creep rupture testing. The effects of this transformation on creep-rupture properties are not known precisely as yet, however detailed understanding of the dispersed phase equilibrium and phase transformation appears to be necessary to evaluate the role of the dispersed carbide phase(s) on mechanical properties.

Summary of Phase Relationships

The experimental results of this portion of the study can be summarized by references to Figures 34, 38, and 39. Figure 34 shows the temperature variation of composition of the $(Cb\text{-}Hf\text{-}W)C_{1-x}$ corner of the three phase equilibrium region. These data are shown schematically on Figure 33. Figure 38 shows the approximate temperature variation of the carbon solvus in the 22-28 w/o W, 2 w/o Hf region of the Cb-W-Hf-C quaternary. Figure 39 is a semi-quantitative representation of the variation of the β solvus and the β rich corner of the three phase equilibrium region. These data essentially define the equilibrium phase relationships as applied to this family of alloys. The explanation of observed phase relationships under non-equilibrium conditions becomes a kinetic problem. Normal furnace cooling rates from above the carbon solvus are sufficient for the formation of the metastable zeta phase in XB-88 (which is probably controlled by carbon diffusion) but are too fast for the precipitation of the equilibrium cubic carbide phase (which is probably controlled by hafnium diffusion).

V. MECHANICAL PROPERTIES

The mechanical property studies conducted in this investigation had two primary objectives:

1. Determination of the effects of thermal-mechanical processing to establish the treatment which provides the optimum combination of high temperature creep resistance and low temperature ductility.
2. Detailed evaluation of the tensile and creep rupture properties of XB-88 in the reference (optimum) condition.

As described previously in this report, initial studies[1] showed that high temperature annealed fully recrystallized structures provided the best creep properties for XB-88 and similar Cb-W-Hf-C alloys. While annealing at 1800 and 2000°C provided excellent creep strength, this was achieved at the sacrifice of adequate room temperature ductility. The poor low temperature ductility of the large grained, high temperature annealed material is a manifestation of the well known effect of increasing grain size raising the ductile-brittle transition temperature range in body centered cubic metals. Large grain size has another undesireable effect. The initiation and duration of third stage creep (and consequently creep life) is strongly influenced by grain size, with the larger grain size favoring intergranular rupture at low total creep strains.

Attempts to provide an optimum combination of high temperature creep strength and low temperature ductility involved three basic approaches:

1. Annealing at temperatures just above the carbon solvus to provide essentially fully recrystallized structures without excessive grain growth.

2. Very short time annealing of wrought material at high temperatures (above the carbon solvus) to provide a fine grained, recrystallized structure.

3. High temperature extrusion to produce a fine grained recrystallized structure having the high temperature carbide phase morphology.

These three approaches were selected on the basis of their capability of providing relatively fine grained recrystallized structures having the high temperature carbide phase morphology. The effects of the various thermal-mechanical treatments were evaluated on the basis of creep-rupture tests at 1315°C (2400°F) and room temperature tensile tests. All creep-rupture testing was conducted at pressures below 5×10^{-6} torr in liquid nitrogen trapped SATEC VC-100 creep rupture units described previously in this report. All test specimens were wrapped in pure tantalum foil to provide additional protection from oxygen and carbon contamination during testing. The calibration and check out procedures used to assure the validity of the creep test data are described in an earlier report.[1]

The tensile data obtained on XB-88 are summarized in Table 9, and the creep-rupture results are listed in Table 10.

Effect of Final Annealing Temperature on Mechanical Properties

Material which had been extruded at 1930°C and swaged at 1300°C (86% reduction by swaging) was machined into test specimens and annealed 1 hour at temperatures ranging from 1400°C to 2000°C. Representative microstructures for most of these annealing treatments were shown previously in Figure 23. The effect of final annealing temperature on room temperature tensile properties is shown in Figure 40. Heat treating at 1800 and 2000°C produced fairly large grained, completely recrystallized structures having essentially no room temperature ductility. The stress relieved specimens (annealed at 1600°C and below) had tensile elongation values of 8%. A modest peak in the ductility versus annealing temperature plot was observed at 1700°C. Approximately 8.5% reduction in area and 11% elongation were obtained with the 1700°C anneal which produced an almost completely recrystallized microstructure (Figure 23). The relatively low ductility of the stress-relieved material was unexpected, since earlier work on XB-88 showed that material stress relieved

TABLE 9 - Tensile Data for XB-88

Specimen No.	Thermal-Mechanical History	Test Temp. (° C)	Test Temp. (° F)	0.2%** Yield Stress (psi)	Ultimate Stress (psi)	Red. of Area (%)	Elong. (%)
T-1	A+1 hr. at 2000° C+H. Q.*	R.T.	R.T.	---	100,600	0	0
T-12	B+1 hr. at 1300° C+H. Q.	R.T.	R.T.	121,000	145,900	10.8	11.3
T-14	B+1 hr. at 1400° C+H. Q.	R.T.	R.T.	120,100	144,300	16.4	17.9
T-24	C+5 mins. at 1800° C+H. Q.	R.T.	R.T.	116,300	122,700	1.1	1.3
T-28	C+15 secs. at 2200° C+H.Q.	R.T.	R.T.	115,500	131,500	3.4	4.0
T-37	C+5 secs. at 2200° C+H.Q.	R.T.	R.T.	123,700	137,700	2.7	3.3
T-31	C+1 min. at 2200° C+H.Q.	R.T.	R.T.	110,000	122,200	2.2	2.7
T-32	C+1 hr. at 1800° C+H.Q.	R.T.	R.T.	---	115,000	0	0.7
T-33	C+1 hr. at 1700° C+H.Q.***	R.T.	R.T.	119,300	137,300	8.8	11.3
T-34	C+1 hr. at 1600° C+H.Q.	R.T.	R.T.	132,800	143,800	6.6	8.0
T-35	C+1 hr. at 1500° C+H.Q.	R.T.	R.T.	129,100	147,200	7.2	8.0
T-38	C+1 hr. at 1400° C+H.Q.	R.T.	R.T.	129,400	153,700	6.1	5.3
T-52	D+1 hr. at 1300° C+H.Q.	R.T.	R.T.	---	70,800	0	0
T-39	Reference Condition	93	200	102,000	107,000	24.2	16.7
T-40	Reference Condition	-79	-110	146,600	151,000	1.0	1.0
T-43	Reference Condition	316	600	80,000	98,000	58.2	19.3
T-72	Reference Condition	648	1200	59,800	97,000	55.0	16.0
T-64	Reference Condition	759	1400	53,500	99,700	53.0	17.0
T-65	Reference Condition	870	1600	51,400	95,700	60.0	17.0
T-66	Reference Condition	980	1800	52,500	97,000	65.0	17.0
T-91	Reference Condition	1092	2000	50,200	86,000	60.7	16.0
T-68	Reference Condition	1204	2200	48,800	71,300	76.0	14.0
T-69	Reference Condition	1315	2400	45,000	53,400	76.0	19.0
T-60	Reference Condition	1370	2500	43,200	46,800	78.0	22.0
T-76	Reference Condition + TRW Coating	R.T.	R.T.	---	70,000	0	0
T-78	Reference Condition TRW Coating	316	600	66,300	86,200	55.4	19.3
T-79	Reference Condition + TRW Coating	R.T.	R.T.	---	60,240	0	0

* See Table 11 for processing history
** Strain Rate = 0.05 in/in/min.
*** Reference Condition
HQ = Helium Quench

TABLE 10 - Creep Rupture Data for XB-88

Specimen No.	Thermal - Mechanical History*	Test Temp. (° C)	Test Temp. (° F)	Stress (psi)	Rupture Time (hrs.)	Min. Creep Rate (%/hrs.)	Transition Time (hrs.)	Deformation	
								Red. in Area (%)	Elongation (%)
T-2	A+1 hr. at 1800° C+H. Q.	1315	2400	30,000	28.6	0.0573	18.4	10.9	4.7
T-3	A+1 hr. at 1800° C+H. Q.	1315	2400	27,000	49.8	0.0384	20.0	10.9	5.3
T-4	A+1 hr. at 2000° C+H. Q.	1315	2400	30,000	18.8	0.0756	14.1	8.8	4.0
T-5	A+1 hr. at 2000° C+H. Q.	1315	2400	27,000	47.9	0.0368	34.5	9.9	4.0
T-11	A(as extruded at 1930° C)	1315	2400	27,000	127.8	0.0384	50.6	57.5	18.0
T-13	B+1 hr. at 1400° C+H. Q.	1315	2400	27,000	21.5	0.3000	5.1	76.4	27.3
T-16	B+1 hr. at 1300° C+H. Q.	1315	2400	27,000	48.5	0.1398	8.3	72.9	34.0
T-22	C+1 hr. at 1800° C+H. Q.	1315	2400	30,000	24.3	0.0756	18.0	15.1	6.0
T-23	C+5 min. at 1800° C+H.Q.	1315	2400	30,000	29.3	0.0980	11.4	28.0	14.7
T-27	C+1 hr. at 1700° C+H. Q.	1315	2400	30,000	26.9	0.0735	15.0	---	11.3
T-29	C+15 secs. at 220[illegible]+H. Q.	1315	2400	30,000	22.1	0.115	11.0	27.1	12.0
T-30	C+5 secs. at 2200° C+H. Q.	1315	2400	30,000	31.3	0.074	13.0	31.7	14.0
T-51	D(as re-extruded in Dynapak, 1930° C)	1315	2400	30,000	41.7	0.0924	21.9	31.6	12.0
T-54	D(as re-extruded in Dynapak, 1930° C)	1315	2400	27,000	62.6	0.0449	37.0	18.2	7.3
T-41	Reference Condition	1315	2400	27,000	69.6	0.0470	30.5	33.6	13.3
T-42	Reference Condition	1204	2200	37,000	53.4	0.0516	27.6	29.0	12.0
T-44	Reference Condition	1204	2200	45,000	13.7	0.1360	5.9	53.0	13.3
T-45	Reference Condition	1092	2000	70,000	16.9	0.0833	9.0	63.5	13.3
T-46	Reference Condition	1092	2000	55,000	96.6	0.0134	59.0	---	10.7
T-48	Reference Condition	980	1800	70,000	144.9	0.0133	103.0	60.7	14.7
T-49	Reference Condition	1315	2400	25,000	93.6	0.0372	41.0	60.7	14.7
T-60	Reference Condition	1315	2400	25,000	107.5	0.040	45.5	28.0	12.0
T-61	Reference Condition	1204	2200	34,000	170.8	0.0161	88.0	26.3	11.3
T-62	Reference Condition	1092	2000	60,000	60.2	0.0246	37.8	41.6	10.7
T-73	Reference Condition	1092	2000	64,000	45.0	0.0344	27.0	61.8	12.0
T-74	Reference Condition	1204	2200	42,000	26.7	0.0800	8.5	59.0	20.6
T-81	C+1 hr. at 1600° C+H.Q.	1315	2400	25,000	73.0	0.0518	11.5	71.5	26.0
T-83	Reference Condition	1315	2400	20,500	293.2	0.0215	92.0	73.3	25.3
T-84	Reference Condition + TRW Coating Thermal Cycle**	1315	2400	25,000	64.4	0.0725	24.5	60.8	23.3
T-85	Reference Condition + TRW Coating Thermal Cycle**	1315	2400	28,000	37.7	0.0946	9.9	75.6	30.0
T-93	Reference Condition + 88 Hours at 1315° C	1315	2400	25,000	117.6	0.0393	38.0	49.9	17.3
T-96	C+1 hr. at 1400° C	1315	2400	25,000	40.8	0.1376	21.9	84.1	28.6

* See Table 11 for processing history

** 8 hrs. at 2325°F + 6 hrs. at 2100°F

TABLE 11 - Processing History

Condition Code	Processing History
A	Extruded at 1930°C, 9:1 Reduction Ratio. Swaged at 1300°C, 65%R. A.
B	Extruded at 2040°C, 9:1 Reduction Ratio. Re-extruded at 2040°C at 2:1 Reduction Ratio.
C	Extruded at 1930°C, 5:1 Reduction Ratio. Swaged at 1300°C, 86%R. A.
D	Extruded at 1930°C, 5:1 Reduction Ratio. Re-extruded in Dynapak at 1930°C at 8:1 Reduction Ratio.
Reference Condition	C above + 1 Hr. at 1700°C + Helium Quench

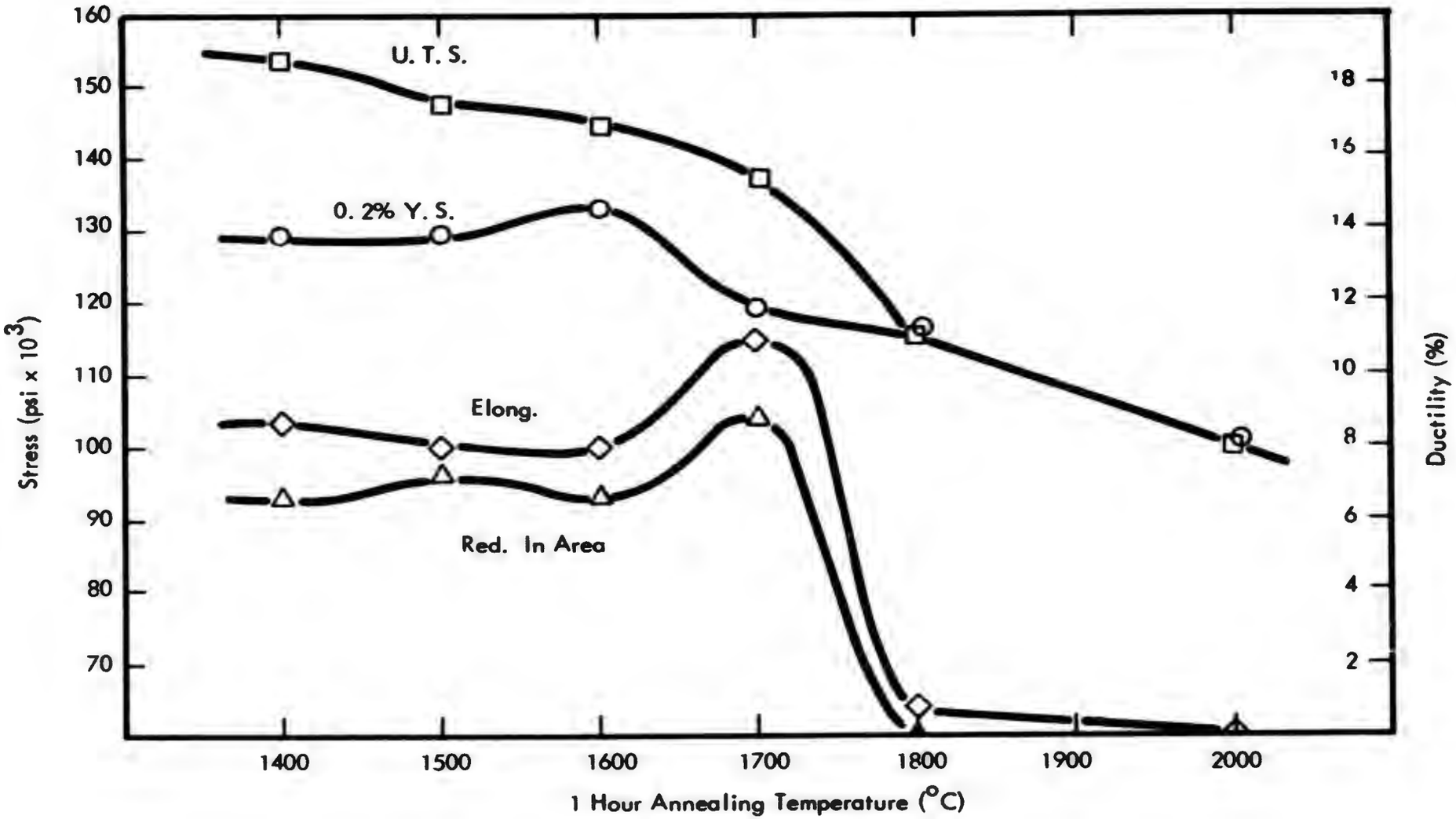

FIGURE 40 - Room Temperature Tensile Properties of XB-88 as a Function of Prior Heat Treatment

at 1400°C had 22% elongation and 32% reduction in area at room temperature. The reason for this discrepancy is not obvious, although the original XB-88 material received more cold work, since ingot breakdown was accomplished by Dynapak extrusion at 1250°C.

The effects of final annealing temperature on the creep-rupture properties of extruded plus swaged XB-88 are illustrated by the data of Figures 41 and 42. Figure 41 shows creep curves obtained at 1315°C (2400°F) and 30,000 psi for material annealed 1 hour at 2000°C, 1800°C, and 1700°C. These heat treatments provided recrystallized structures having grain sizes of 0.03 mm average grain diameter for the 1700°C anneal, 0.05 mm for the 1800°C anneal, and 0.14 mm at 2000°C. The secondary creep rates were essentially identical for all three conditions. Rupture time was somewhat shorter for the coarse grained 2000°C annealed specimen, while the finer grained specimens had fairly equivalent rupture times. Rupture strain decreased with increasing annealing temperature which is in agreement with earlier observations that rupture strain was inversely related to grain size. Figure 42 shows the 1315°C 25,000 psi creep curves for XB-88 annealed 1 hour at 1700°C, 1600°C, and 1400°C. The secondary creep rate increases from 0.037%/hr. for the 1700°C anneal to 0.137%/hr. for the 1400°C anneal. These results confirm previous observations that worked plus stress-relieved structures provide considerably poorer creep properties, both in terms of secondary creep rates and rupture lives, than high temperature annealed, recrystallized structures. The essentially equivalent secondary creep rates of material annealed at 1700°C and above suggest that the structure and/or the precipitate phases stabilized by the high temperature anneal are responsible for the improved creep behavior.

In view of the adequate room temperature ductility and attractive 1315°C creep properties exhibited by the material annealed 1 hour at 1700°C following extrusion and swaging, this treatment was selected as the reference treatment or base line against which other processing variations would be evaluated. The insert plots of log stress versus log rupture time shown in Figures 41 and 42 compare the reference treatment properties with the rupture times obtained from both higher and lower final annealing temperatures.

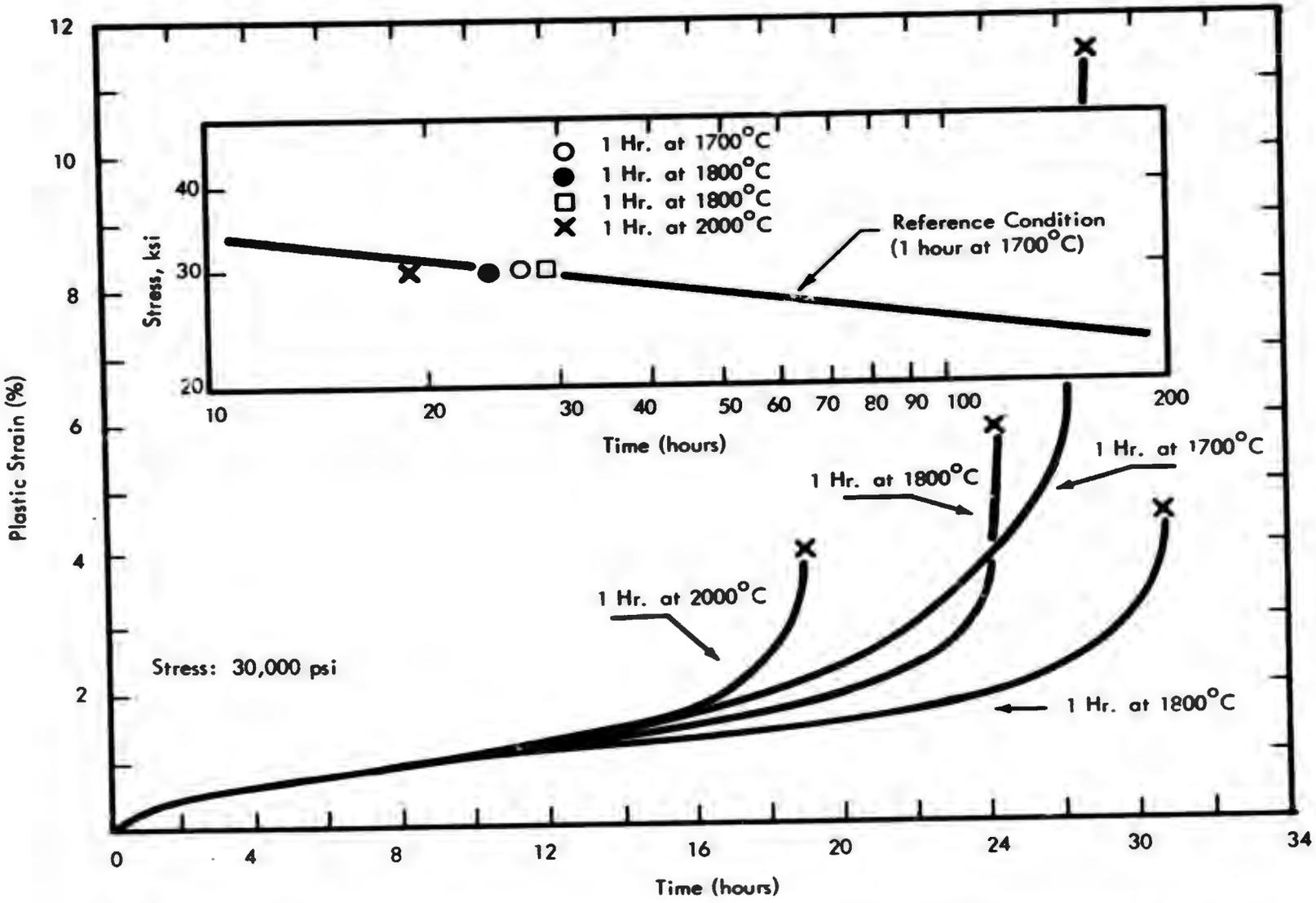

FIGURE 41 - Effect of Prior Annealing Temperature on the 1315°C (2400°F) Creep Properties of XB-88

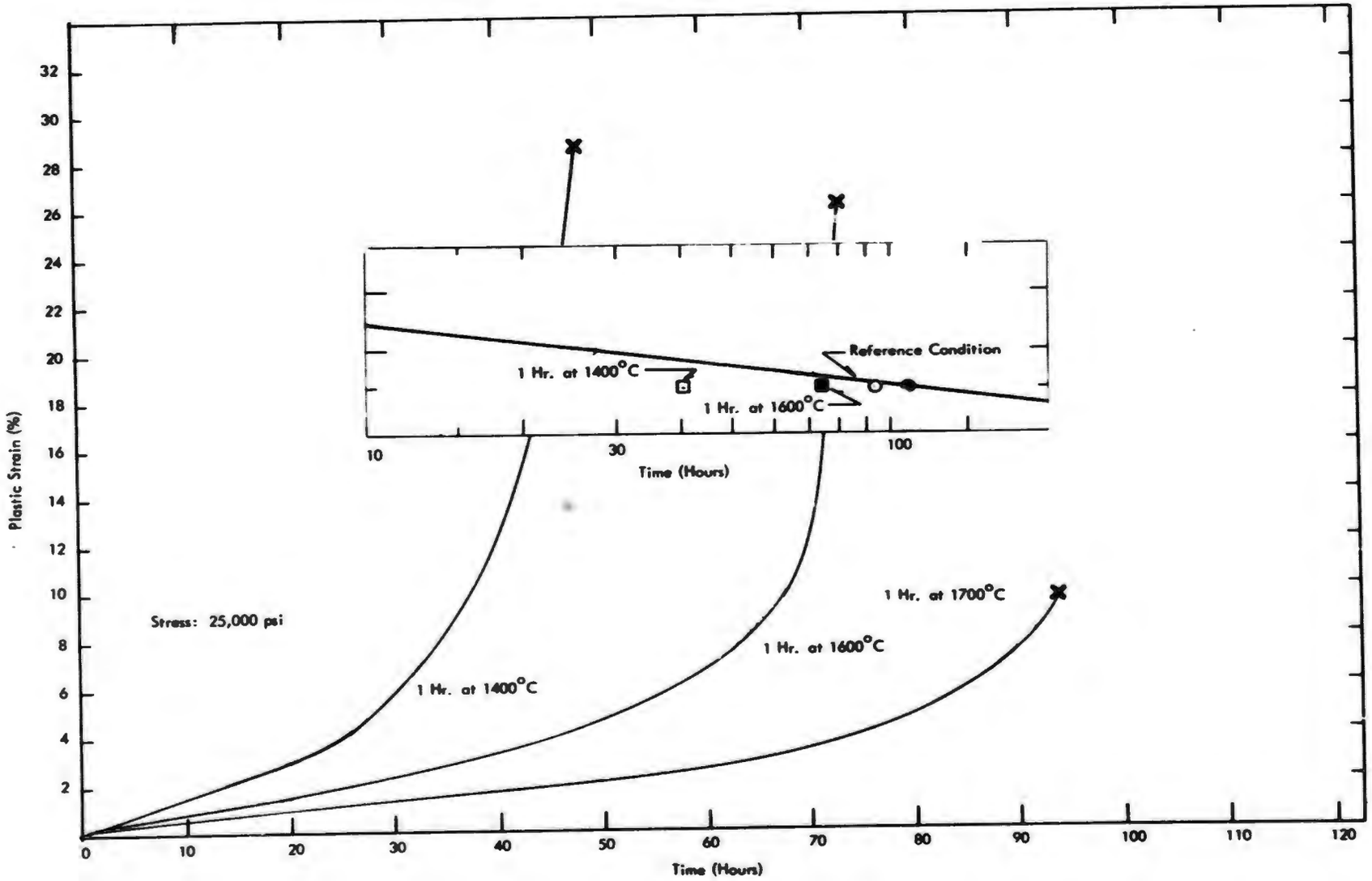

FIGURE 42 - Effect of Prior Annealing on the Creep-Rupture Properties of XB-88 at 2400°F (1315°C)

High Temperature Fracture Behavior. Previous work had indicated that rupture life and rupture strain were strongly influenced by high temperature fracture behavior. Photomicrographs of head and gauge sections of fractured creep specimens annealed 1 hour at 2000°C, 1700°C, and 1400°C prior to creep testing at 1315°C are shown in Figures 43, 44 and 45. The microstructure of the gauge section of the specimen annealed at 2000°C (Figure 43) shows intergranular (W-type) cracks generally orientated perpendicular to the stress axis. This type of cracking arises from grain boundary sliding as described by Begley and Godshall[14]. Evidence of grain boundary sliding is shown by the apparently deformed areas adjacent to grain boundaries in Figure 43c. The creep-rupture specimen annealed 1 hour at 1700°C shows similar grain boundary separations (Figure 44d). However, this finer grained material can accommodate more grain boundary deformation than the larger grained equiaxed recrystallized structures without early rupture at low strain values. The pre-test microstructures of the 1700°C annealed material (illustrated in Figures 23 and 24) show a few unrecrystallized bands and a well developed substructure decorated with precipitates. This material has fewer boundaries oriented perpendicular to the stress axis and greater boundary "roughness" than that of the 2000°C material. This structure reduces stress concentrations at triple points, reducing the tendency for crack initiation and propagation, permitting a greater amount of deformation to be accommodated by the matrix, and thus a longer, more gradual tertiary creep stage.

The microstructure of the specimen stress relieved at 1400°C prior to creep testing (Figure 45) showed little if any evidence of grain boundary separation, and consequently a relatively high rupture strain, although there was some evidence of recrystallization during creep testing. However, as shown previously in Figure 42, the creep rate of this material was considerably greater than that of material annealed at higher temperatures.

Effect of High Temperature, Short Time Annealing

In order to explore the effect of finer grain size on the mechanical properties of high temperature annealed XB-88, specimens were annealed for short times at temperatures well

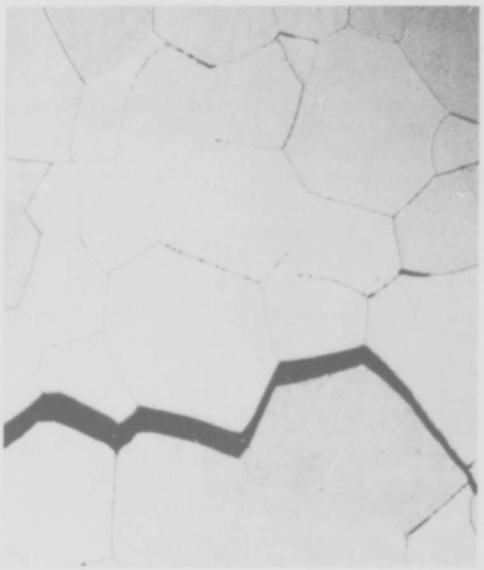

(a) Gauge Section Near Fracture 100X

(b) Head Section 1500X

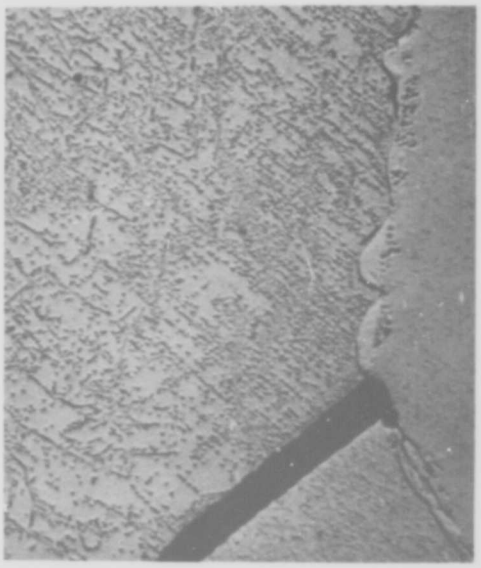

(c) Gauge Section Near Fracture 1500X

FIGURE 43 - Microstructure of XB-88 Creep Specimen (T-4) Annealed 1 Hr. at 2000°C. Failed after 18.8 Hrs. at 30,000 psi (1315°C(2400°F)

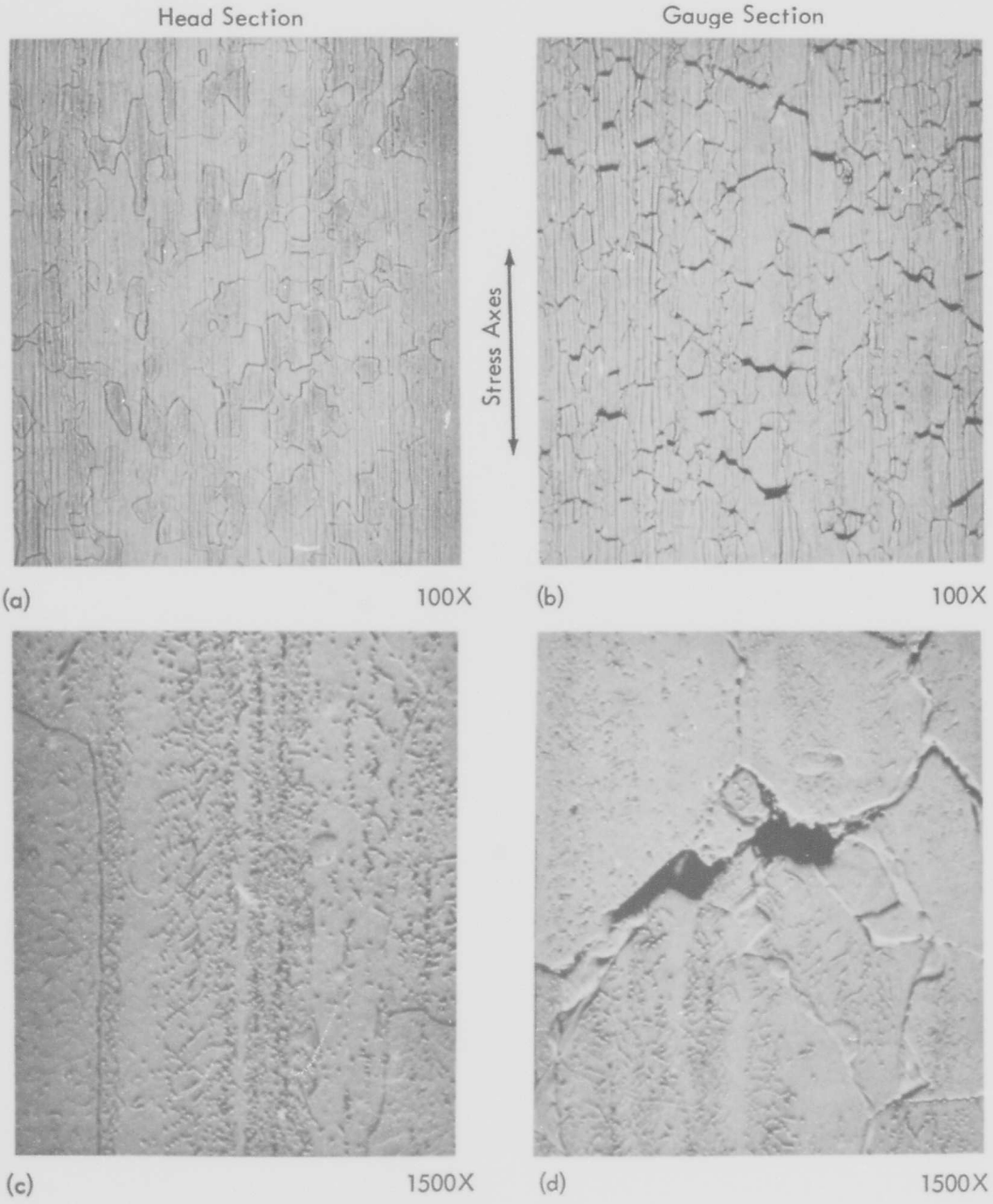

FIGURE 44 - Microstructure of XB-88 Creep Specimen (T-27) Annealed 1 Hr. at 1700°C. Failed after 26.9 Hrs. at 30,000 psi (1315°C(2400°F)

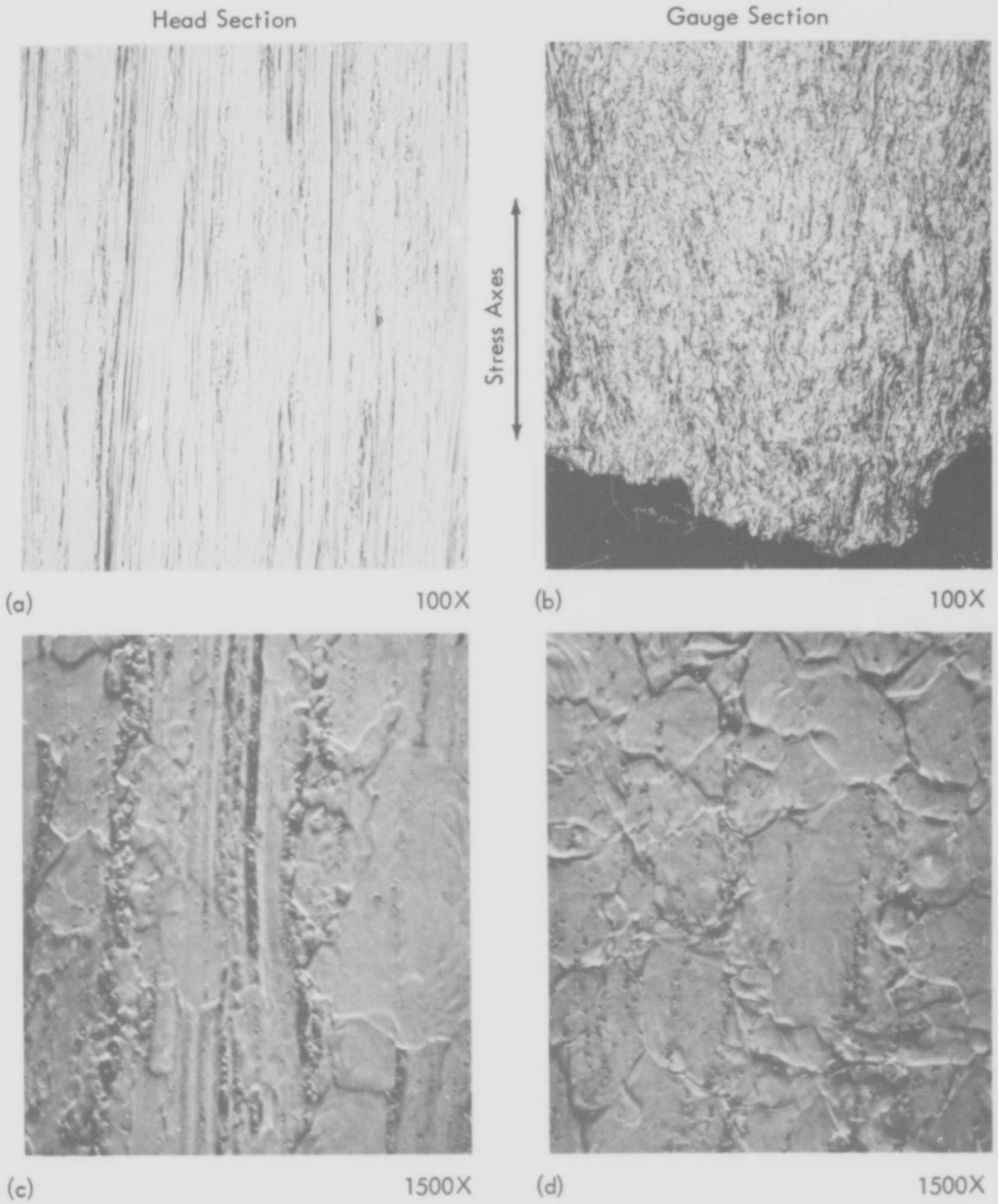

FIGURE 45 - Microstructure of XB-88 Creep Specimen (T-96). Annealed 1 Hr. at 1400°C. Failed after 40.8 Hrs. at 1315°C (2400°F), 25,000 psi

above the carbon solvus for XB-88. Specimens were annealed 5 minutes and 1 hour at 1800°C (providing mean grain diameters of 0.032 mm and 0.065 mm respectively) and 5 seconds and 15 seconds at 2200°C (0.016 mm and 0.028 mm mean grain diameters respectively). The 1315°C (2400°F) creep data representative of the 5 minute and 1 hour 1800°C annealing treatments are shown in Figure 46. The 1 hour anneal provided a slightly lower secondary creep rate but a shorter rupture time than the 5 minute anneal. The difference in rupture time was quite small however, (24.3 hours versus 29.3 hours). Again, rupture strain increased significantly with decreasing grain size. Metallographic examination of the specimens annealed 5 minutes at 1800°C showed that recrystallization was complete with a structure very similar to that shown previously in Figures 27a and 27b. A well defined substructure was formed which was decorated by precipitates (initially the metastable zeta and cubic phases, both of which later transformed to the fcc carbide during creep testing).

Creep curves for the 5 second and 15 second 2200°C annealing treatments are shown in Figure 47. The data are not entirely consistent with the 1800°C results, for in this case the finer grain size material had a lower secondary creep rate as well as a longer rupture life. The microstructures of the two creep specimens did not differ greatly and were quite similar to the specimen annealed 5 minutes at 1800°C.

The room temperature tensile properties of high temperature, short time annealed specimens are listed in Table 12. Decreasing the annealing time from 1 hour to 5 minutes at 1800°C raised room temperature ductility to only 1%. It would not be correct to assume from these data, however, that decreasing the annealing time (and consequently the grain size) had no significant effect on low temperature ductility, for a considerable shift in the ductile-brittle transition may have occurred. The shift in transition temperature cannot be established with single point tests. Nevertheless, the room temperature ductility of the 5 minute annealed material is below the target properties. The room temperature tensile data for specimens annealed 5, 15, and 60 seconds at 2200°C also showed improvement in room temperature ductility. Again, the elongation values of 2 to 3.4% are below the target minimum of 5%.

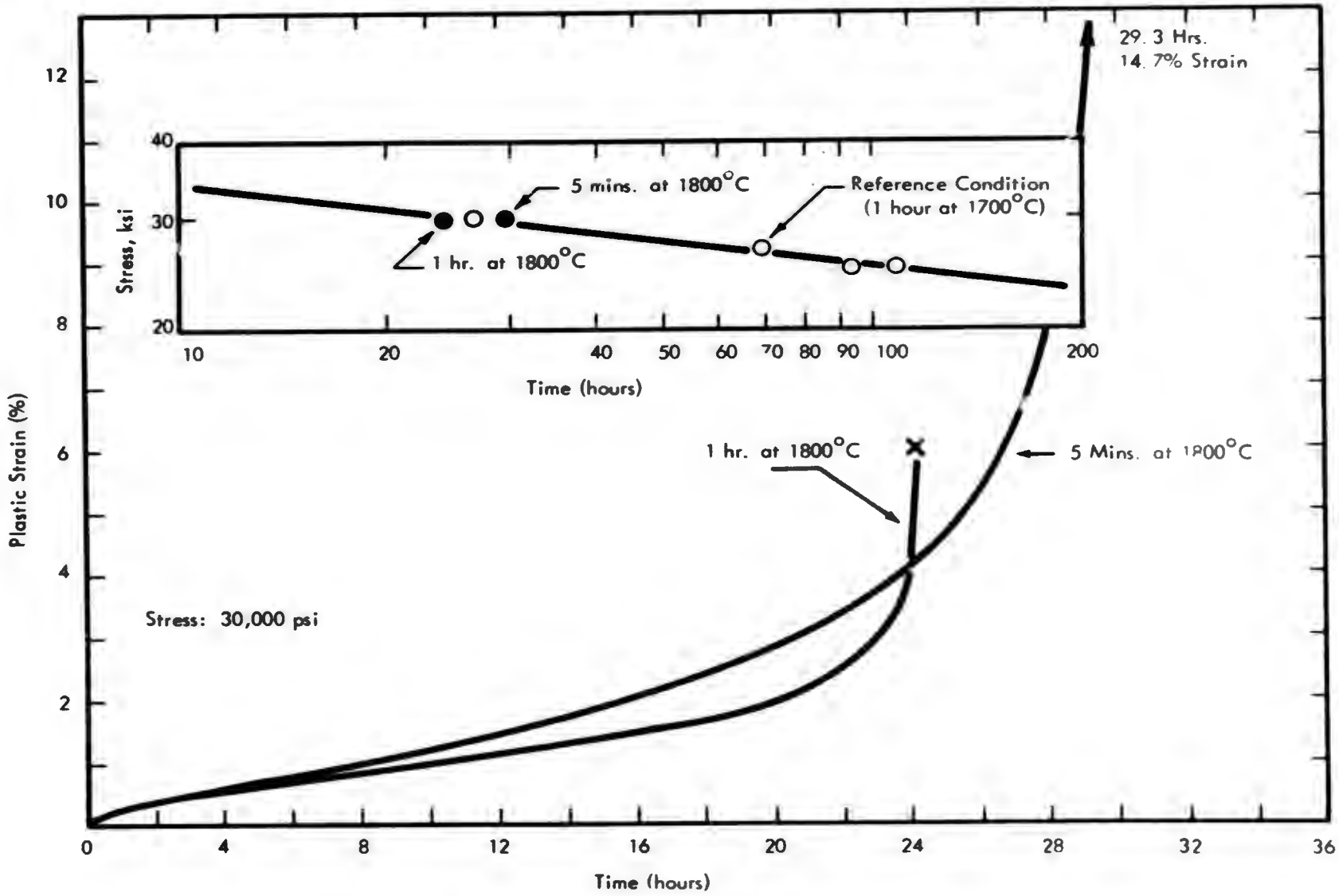

FIGURE 46 - Effect of Annealing Time at 1800°C on the 1315°C (2400°F) Creep Properties of XB-88

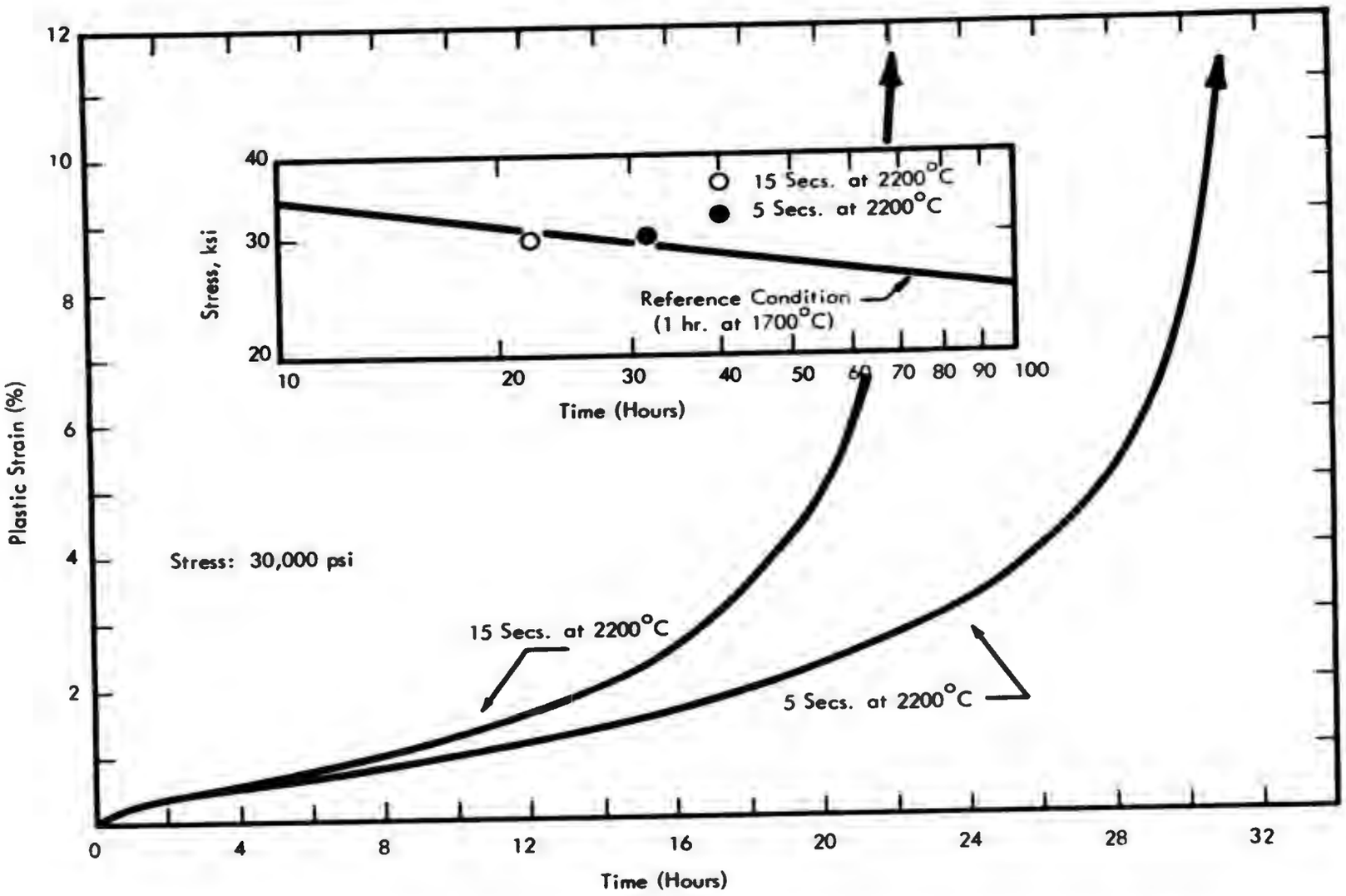

FIGURE 47 - Effect of Annealing Time at 2200°C on the1315°C (2400°F) Creep Properties of XB-88

TABLE 12 - Room Temperature Tensile Properties of Annealed XB-88

Specimen No.	Condition	0.2% Yield Strength (psi)	Ultimate Strength (psi)	Elong. (%)	Red. In Area (%)	Average Grain Diameter (mm)
T-24	Annealed 5 min. at 1800°C	116,300	122,700	1.1	1.3	0.032
T-32	Annealed 1 hr. at 1800°C	---	115,000*	0.0	0.7	0.065
T-37	Annealed 5 secs. at 2200°C	123,700	137,200	2.7	3.3	0.016
T-28	Annealed 15 secs. at 2200°C	115,500	131,500	3.4	4.0	0.028
T-31	Annealed 60 secs. at 2200°C	110,100	122,200	2.2	2.7	0.048

*True stress at fracture

The results of the short time annealing study showed that both creep rupture strain and low temperature ductility could be improved by reducing grain size. The creep rupture strength did not show any significant improvement over that obtained by the 1 hour at 1700°C reference heat treatment, at least at high stresses (30,000 psi). While an improvement in room temperature ductility was observed, it was not as good as that obtained by the reference treatment.

Effects of High Temperature Extrusion

To complement the experiments involving heat treatment of swaged rod, studies of structures produced by extrusion at temperatures well above the carbon solvus of XB-88 were carried out. It was anticipated that a fine grained or polygonized structure having a favorable carbide phase morphology could be produced which would yield improved creep rupture properties, especially with respect to the tendency toward intergranular rupture at

low creep strains. Sections of XB-88 in the following conditions were evaluated:

A. Extruded at 1930°C (3500°F), 9:1 extrusion ratio.

B. Extruded at 2040°C (3700°F), 9:1 extrusion ratio plus re-extruded at 2040°C (3700°F), 2:1 extrusion ratio.

C. Extruded at 1930°C (3500°F), 5.5:1 extrusion ratio, re-extruded (Dynapak) at 1930°C (3500°F, 8:1 extrusion ratio.

Creep-rupture specimens were machined from each of the extrusions and creep tested at 1315°C (2400°F). The creep data are presented in Figure 48. The secondary creep rate at 1315°C (2400°F) and 27,000 psi was 0.038%/hr., compared to a slightly higher value, 0.047%/hr., for material in the reference condition, but the extent of third stage creep was greater for the extruded specimen. The material which was double extruded, at 2040°C, demonstrated poor creep properties. The Dynapak re-extruded XB-88 had creep properties quite comparable to those provided by the reference condition (annealed 1 hr./1700°C). The relatively wide variation in the creep properties of the various hot extruded conditions can be rationalized in terms of the structure produced by the various processing treatments.

The 9:1 extrusion ratio, 1930°C extrusion, condition A, had a duplex structure consisting of approximately 60% fine grained (0.007 mm) recrystallized areas separated by bands of apparently unrecrystallized material, as shown in Figure 11. The bands had a well developed substructure, as shown in the high magnification photomicrograph of Figure 11b. Photomicrographs of the gauge section adjacent to the fracture area of the creep specimen (Figure 49) reveals that grain boundary separations have occurred in the recrystallized regions but are terminated in the areas containing the sub-boundary network. The combination of the fine grain size in the recrystallized areas and the banded structure of the as-extruded specimen provides greater resistance to crack initiation and propagation which results in

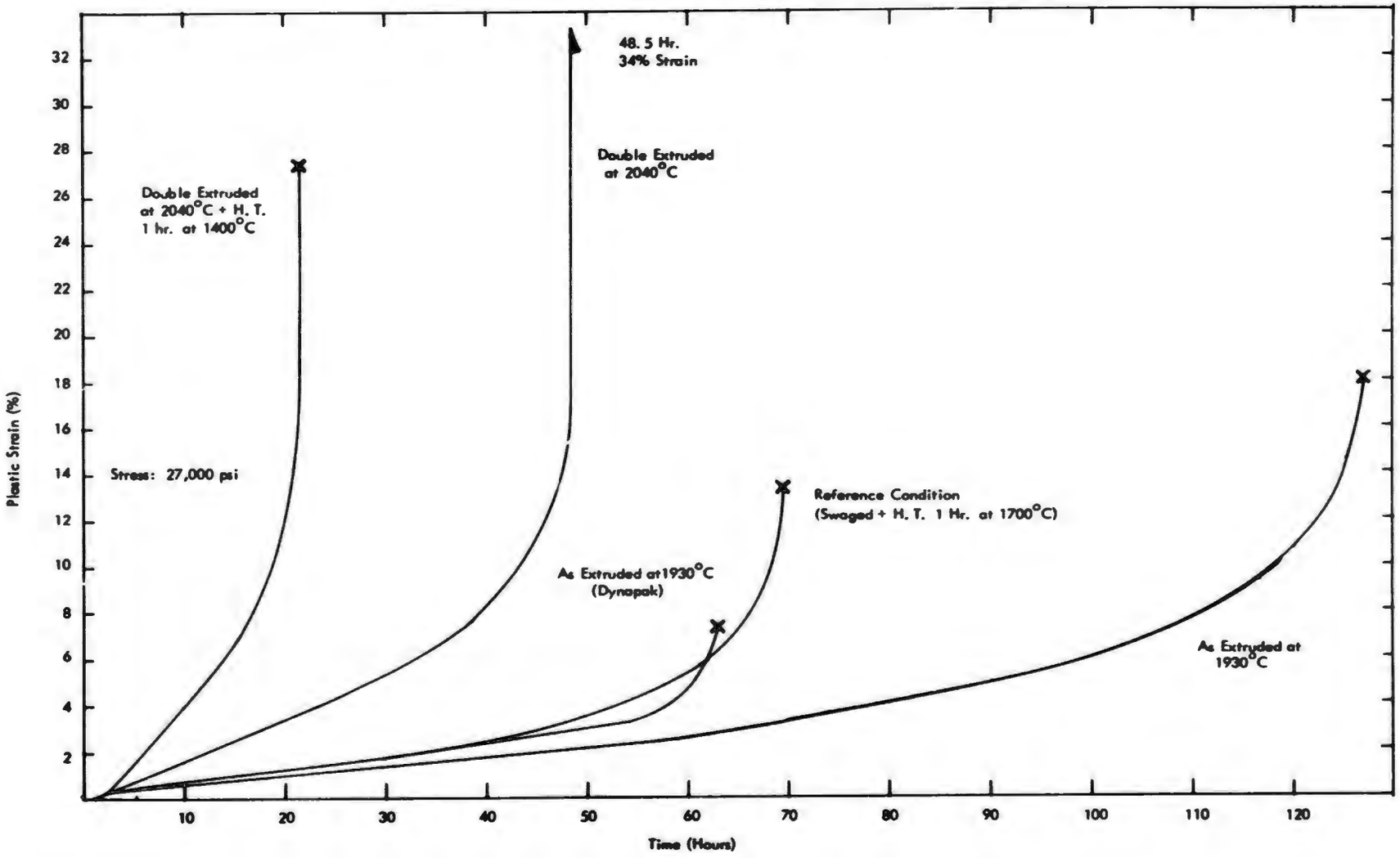

FIGURE 48 - Effect of Thermal Mechanical Treatment on the Creep-Rupture Properties of XB-88 at 1315°C(2400°F)

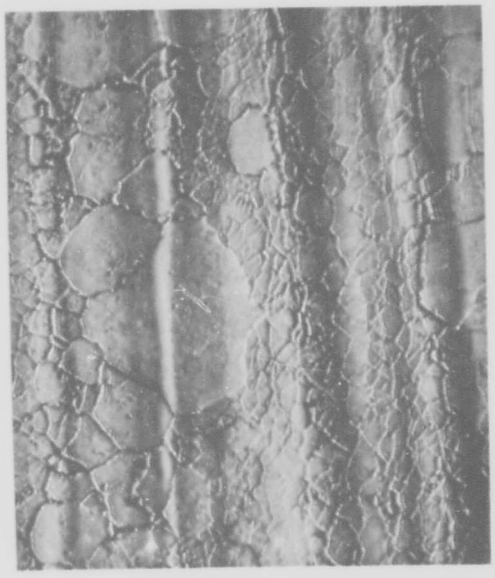

(a) As Extruded 1500X

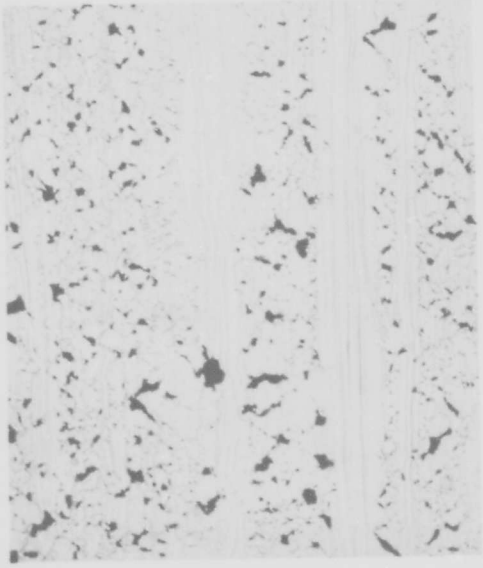

(b) Gauge Section 100X

(c) Gauge Section 1500X

FIGURE 49 - Microstructure of XB-88 Creep Specimen (T-11). Extruded at 1930°C and Creep Tested at 1315°C and 27,000 psi. Failed After 127.8 Hours.

larger rupture strains and consequently larger rupture life.

The Dynapak re-extruded material (1930°C, 8:1 reduction) showed a similar type of duplex structure (see Figure 14), except that the grain size was larger, in wider recrystallized bands, with a higher percentage of grain boundaries perpendicular to the extrusion axis. These differences in structure between the conventionally extruded material, condition A, and the Dynapak re-extruded stock apparently arise from the adiabatic heating which occurs during high energy rate deformation, since the initial billet temperatures and extrusion ratios were quite comparable. As a consequence of its larger grain size and the fewer, coarser bands of unrecrystallized material to arrest grain boundary separations, the Dynapak re-extruded bar had a shorter tertiary creep stage and lower rupture life than the conventionally extruded XB-88.

The microstructure of a Dynapak re-extruded specimen creep tested at 1315°C and 30,000 psi is shown in Figures 50 and 51. The microstructure of the head section of the creep specimen in Figure 50 shows the typical aged precipitate within the recrystallized grain volumes The substructure in the banded region has not changed appreciably from aging during the creep test. Photomicrographs of the gauge section of this creep specimen show grain boundary separations terminated in the unrecrystallized bands containing the well developed sub-boundary networks. Examination of the gauge sections revealed a microstructural feature along the grain boundaries which was not observed in the relatively unstressed head section. Small, irregularly shaped areas along the boundaries had the appearance of being rather heavily deformed. These areas may result from sliding along a serrated or jogged boundary, causing high stress to be developed within the matrix between the serrations and consequent deformation of these local matrix areas. These areas along the boundary do not have the appearance of large precipitates; indeed the precipitation within the gauge section appears to be somewhat finer after test than in the head section.

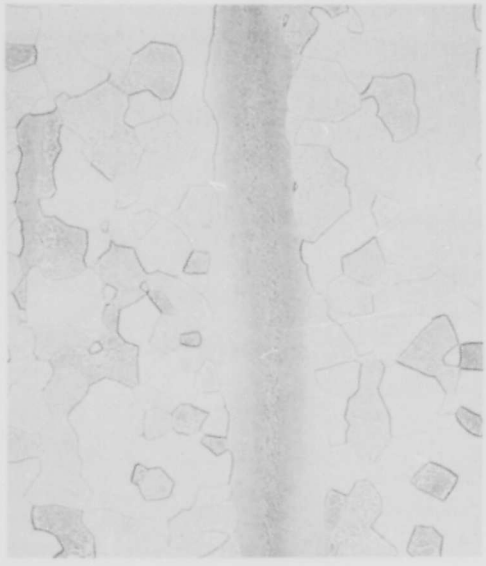

(a) 100X

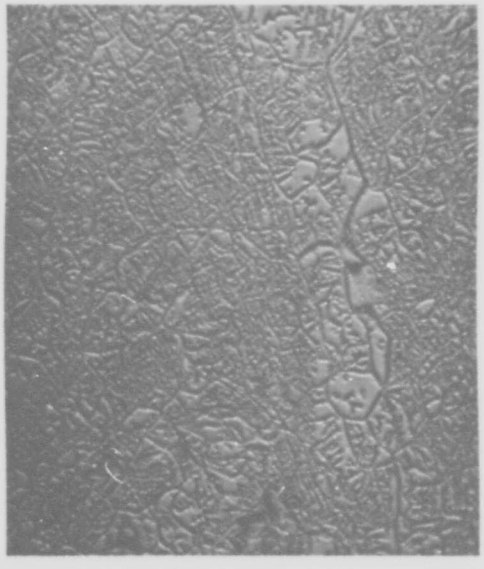

(b) 1500X

(c) 1500X

FIGURE 50 - Microstructure of XB-88 Creep Specimen Head Section. Dynapak Extruded at 1930°C(3500°F). Failed After 41.7 Hours at 1315°C (2400°F), 30,000 psi.

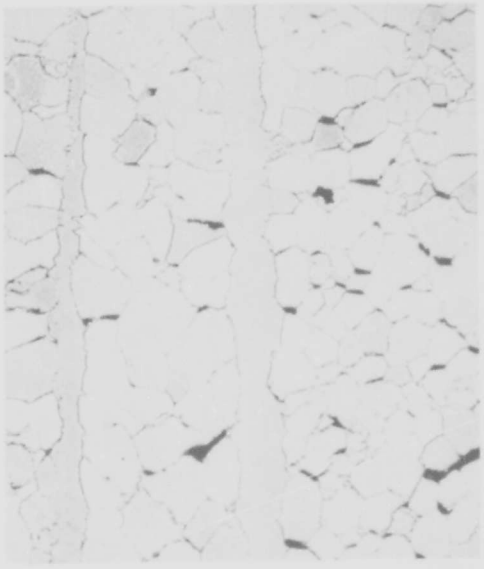

(a) 100X

(b) 1500X

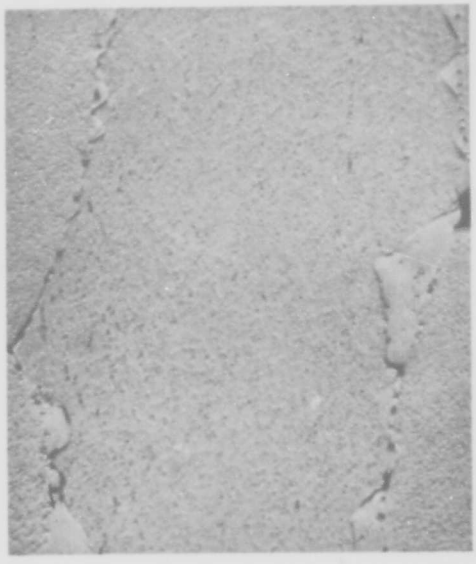

(c) 1500X

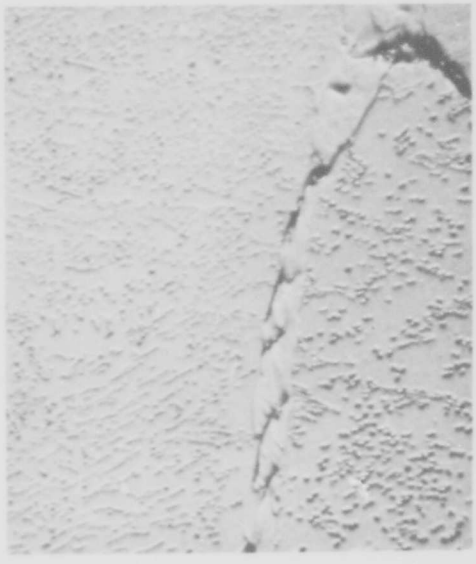

(d) 1500X

FIGURE 51 - Microstructure of XB-88 Creep Specimen Gauge Section. Dynapak Extruded at 1930°C(3500°F). Creep Tested at 1315°C and 30,000 psi. Failed After 41.7 Hours.

The material double extruded at 2040°C, 9:1 reduction, plus 2:1 reduction, had the poorest creep properties. The final extruded microstructure (Figure 13)had a typically worked structure apparently resulting from the relatively low reduction on the final extrusion, providing insufficient strain energy to permit recrystallization during the short time at temperature. The structure did not show any evidence of the precipitate (as indicated) decorated sub-boundary network present in the other high temperature annealed and high temperature extruded conditions evaluated. The microstructures of a creep specimen tested at 1315°C and 27,000 psi (Figure 52) shows some recrystallization during test in the gauge length and substructure formation in the heat section. Voids have been formed, possibly at the new grain boundaries, but the incidence of void formation was not very great. The rupture strain of this specimen was quite high, 34%. The fracture was a ductile shear type rather than intergranular rupture which is typical of recrystallized structures.

Room temperature tensile data were obtained on the wrought double extruded bar after stress relieving 1 hour at 1300°C and 1400°C and are listed in Table 13.

TABLE 13 - Room Temperature Tensile Properties of Double Extruded XB-88

Specimen No.	Condition	0.2% Yield Strength (psi)	Ultimate Strength (psi)	Elong. (%)	Red. In Area (%)
T-12	Double Extruded at 2040°C+ Annealed 1 Hr. at 1300°C	121,000	145,900	11.3	10.8
T-14	Double Extruded at 2040°C+Annealed 1 Hr. at 1400°C	120,100	144,300	17.9	16.4

The double extruded bar had satisfactory room temperature ductility with the highest values obtained after a 1 hour at 1400°C stress relief anneal.

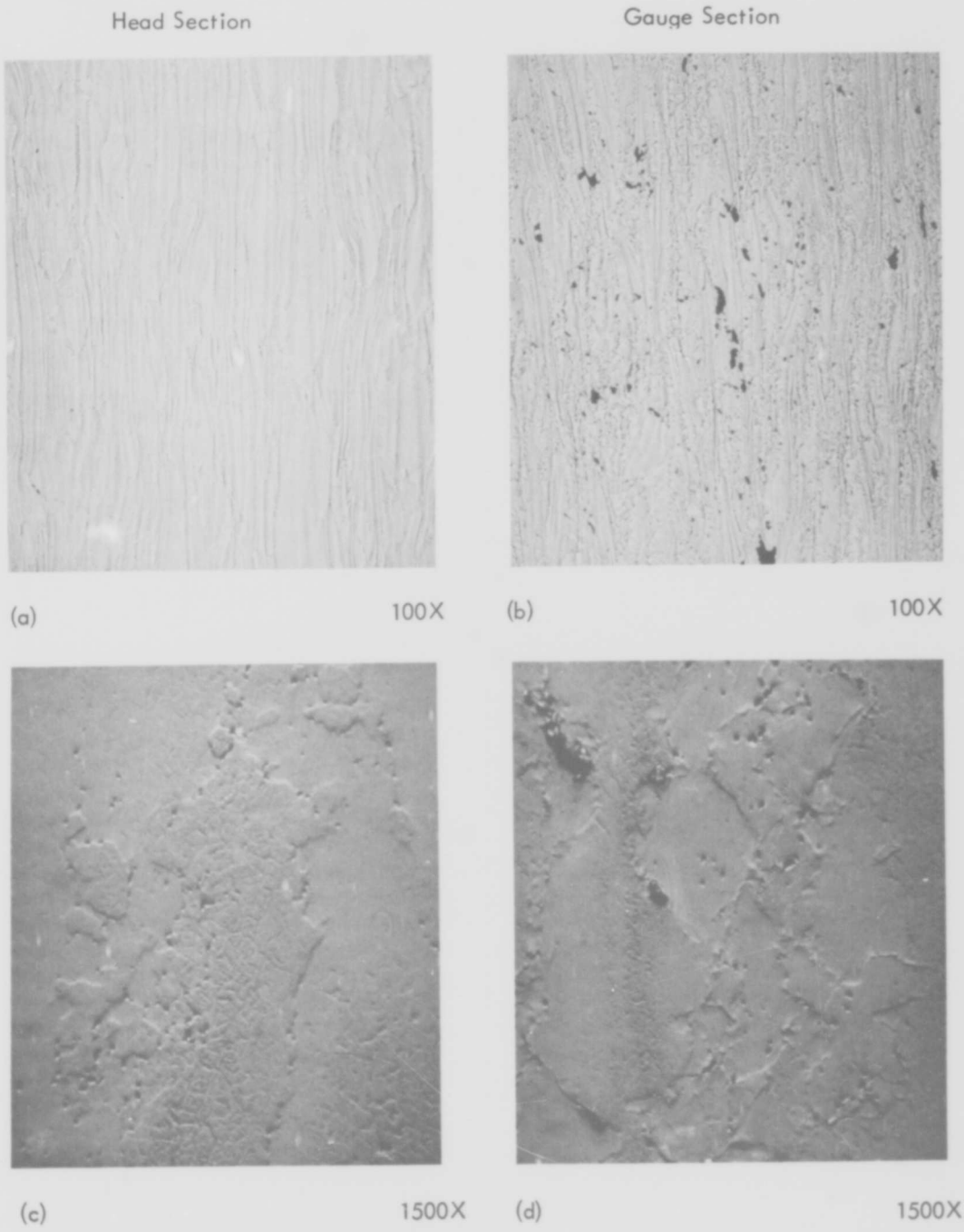

FIGURE 52 - Microstructure of XB-88 Creep Specimen. Double Extruded at 2040°C(3700°F). Creep Tested at 1315°C(2400°F) and 27,000 psi. Failed After 48.5 Hours.

The XB-88 produced by extrusion at 1930°C (3500°F), 9:1 extrusion ratio, Condition A, exhibited the best creep-rupture strength of all the conditions evaluated. More detailed studies of this thermal-mechanical processing sequence were not pursued, however, because of the obvious difficulties of producing the desired structure in a complex component such as a turbine blade. However, this processing sequence can be utilized to produce very high strength bar stock and simple shapes if subsequent deformation of the extruded material is not necessary.

Discussion of Thermal-Mechanical Treatments

The results of the thermal-mechanical treatments evaluated in this program may be summarized as follows:

1. The best creep-rupture properties were obtained with fully or partially recrystallized structures produced by high temperature processing.
2. Wrought, stress relieved structures had considerably poorer creep strength.
3. The initiation and propagation of intergranular cracking controls the extent of tertiary creep, and thus has a significant influence on rupture life.
4. Refining the grain size increases rupture strain. Duplex structures composed of a fine grained matrix and bands of unrecrystallized, polygonized material had good rupture life and relatively high rupture strains.
5. The best low temperature ductility was obtained with wrought plus stress-relieved,and fine grained recrystallized structures.

Analysis of creep mechanisms in an alloy as complex as XB-88 is difficult. The structural heterogeneities observed, particularly with respect to substructure, the variations in precipitate identity and morphology, and the strong influence of intergranular fracture on

rupture life, preclude a detailed analysis of mechanisms. There are, however, a number of significant observations which are worthy of discussion. All of the material annealed at 1700°C and above prior to creep testing exhibited very comparable secondary creep rates for equivalent stress levels. The observed differences in rupture life were controlled primarily by the initiation and propagation of intergranular separations arising from grain boundary sliding, as previously described. In addition, partially recrystallized duplex structures produced by high temperature extrusion also exhibited creep rates quite equivalent to high temperature annealed structures. This indicates that the structure and/or precipitate morphology produced by high temperature annealing (~1700°C and above) are responsible for the strength properties. It is not precipitate identity per se which improves strength, for as previously shown the complex carbide phases resulting from high temperature annealing are very rapidly converted to the $(Cb,Hf)C_{1-x}$ monocarbide during exposure to creep testing temperatures. Merely heating above the carbon solvus temperature for XB-88 (~1675°C) in itself is not sufficient to produce optimum creep strength, for the material double extruded at 2040°C (3700°F) had poor creep properties. The wrought structure of the 2040°C double extruded material resulted in high secondary creep rates despite the presence of a fine carbide precipitate in the matrix. The substructure morphology rather than the carbide identity per se appears to be the controlling factor with respect to high temperature creep strength.

The role of the carbide phase in creep strengthening XB-88 and similar alloys is of considerable interest. Previous studies[1] of a Cb-22W-2Hf alloy containing varying carbon levels (0.067, 0.13, 0.17 w/o C) showed that elevated temperature tensile strength increased with increasing carbon level. At 1095°C (2000°F) creep strength increased with carbon content but at 1205°C (2200°F) and 1315°C (2400°F), the creep strength was not significantly affected by the carbon level. This is not to say that the carbide phase has no effect on high temperature creep strength, for a carbon-free alloy of the same matrix composition (Cb-22W-2Hf) had considerably poorer creep properties than the carbon-containing alloys, indicating that a certain minimum carbon level (0.067 w/o C or below) is required to enhance creep strength in alloys of this type.

It is unlikely that direct dislocation-precipitate interactions contribute to the creep strength of XB-88, as in the Mott-Nabarro, Orowan, and Fisher, Hart, and Prye mechanisms, because of the ability of screw dislocations to cross slip and because of the large number of slip planes for edge components in body centered cubic alloys. The role of the carbide phase in creep strengthening is more likely to be associated with stabilization of dislocation networks to a temperature higher than their normal recovery temperature, as described by Gregory and Rowe[15]. The microstructures of the high temperature annealed and the high temperature extruded material (with the exception of the 2040°C double extruded bar having a wrought structure) show the presence of a well developed sub-boundary network heavily decorated with precipitates. If a strengthening mechanism is operative in which mobile dislocations within the subgrains are entangled at precipitate stabilized sub-boundaries, then the stability of precipitates which stabilize the sub-boundary network is critical. In order to provide some information on structural stability a creep specimen was annealed 1 hour at 1700°C(reference condition) and then aged 88 hours at 1315°C in a vacuum of 1×10^{-8} torr prior to testing at 1315°C(2400°F). The creep data are listed in Table 14, compared to a specimen tested in the reference condition.

TABLE 14 - Creep Rupture Data for XB-88 at 1315°C(2400°F)

Specimen No.	Condition	Stress (psi)	Rupture Time (hrs.)	Minimum Creep Rate (%/hr.)	Transition Time (hrs.)	Elong. (%)	Red. In Area (%)
T-60	Annealed 1 hr. at 1700°C	25,000	107.5	0.040	45.5	12.0	28.0
T-93	Annealed 1 hr. at 1700°C + 88 hrs. at 1315°C	25,000	117.6	0.039	38.0	17.3	49.9

The aged specimen had a slightly longer rupture life than the reference material but the secondary creep rates were virtually identical. The microstructure of the aged creep specimen is shown in Figure 53. The resultant structure is very similar to the original, 1 hour at 1700°C, condition. This test further indicates that the substructure stabilization rather than the species or composition of the precipitate is responsible for the better creep resistance of the high temperature annealed material. Mechanisms such as strain-induced precipitation do not seem to provide a likely explanation for the observed creep strengthening because the carbides should be equilibrated . Any supersaturation of carbon should have been removed by aging 88 hours at 1315°C prior to creep testing. The fact that a fairly extended aging treatment at 1315°C resulted in no decrease in creep strength is encouraging, since it indicates that the structure developed by high temperature annealing is quite stable. It should be pointed out, however, that a Cb-22W-2Hf-0. 167C alloy investigated in an earlier phase of this program showed a significant loss in creep strength at 1205°C (2200°F) when aged 100 hours at 1200°C prior to creep testing. More extensive aging studies are in progress to better define the structural stability of XB-88.

The relatively poor creep strength of worked plus stress relieved material may result from the lack of precipitate-stabilized sub-boundary networks plus a higher density of mobile dislocations in the wrought material.

Electron Microscopy

Electron microscopy studies were carried out to provide a more detailed structural characterization of XB-88 in the reference condition (annealed 1 hr./1700°C). Electron micrographs of surface replicas and bulk extracted dispersed phase replicas are shown in Figure 54. Figure 54a clearly illustrates the sub-boundary structure in the polygonized areas of XB-88. This micrograph shows a number of precipitate decorated tilt boundaries. The recrystallized areas have a more poorly defined substructure. Figure 54c indicates that most of the precipitate is in the form of polyhedra, measuring less than 0. 5 microns in diameter.

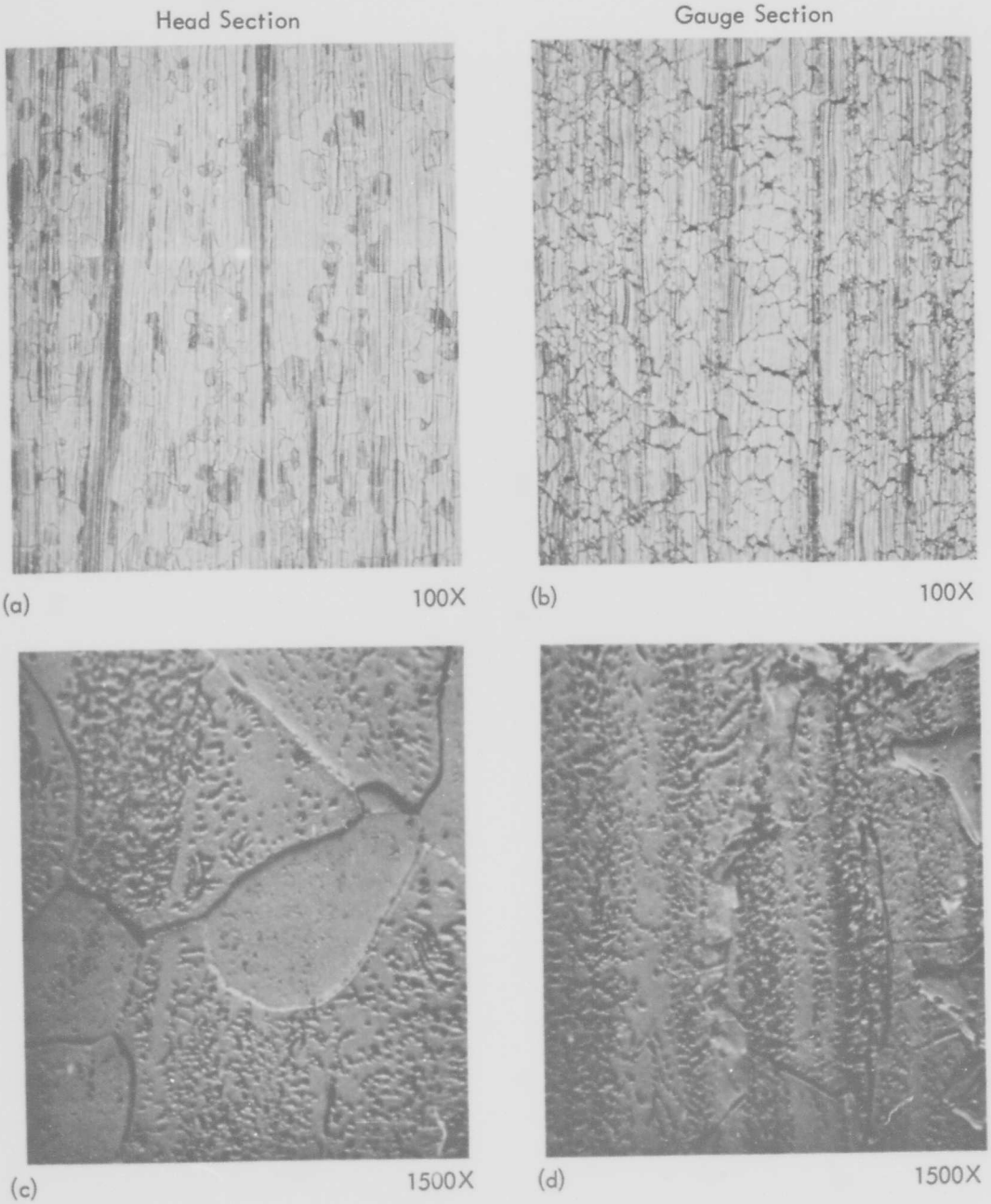

FIGURE 53 - Microstructure of XB-88 Creep Specimen (T-93) Annealed 1 Hr. at 1700°C, Aged 88 Hrs. at 1315°C. Failed after 117.6 Hrs. at 1315°C (2400°F), 25,000 psi.

(a) 3200X

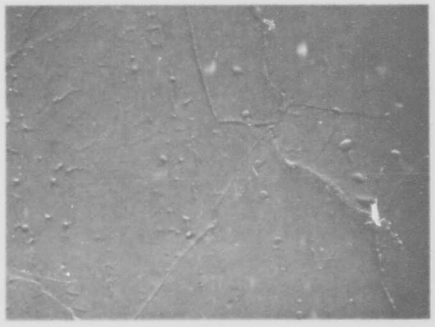

(b) 3200X

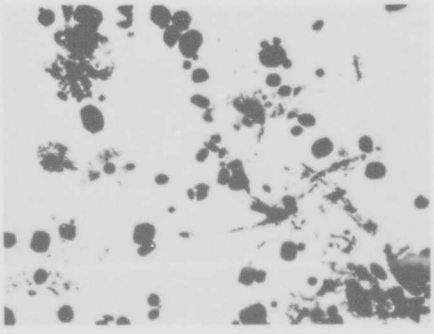

(c) 10,000X

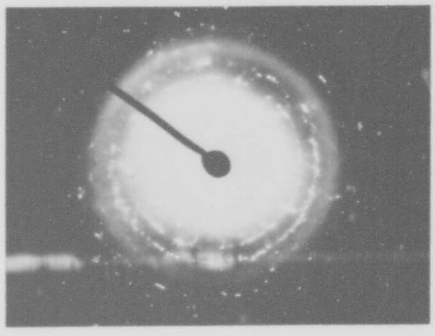

(d)

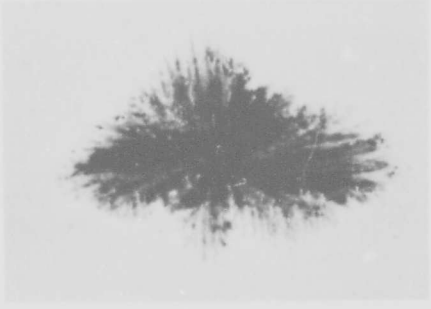

(e) 20,000X

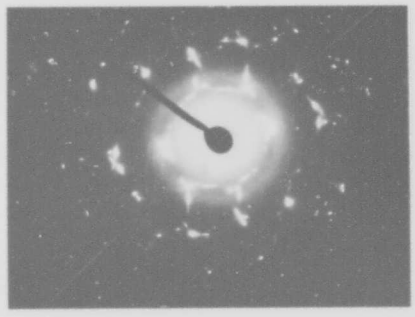

(f)

FIGURE 54 - Electron Micrographs (Surface and Dispersed Phase Replicas) of XB-88 in the Reference Condition (Annealed 1 Hr. at 1700°C)

The ring pattern (Figure 54d) and selected area electron patterns of these polyhedra confirm that they are the cubic $(Cb,Hf)C_{1-x}$ phase as originally determined by x-ray analysis of extracted residues. Also observed are a few platelets which are more transparent to the electron beam. These platelets have been identified as the zeta phase by selected area electron diffraction. A typical platelet and its diffraction pattern are shown in Figures 54e and 54f. The crystallographic structure of the zeta phase has not been successfully indexed. The platelets are badly faulted with stacking faults and/or microtwins as indicated by the electron diffraction pattern.

Transmission electron micrographs of thin foils are shown in Figures 55 and 56. Extensive dislocation networks and what appear to be tilt boundaries are observed in the polygonized areas (Figures 55a,b,c, and 56). Most of the sub-boundaries are decorated with precipitate as observed both optically and by means of surface replicas. Note especially the undecorated hexagonal network of dislocations associated with body centered cubic materials in the recovered condition. Also note the grain boundary extinction contours and precipitates in Figure 55c, and the precipitate decoration of the nodes of the extended dislocation network in Figure 56. As should be expected, very few dislocations or dislocation networks were observed in the recrystallized grains (Figures 55d,e,and f).

Effect of Creep Strain on Structure. Creep specimens strained to the end of primary creep (specimen T-86, strained 0.2% at 25,000 psi and 1315°C/2400°F) were examined to evaluate the structural changes which occur during creep. A well developed, precipitation-decorated subgrain structure forms within the recrystallized grains during primary creep. This subgrain structure, which consists of more or less irregular dislocation networks in long bands parallel to the stress axis, is illustrated in the transmission electron micrographs of Figure 57. During steady-state creep an apparent degeneration of the decorated subgrain structure and/or dislocation networks that formed within the recrystallized grain during primary creep occurs. Many more platelet type precipitates are present, especially in the recrystallized areas, but they no longer appear to be in the form of decorated dislocations or dislocation networks.

(a) 10,000X

(b) 16,000X

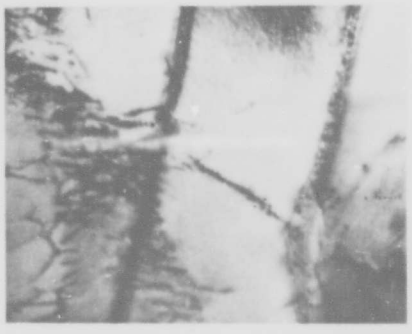

(c) 25,000X

(d) 7,800X

(e) 10,000X

(f) 16,000X

FIGURE 55 - Transmission Electron Micrographs of XB-88 in the Reference Condition (Annealed 1 Hr. at 1700°C)

FIGURE 56 - Transmission Electron Micrograph of XB-88 in the Reference Condition (Annealed 1 Hr. at 1700°C) 40,000X

(a) 7,000X

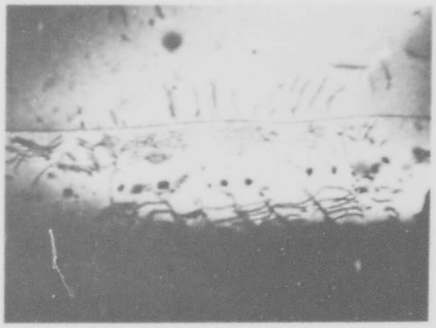

(b) 3,600X

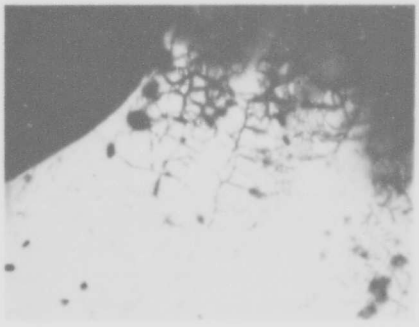

(c) 3,600X

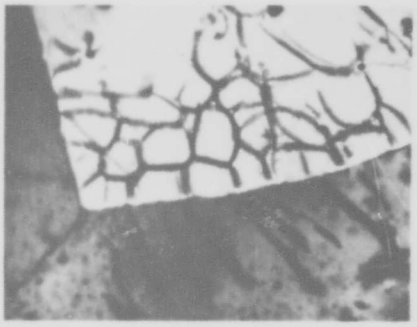

(d) 8,500X

FIGURE 57 - Transmission Electron Micrographs of XB-88 Specimen T-87 Creep Tested to End of Primary Creep at 1315°C (2400°F) (1.6 Hrs./ 25,000 psi/0.2% ϵ)

The degeneration of the subgrain structure and/or decorated dislocation networks formed during primary creep into long bands of precipitate parallel to the stress axis during steady state creep is clearly illustrated in the electron micrographs of surface replicas in Figures 58a, b, and c. No decorated low-angle tilt boundaries are seen between the parallel bands of precipitates and the dispersed phase appears to be considerably larger than previously observed. In agreement with the metallographic results, grain boundary pinning and migration are apparent in Figure 58c.

Examination of the dispersed phase indicates that a significant change occurred in the precipitate morphology. Elongated, transparent platelets, exhibiting many extinction (bend) contours, are illustrated in Figures 58d and e. Growth of these platelets appears to be crystallographic in nature as indicated by the common direction of growth facets. The thicker, non-transparent precipitates appear to be transforming from the many sided polyhedra into thick, but geometrically shaped platelets, probably similar in nature to the thinner platelets. An x-ray diffraction analysis of the extracted residue indicates that it consists primarily of a fcc carbide phase having a lattice parameter a_o of 4.58 Å and a minor amount of a second fcc carbide phase having a lattice parameter a_o of 4.54 Å. Thus evidently stabilization of the dispersed phase to the higher lattice parameter is occurring during creep, and the thin, transparent platelets are expected to have a lattice parameter of 4.58 Å. The selected area electron diffraction pattern (Figure 58f) of the thin fcc platelet shown in Figure 58_e confirms that it has a (100) zone axis. A careful analysis of the diffraction pattern, using an aluminum ring pattern to accurately determine the camera constant (λL), indicates that the lattice parameter is probably 4.58 Å as expected. However, as the inherent errors in electron diffraction are on the same order of magnitude as the difference between the lattice parameters of the two fcc carbide phases (i. e., about 10%), it is impossible to be entirely sure of the lattice parameter by electron diffraction alone.

(a) 3200X

(b) 3200X

(c) 3200X

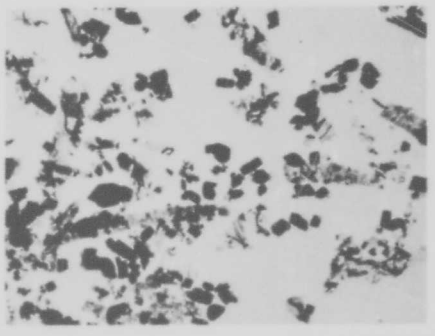

(d) 10,000X

(e) 30,000X

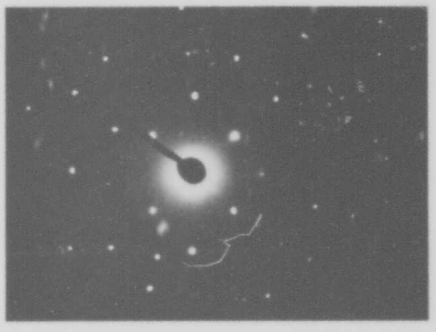

(f)

FIGURE 58 - Electron Micrographs of XB-88 Specimen T-87 Creep Tested to End of Secondary Creep at 1315°C(2400°F)

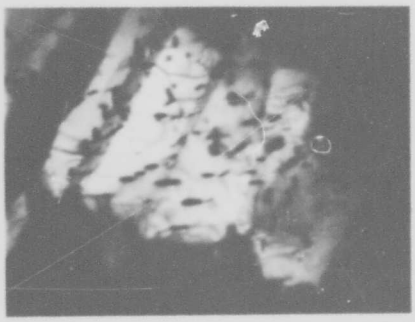

(a) 10,000X

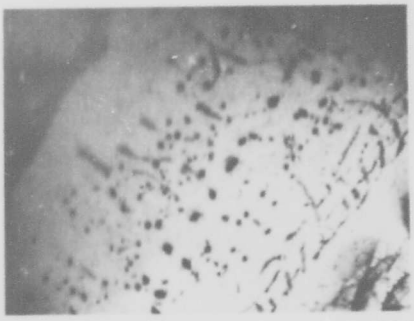

(b) 3700X

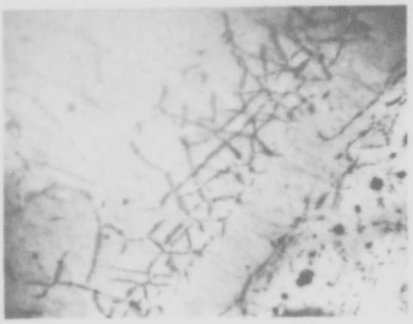

(c) 3700X

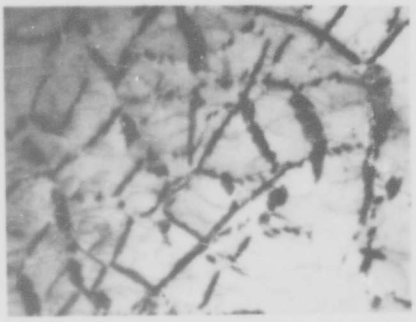

(d) 10,000X

(e) 40,000X

FIGURE 59 - Transmission Electron Micrographs of XB-88 Specimen T-87 Creep Tested to End of Secondary Creep at 1315°C(2400°F) (42 Hrs./25,000 psi/1.3%ε)

At the beginning of tertiary creep (Figure 59) the polygonized substructures have degenerated as the precipitates decorating the sub-boundaries either transformed to a more stable fcc monocarbide or dissolved. With the degeneration of the precipitate-stabilized substructure, weaker dislocation-dislocation and dislocation-precipitate interactions may be the rate controlling mechanism. Dislocation-dislocation interactions are not particularly effective at elevated temperatures where jogs disappear quickly by diffusion, and dislocation-precipitate interactions are also ineffective due to the ease of dislocation climb. The changes in the fcc cubic carbide leading to the degeneration of the substructure may be accelerated by stress, hence static aging prior to creep testing may not indicate the stability of the structure.

The results of the electron microscopy studies suggest that substructure stabilization by precipitates may have a significant effect in controlling creep behavior of XB-88 and similar dispersed phase-containing bcc alloys. However, more detailed studies are required to assess the effectiveness of this strengthening mechanism. One of the many factors affecting strength which must be considered is the role of grain boundary sliding, not only with respect to its influence on intergranular cracking, but also with respect to its contribution to total creep strain. The transition from second to third stage creep in XB-88 occurs at low strain values, on the order of 2%. Extending the duration of second stage creep to high strain levels could considerably increase the useful strength of alloys of this type. Understanding of the factors which control this transition could contribute significantly to the development of improved mechanical properties.

Mechanical Properties of XB-88 in the Reference Condition

The thermal-mechanical processing studies of XB-88 showed that material processed by extruding at 1930°C (3500°F), followed by swaging at 1300°C, with a final anneal at 1700°C, exhibited the best condition of high temperature creep strength and low temperature ductility. Consequently, this processing sequence was chosen as the reference condition for detailed evaluation of creep rupture and tensile properties.

The tensile properties of XB-88 in the reference condition were determined over the temperature range of -110°F (-80°C) to 2500°F (1370°C), and the data are plotted in Figure 2*. The low temperature ductility values improve markedly slightly above room temperature, with reduction in area increasing from 8% at room temperature to 24% at 200°F (93°C). The plot of ultimate strength versus temperature showed typical strain aging response, with a strength maxima extending over the range from 760°C (1400°F) to 980°C (1800°F). High temperature tensile strength values were quite high, 86,000 psi at 1095°C (2000°F) and 46,800 psi at 1370°C (2500°F). The tensile strength values are quite comparable to those obtained initially on XB-88 processed from a 2 inch diameter ingot.[1] The elevated temperature tensile ductility was excellent.

Creep rupture properties were evaluated over the temperature range 980°C (1800°F) to 1315°C (2400°F). The rupture properties of XB-88 in the reference condition for the various test temperatures are given in the log stress versus log rupture time plot of Figure 3*. Both rupture and 1% creep data are summarized in the Larsen-Miller plot of Figure 4*. In addition to attractive creep-rupture properties, XB-88 in the reference condition had low secondary creep rates. The transition from second to third stage creep, however, occurred at low strain values, on the order of 2%.

The 100 hour rupture strength of XB-88 at 1315°C (2400°F) is 25,500 psi, corresponding to a stress/density ratio of 68,500 inches which is quite close to the target value of 70,000 inches. At 1095°C (2000°F) this 100 rupture strength is 56,000 psi, providing a stress/density ratio of 150,000 inches.

The stress dependency of the minimum creep rate of XB-88 in the reference condition is at 1095, 1205, and 1315°C (2000, 2200, and 2400°F) is shown in Figure 60. These data fit the equation

$$\epsilon_s = A_T G_T^n$$

where ϵ_s is the steady state creep rate, A_T is a constant containing the geometric, frequency,

*These curves presented previously in the Introduction and Summary Section of this report.

and activation energy terms, and n is the stress exponent. At temperatures of 1205°C ($0.49T_M$) and below n is approximately 7.7, while at 1315°C ($0.54T_M$) n decreases to 3.4. The stress exponent obtained at 1315°C is consistent with that predicted by Weertman's dislocation climb model for creep[22]. Experimental data on pure polycrystalline metals (as well as a number of alloys) shows the stress exponent to normally fall within the range 3-5.

At temperatures below 1315°C (2400°F) a considerably higher stress for XB-88 was observed. It is interesting to note that the observed stress dependency (7.7) is very similar to that found by Clauer and Wilcox[23] for a series of dispersion strengthened nickel alloys. They point out that $n \cong 6\text{-}8$ is common to a variety of recrystallized dispersion strengthened metals subjected to high temperature creep, and suggest that the high stress exponent may be attributed to internal stresses which are higher in dispersion-strengthened metals as a result of dispersed phases promoting a stable fine dislocation substructure. These data suggest the possibility of a difference in creep mechanism in XB-88 between 1205°C (2200°F) and 1315°C (2400°F).

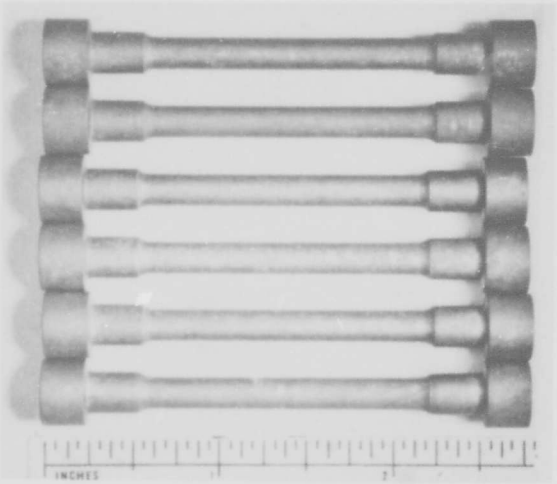

As Coated XB-88 Specimens

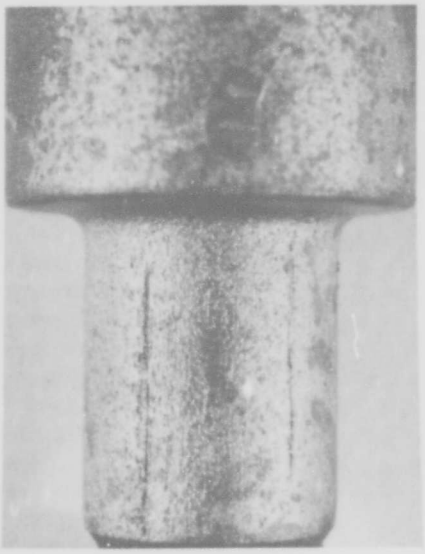

Shoulder Flaws

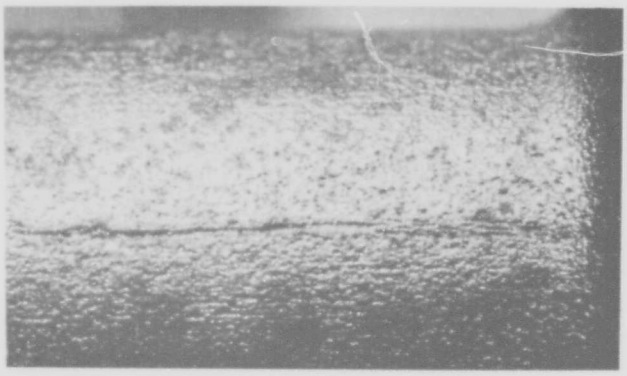

Gauge Section Flaw

FIGURE 61 - Typical Coating Flaws in XB-88 Test Specimens

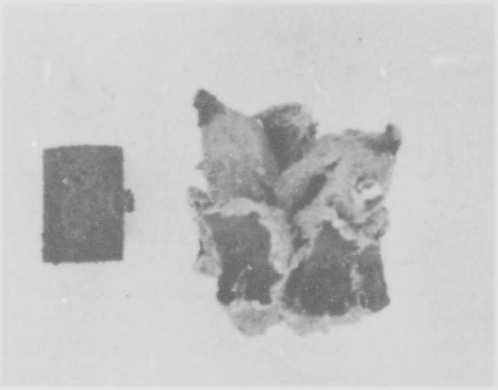

(a) 4 Hrs. 197 Hrs.

XB-88 Specimen Tested in Air at 1315°C(2400°F

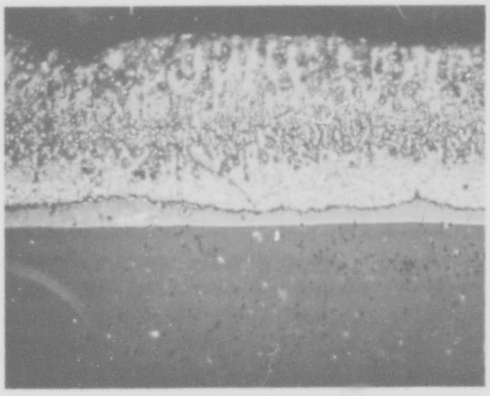

(b) As Coated XB-88

(c) Coated XB-88 Exposed to Slowly Moving Air 4 Hrs. at 1315°C

FIGURE 62 - Micrographs of Cr-Ti-Si Coated XB-88 Specimens

XB-88, since only one set of specimens was supplied. Subsequently, Friedreich[16] reported sound coatings of XB-88 with a modified coating sequence. It was therefore decided to defer evaluation of the high temperature properties of coated XB-88 until additional specimens could be supplied for coating using the modified sequence. The available specimens were utilized to determine the effect of the coating on low temperature ductility. Room temperature tensile tests were carried out on the coated samples, and the results are listed in Table 15. The coated specimens had no room temperature ductility, but raising the test temperature to 315°C (600°F) resulted in good elongation and reduction in area values. The coating has increased the ductile-brittle transition temperature to between room temperature and 315°C (600°F). A more detailed coating evaluation of XB-88 is being developed.

TABLE 15 - Tensile Data for Cr-Ti-Si Coated XB-88

Specimen No.	Temperature (°F)	0.2% Yield Strength (psi)	Ultimate Strength (psi)	Red. In Area (%)	Elong. (%)
T-76	R. T.	---	70,000	0	0
T-79	R. T.	---	60,240	0	0
T-78	600	66,300	86,200	55.4	19.3

VII. TURBINE BLADE FORGING EVALUATION

The capability of XB-88 to be precision forged into a complex turbine blade configuration was evaluated by TRW Equipment Laboratories on another Air Force sponsored program. Two XB-88 preforms were machined from a 1.25 inch diameter extruded bar (extruded at 1930°C, 4.5:1 extrusion ratio) and then annealed 1 hour at 1700°C. These preforms were then processed through the forging cycle developed by TRW for precision forging Cb-132M turbine blades to a JT-3D first stage rotor blade configuration.

The forging operations include coin, upset, and forming operations on the shroud end, two roll-forging operations on the airfoil and rod sections, and three press forging operations (blockdown, semi-coin, and coin) to obtain the final configuration. One XB-88 preform cracked in the shoulder of the shroud end after the final shroud end forming operation because of what appeared to be a defect in the original extrusion. The remaining preform was successfully processed through the complete cycle. Photographs of the finished blade in Figure 63 show that material completely filled the dies, producing a high quality precision forging thus demonstrating the capability of this high strength alloy to be forged into complex components. Details of processing sequence are given in the TRW progress reports on Contract AF 33(615)-1391.[17]

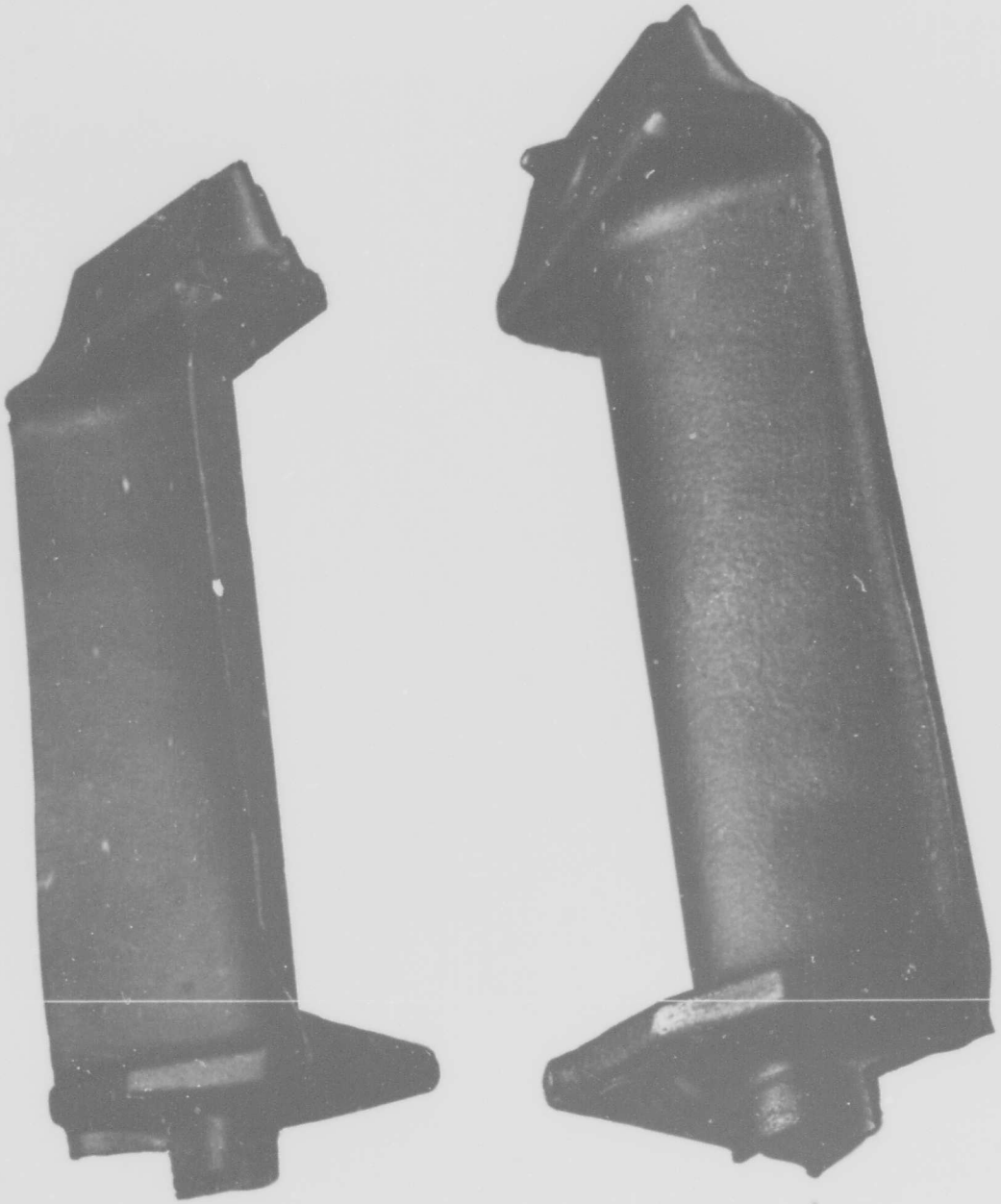

FIGURE 63 - XB-88 Forged into JT-3D Turbine Bucket Configuration

VIII. EFFECT OF THERMAL TREATMENT ON CREEP RUPTURE PROPERTIES OF SOLID SOLUTION AND CARBIDE STRENGTHENED ALLOYS

In addition to the studies of the XB-88 alloy described earlier in this report, several additional tests were carried out to provide a better understanding of the role of heat treatment on creep properties. The effect of varying pretest thermal treatment was evaluated on an alloy containing a dispersed carbide phase, VAM-85 (Cb-22W-1Hf-0.067C), and a solid solution alloy VAM-77 (Cb-18W-2Hf) produced during the first phase of this program. These alloys prepared as 2 inch diameter ingots, were processed to bar by Dynapak extrusion, at 1250°C, followed by warm swaging[1]. Both alloys were given a series of annealing treatments ranging from 1600°C to 2000°C, and then creep rupture tested. Grain size was determined on sections of the as-tested specimens in areas removed from the fracture.

Grain size and creep rupture data for alloys VAM-77 and VAM-85 are tabulated in Table 16. The solid solution alloy VAM-77 was creep tested at 1205°C (2200°F), and the carbide strengthened alloy, VAM-85, at 1315°C (2400°F) and 1205°C (2200°F).

The secondary creep rate of the alloys are plotted as a function of both annealing temperature and grain size in Figure 64. The behavior of the solid solution alloy and the alloy containing the dispersed carbide phase were quite different. The solid solution alloy, VAM-77, exhibited a pronounced increase in creep rate with increasing annealing temperature, or equivalently with increasing grain size. The carbide strengthened alloy, VAM-85, showed a decrease in creep rate as the annealing temperature was raised from 1600°C to 1700°C. Thereafter, creep rate was relatively insensitive to annealing temperature. This is the same trend observed for XB-88. Reference to Figure 39 indicates that annealing at about 1700°C is also above the carbon solvus for VAM-85 as it is for XB-88. The relationship between rupture life and annealing temperature (and grain size) also showed the same trend as the secondary creep rate data, Figure 65.

BLANK PAGE

TABLE 16 – Effect of Prior Thermal Treatment on the Creep Rupture Properties of Alloys VAM-77 and VAM-85

Specimen No.	Initial Heat Treatment	Temperature (°C)	Temperature (°F)	Stress (psi)	Rupture Time (hrs.)	Minimum Creep Rate (%/hr.)	Transition Time** (hrs.)	Red. In Area (%)	Elong. (%)	Grain Size ASTM No.	Grain Size Avg. Grain Dia. (mm)
Cb-18W-2Hf											
VAM-77-T9	2 hrs/2000°C	1205	2200	25,000	0.75	6.65	---	32.7	16.8	2.6	0.168
VAM-77-T10	1 hr/1800°C	1205	2200	25,000	4.25	1.57	0.5	71.5	34.7	6.2	0.042
VAM-77-T11	1 hr/1600°C+	1205	2200	25,000	39.7	0.034	12.5	85.0	18.7	7.7	0.029
VAM-77-T12	1 Hr/1600°C	1205	2200	25,000	14.5	0.036	8.8	84.5	22.0	7.2	0.034
Cb-22W-1Hf-0.067C											
VAM-85-T4	2 hrs/2000°C	1315	2400	22,000	75.1	0.044	23.0	35.5	14.0	1.8	0.220
VAM-85-T16	1 hr/1800°C	1315	2400	23,000	46.8	0.085	17.5	61.8	23.3	5.8	0.054
VAM-85-T14	1 hr/1700°C	1315	2400	23,000	57.0	0.068	19.0	73.2	22.7	6.7	0.041
VAM-85-T17	1 hr/1600°C	1315	2400	23,000	25.0	0.160	7.0	83.6	29.3	8.5	0.023
VAM-85-T1A	2 hrs/2000°C	1205	2200	25,000	400.0+	0.0085	180.0	5.5+	4.7+	---	---
VAM-85-T2A	1 hr/1800°C	1205	2200	25,000	413.5	0.0062	230.0	49.1	12.0	---	---
VAM-85-T3A	1 hr/1600°C	1205	2200	25,000	360.0	0.0121	180.0	84.5	29.3	---	---

* 1 Hr. at 1600°C plus 5 minutes at 1750°C

** Transition to third stage creep

\+ Test terminated at 310 hrs., rupture time was estimated.

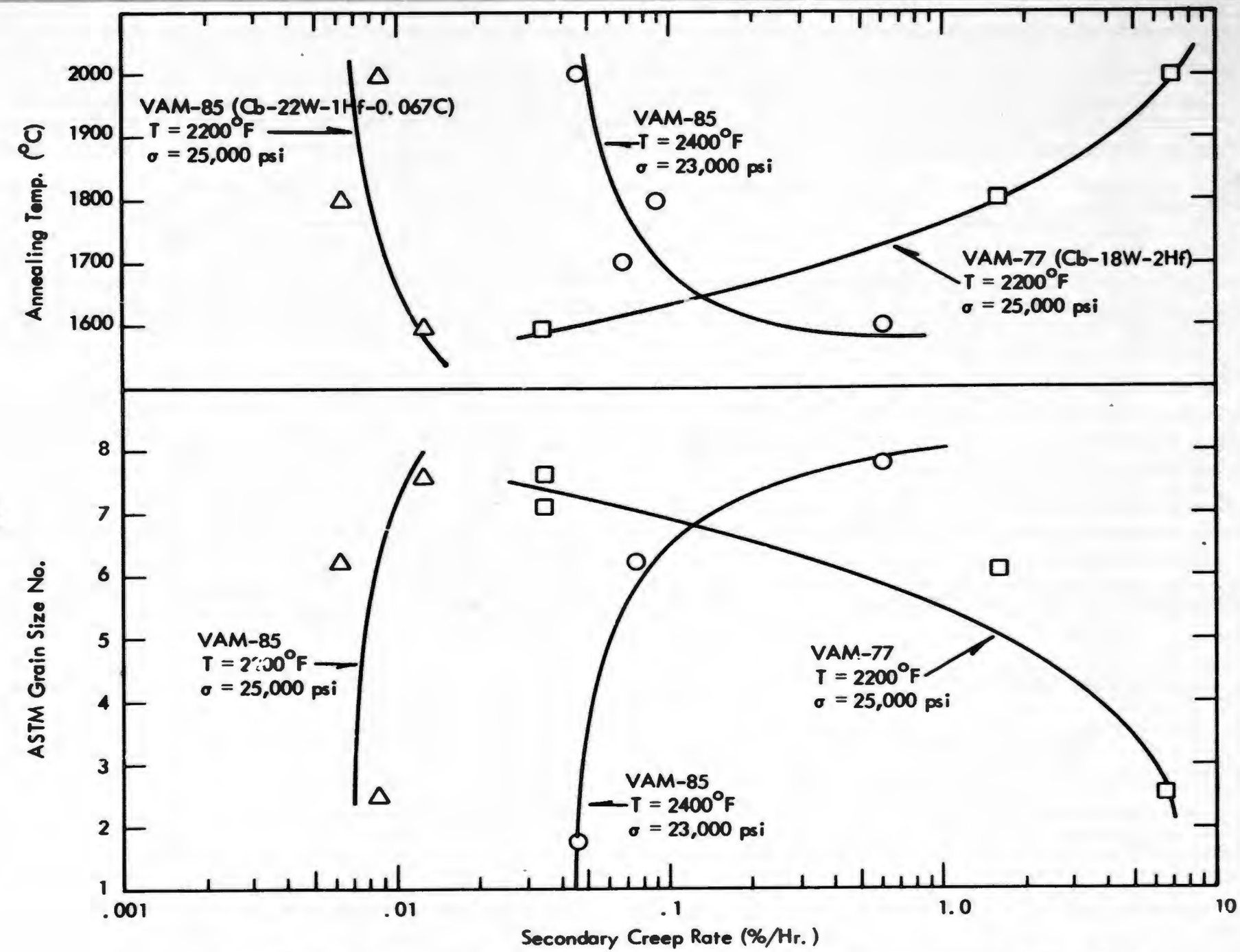

FIGURE 64 - Variation of Secondary Creep Rate with Annealing Temperature and Grain Size

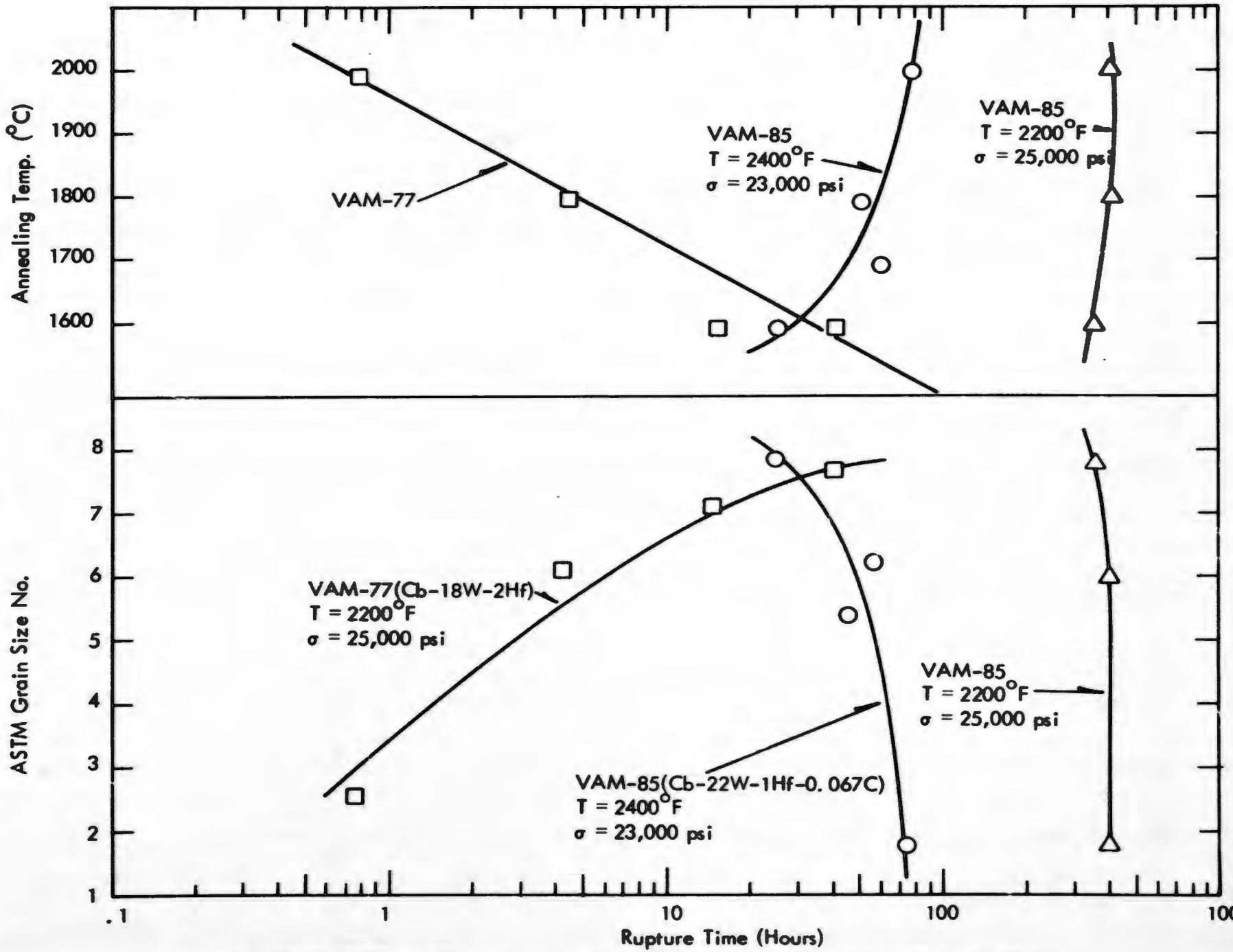

FIGURE 65 - Variation of Rupture Time with Annealing Temperature and Grain Size

The dependence of secondary creep rate on grain size has been investigated in considerable detail in a number of metals and alloys, but apparently not to any significant extent in the refractory metals. Observations on copper and brass have shown creep rate to be proportional to the square of the grain diameter[18,19]. However in lead the creep rate has been observed to decrease with increasing grain size[20]. One of the most significant studies of grain size effects was carried out by Shahinian et al[21], who investigated the effect of grain size on the creep of Monel at various temperatures. Their studies showed well defined minima in the curves of grain size versus secondary creep rate. That is, at each temperature there was an optimum grain size for maximum creep resistance. The optimum grain size increased with increasing temperature. It is not possible from the limited data of the present investigation to determine if an optimum grain size for best creep resistance exists for the solid solution alloy, VAM-77. However, the data serve to show rather conclusively that the effect of heat treatment on the creep properties of the solid solution alloy and the alloy containing a dispersed carbide phase is quite different. These data clearly indicate that primary grain size, per se, does not influence the creep strength of the carbide strengthened alloys, as it apparently does in the solid solution material. These results are not inconsistent with the precipitate-stabilized sub-boundary strengthening mechanism discussed previously.

IX. COMPARISON OF ZIRCONIUM AND HAFNIUM AS REACTIVE METAL ADDITIONS

While the scale-up and evaluation of the XB-88 alloy comprises the major part of this investigation, a limited study of the effectiveness of zirconium versus hafnium as reactive element additions was carried out. Alloy VAM-87 (Cb-22W-1Zr-0.13C) was prepared to permit direct comparison with alloy VAM-78 (Cb-22W-2Hf-0.13C) investigated in an earlier phase of this program. These alloys are essentially identical in composition with the exception of a replacement of 1 atom percent Hf with 1 atom percent zirconium.

Alloy VAM-87 was double arc melted to produce a 2 inch diameter ingot, which was Dynapak extruded and warm swaged to 0.44 inch diameter bar, using the standard techniques described in an earlier report[1]. Chemical analyses data listed in Table 17 show that, with the exception of the substitution of zirconium for hafnium, both alloys have very similar compositions.

TABLE 17 - Chemical Analysis Data for Alloys VAM-78 and VAM-87

Alloy No.	Nominal Composition	Ingot Location	Analysis (w/o)					
			W	Zr	Hf	C	N	O
VAM-78	Cb-22W-2Hf-0.13C	Top	21.8	---	1.78	0.14	0.006	0.0051
		Bottom	22.4	---	1.94	0.12	0.005	0.025*
VAM-87	Cb-22W-1Zr-0.13C	Top	21.9	0.91	---	0.121	0.0073	0.0030
		Bottom	22.4	0.73	---	0.123	0.0041	0.0041

*Apparent contamination from starting pad.

Hardness data for the two alloys are plotted as a function of aging temperature in Figure 66. The zirconium-containing alloy, VAM-87, exhibited slightly higher hardness values than VAM-78 in the as-cast, as-extruded, and as-swaged conditions. Aging the high temperature annealed material for 1 hour at temperatures ranging from 800 to 1800°C indicated little response to thermal treatment for VAM-78 (Cb-22W-2Hf-0.13C). There is evidence of a slight hardness peak after aging at 1200°C. The zirconium-containing alloy showed a similar response to the aging treatments, with a slight hardness peak at 1100°C. This alloy exhibited

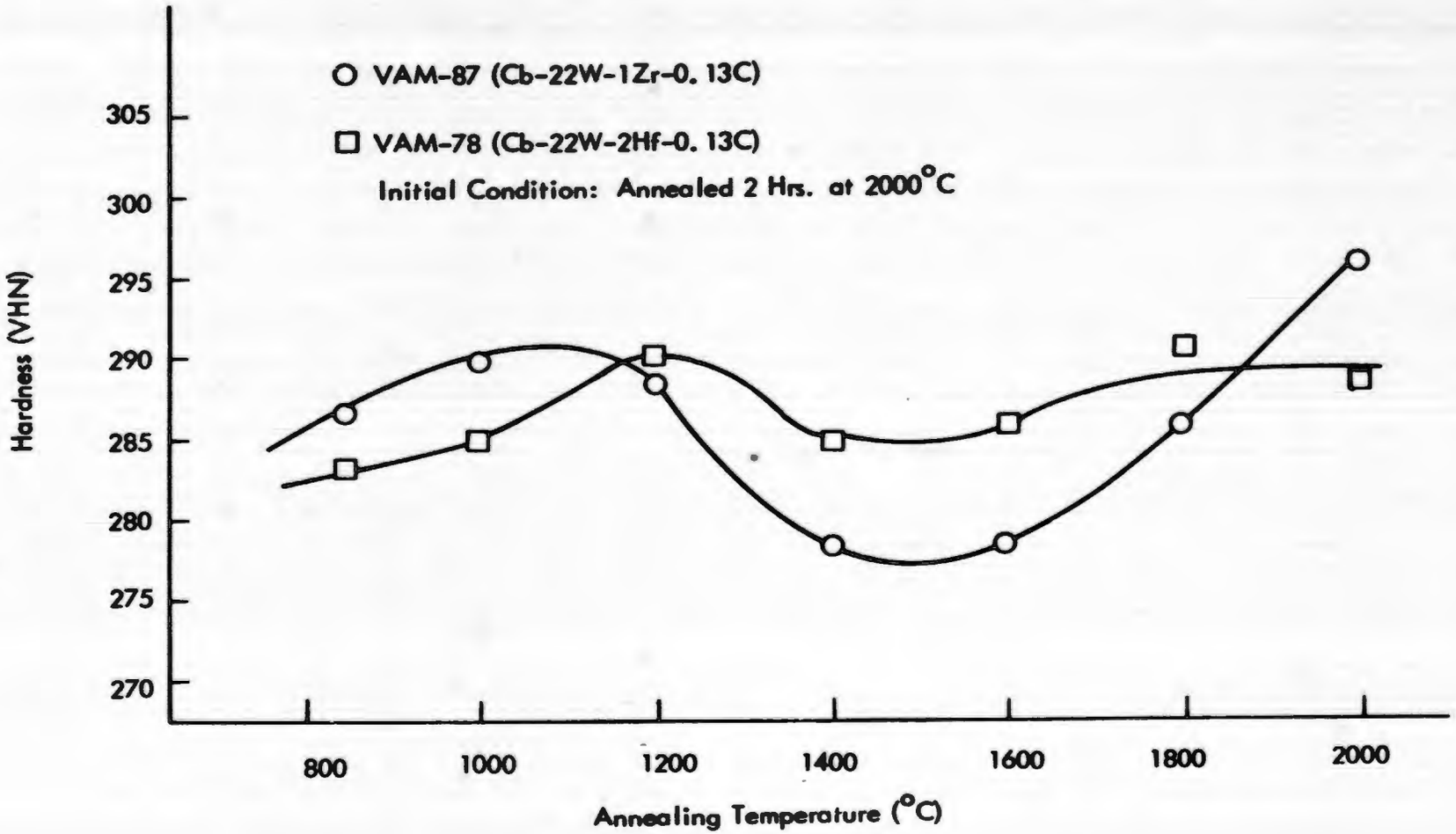

FIGURE 66 - Hardness of VAM-78 and VAM-85 as a Function of Annealing Temperature (1 Hour Anneals)

somewhat greater softening than the hafnium-containing VAM-78 as the aging temperature was increased, and then an increase in hardness at annealing temperatures above 1600°C. The hardness changes observed were quite small, however.

The previous section of this report and previous studies in this program[1] indicate the presence of a zeta and "complex" carbide phases in Cb-W-Hf-C and Cb-W-Zr-C alloys after high temperature (>1700°C) annealing. With lower annealing temperatures a fcc carbide phase is observed, which contains a significant amount of hafnium. The slight hardness peaks shown in Figure 66 may arise from the transformation of the high temperature metastable zeta and "complex" carbide phases to the fcc carbide structure. The hardness increase of VAM-87 at the higher annealing temperatures apparently arises from solution of both carbon and zirconium in the matrix. Metallographic examination of the zirconium containing alloy showed structure virtually identical with those observed in Cb-W-Hf-C alloys of equivalent carbon level and treatment.

Room temperature tensile data for VAM-78 and VAM-87 in the high temperature annealed condition (2 hours at 2000°C) are listed in Table 18. The yield and ultimate strength values for the two alloys were virtually the same. Both materials had low room temperature ductility, resulting from the large grain size (~ASTM 2) of the high temperature annealed material. However, previous work has shown that excellent room temperature ductility can be achieved in these alloys when the proper microstructure is developed. Both wrought plus stress-relieved and fine grained, fully recrystallized structures provide good room temperature ductility.

Limited creep-rupture data obtained on VAM-78 and VAM-87, for identical thermal treatments, are shown in Figures 67 and 68. At 1205°C (2200°F) both alloys had the same initial creep rates, but VAM-87 (Cb-22W-1Zr-0.13C) entered third stage creep after 18 hours test duration, and fractured a short time thereafter (Figure 67). In contrast

TABLE 18 - Room Temperature Tensile Data*

Specimen No.	Composition	0.2% Yield Strength (ksi)	Ultimate Strength (ksi)	Elongation (%)	Reduction in Area (%)
VAM-78 L-1	Cb-22W-2Hf-0.13C	91.2	107.0	2.0	2.46
VAM-87 T-1	Cb-22W-1Zr-0.13C	95.8	102.4	1.3	1.2

* All Specimens Dynapak Extruded at 1250°C - Swaged at 1000°C - Annealed 2/2000°C H. Q.
Strain Rate - 0.05 in/in/min.

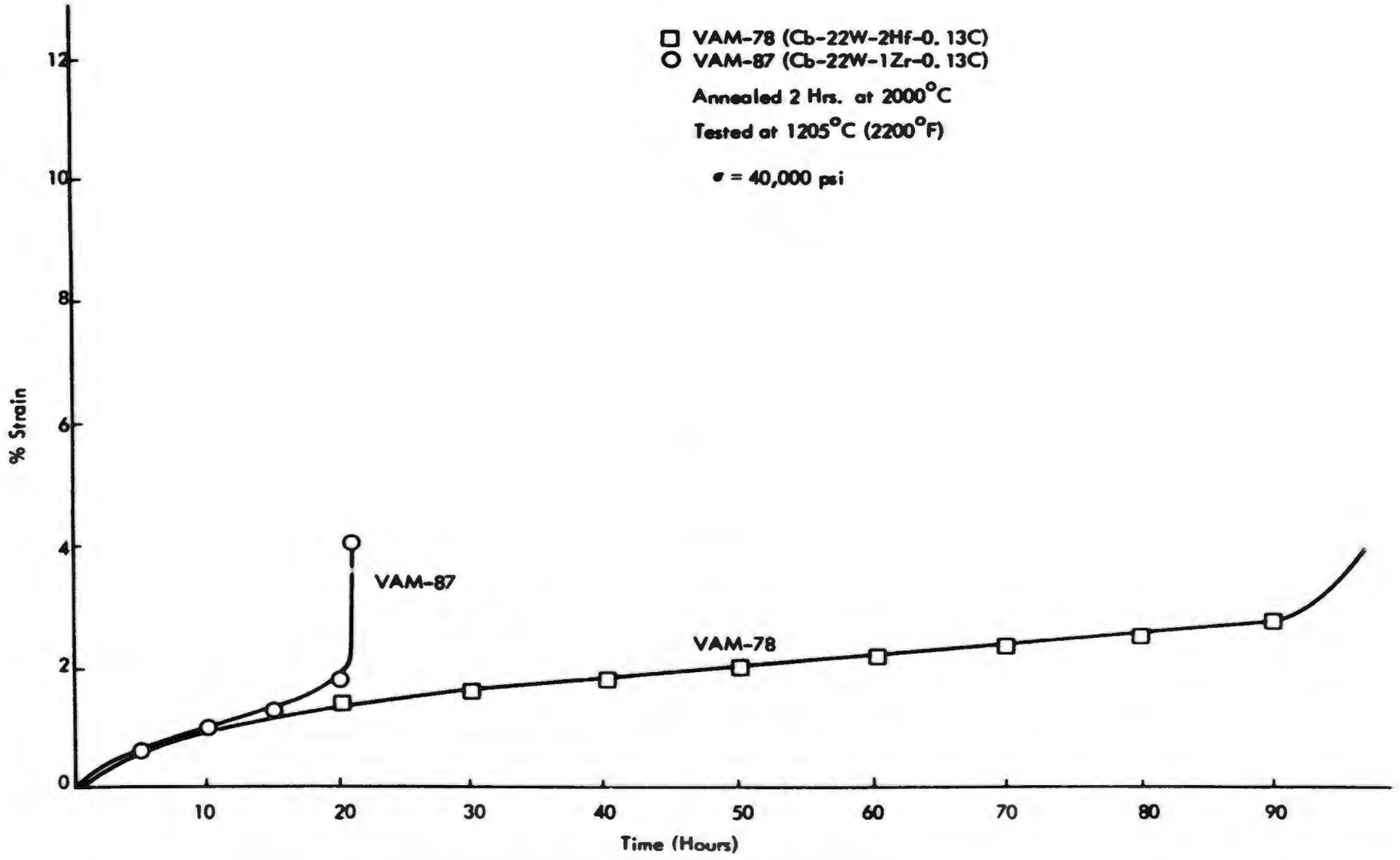

FIGURE 67 - Effect of Substitution of Zr for Hf on Creep Behavior of VAM-78 (Cb-22W-2Hf-0. 13C) at 1205°C (2200°F)

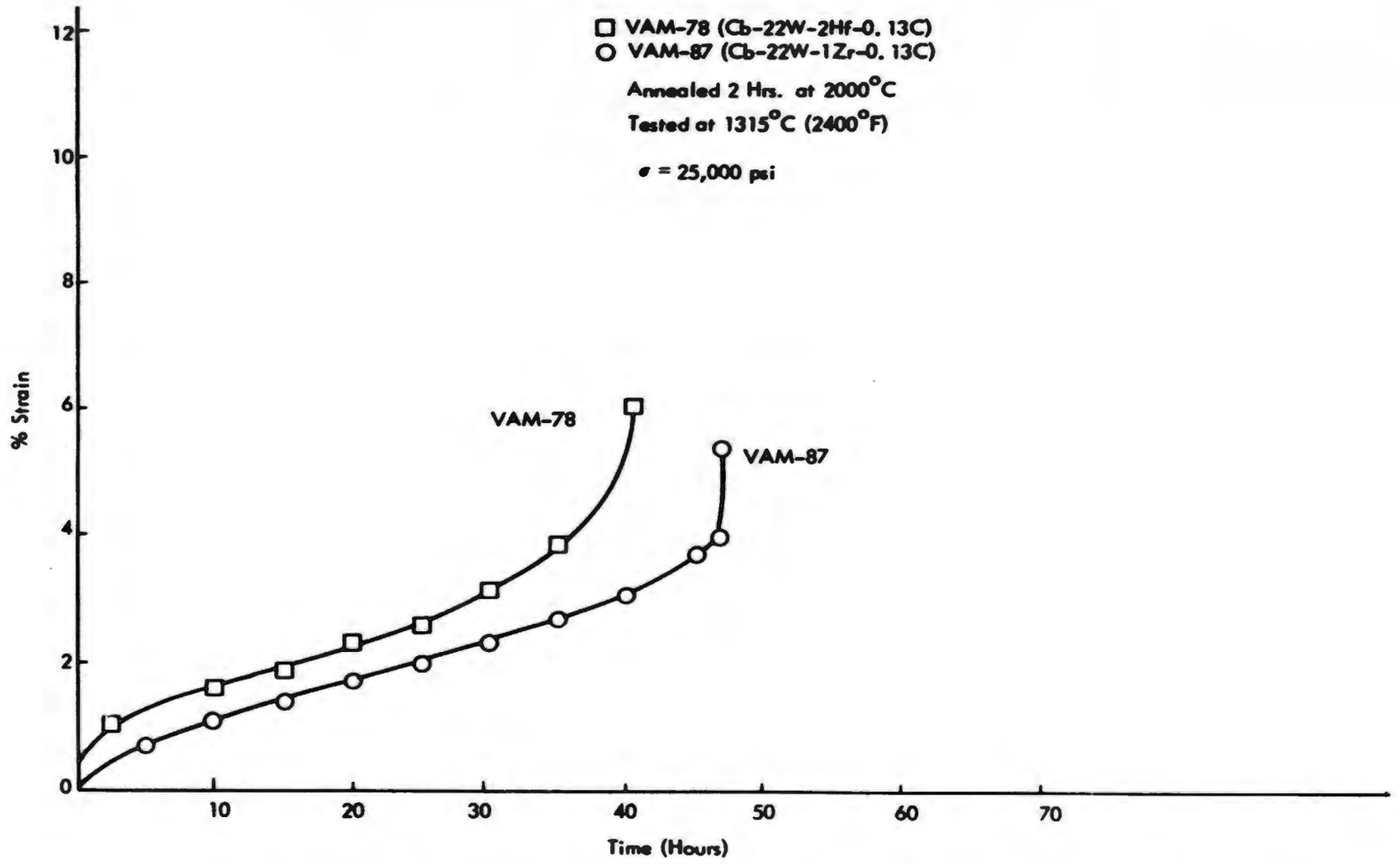

FIGURE 68 - Effect of Substitution of Zr for Hf on Creep Behavior of VAM-78 (Cb-22W-2Hf-0. 13C) at 1315°C (2400°F)

VAM-78 (Cb-22W-2Hf-0.13C) had a rupture life of over 90 hours. The apparent pronounced superiority of the hafnium-containing alloy is a result of its greater resistance to intergranular fracture at low total creep strain.

The transition from secondary to tertiary creep for VAM-87 occurred at less than 2% total strain. In general, a number of factors may be associated with the inception of tertiary creep, including the increasing stress during necking, recrystallization, precipitation or resolutioning of a second phase, and intercrystalline cracking. However, it is apparent that the initiation and growth of intercrystalline cracks is the factor responsible for the early fracture of the Cb-22W-1Zr-0.13C alloy as it is in the Cb-W-Hf-C alloys. At 1315°C (2400°F), the creep behavior of the zirconium-and hafnium-containing alloys were much more comparable. The zirconium-bearing alloy was in fact slightly superior in terms of secondary creep rate and rupture life, as illustrated in Figure 68. However, the differences in properties between the two alloys are insignificant.

The results of this limited study indicate that zirconium and hafnium are equivalent with respect to their effectiveness as reactive metal additions in columbium alloys. The microstructures, response to heat treatment, and creep-rupture properties were very similar for equivalent conditions. Additional creep tests are required to determine if the low rupture life observed for VAM-87 at 1205°C (2200°F) is a real or spurious effect.

The primary consideration leading to the choice of hafnium over zirconium as the reactive metal addition in this program was enhanced fabricability. Previous work at Westinghouse had indicated that the substitution of hafnium for zirconium in Cb alloys provided somewhat better working characteristics at equivalent strength levels. While both VAM-78 and VAM-87 exhibited very satisfactory extrusion and swaging characteristics, the processing characteristics of the hafnium-containing alloy appeared somewhat superior to those of the zirconium-containing heat.

X. REFERENCES

1. R. T. Begley, J. L. Godshall, and D. L. Harrod, Development of Columbium Base Alloys, AFML-TR-65-385, Air Force Materials Laboratory, Wright-Patterson Air Force Base, Ohio, January 1966.

2. J. W. Christian, The Theory of Transformation in Metals and Alloys, p. 734-740, Pergamon Press (1965).

3. W. H. Chang, Private Communication.

4. J. Cornie and E. Delgrosso, Phase Diagram of the Cb-Zr-C System at 1538°C, PWAC 461, September 1965.

5. C. Faunce and D. Peacock, Pratt and Whitney Aircraft, North Haven, Connecticut, Private Communication.

6. W. F. Brizes and J. M. Tobin, Isolation of the Zeta Phase in the Tantalum-Carbon System, Submitted to Journal of American Ceramic Soc., 50, 2 February 1967.

7. I. Zaplatynsky, Observations of the Zeta Phase in the System Ta-C, Journal of American Society, 49, 2 February 1966, 109-110.

8. H. Nowotny, Private Communication.

9. P. Stecher, F. Benesovsky, A. Neckel, and H. Nowotny, Untersuchungen in den Systemen Titan (Zirkonium, Hafnium)-Niob-Kohlenstoff, Monatsh. fur Chemie 95, 6, pp. 1630-45 (1964).

10. A. Taylor, Research for Solubility of Interstitials in Columbium, Ternary System Cb-Hf-C, AFML-TR-65-48, Part II, Air Force Materials Laboratory, Wright-Patterson Air Force Base, Ohio, October 1965.

11. A. Taylor, Research for Solubility of Interstitials in Columbium, AFML-TR-45-48, Part I, Air Force Materials Laboratory, Wright-Patterson Air Force Base, Ohio, March 1965.

12. E. Rudy, Elizabeth Rudy, and F. Benesovsky, Untersuchungen in System Tantal-Wolfram-Kohlenstoff. Monatsh fur Chemie, 93, 1176-95, 1962.

X. REFERENCES (CONTINUED)

13. R. L. Ammon and R. T. Begley, "Pilot Production and Evaluation of Tantalum Alloy Sheet", Summary Phase Report, Contract NOw 62-0656-d, June 15, 1963.

14. R. T. Begley and J. L. Godshall, "Some Observations on the Role of Grain Boundaries in High Temperature Deformation and Fracture of Refractory Metals", Presented at AIME Symposium on the Physical Metallurgy of Refractory Metals, French Lick, Indiana, October 3-5, 1965.

15. D. P. Gregory and G. H. Rowe, J. Metals 13, 670, 1961.

16. L. Friedreich, Private Communication.

17. F. N. Lake and C. R. Smeal, "Process Development for Precision Forging Columbium Base Alloys", Interim Progress Report, Contract AF 33(615)-1391, May, 1966.

18. P. Feltham and J. D. Meakin, Acta Met., 7, p. 614, 1959.

19. P. Feltham and G. J. Copley, Phil. Mag., 5, p. 649, 1960.

20. J. McKeown, Journal Inst. of Metals, 60, p. 201, 1937.

21. P. Shahinian and J. R. Lane, Trans. ASM, 45, p. 177, 1953.

22. J. Weertman, "Theory of Steady-State Creep Based on Dislocation Climb", J. Applied Physics 26, pp 1213-1217, 1955.

23. A. H. Clauer and B. A. Wilcox, Steady-State Creep of Dispersion-Strengthened Nickel, Metal Science Journal, pp 86, May 1967.

INSTRUCTIONS TO FILL OUT DD FORM 1473 - DOCUMENT CONTROL DATA
(See ASPR 4-211)

1. ORIGINATING ACTIVITY: Enter the name and address of the contractor, subcontractor, grantee, Department of Defense activity or other organization *(corporate author)* issuing the report.

2a. REPORT SECURITY CLASSIFICATION: Enter the overall security classification of the report. Indicate whether "Restricted Data" is included. Marking is to be in accordance with appropriate security regulations.

2b. GROUP: Automatic downgrading is specified in DoD directive 5200.10 and Armed Forces Industrial Security Manual. Enter the group number. Also, when applicable, show that optional markings have been used for Group 3 and Group 4 as authorized.

3. REPORT TITLE: Enter the complete report title in all capital letters. Titles in all cases should be unclassified. If a meaningful title cannot be selected without classification, show title classification in all capitals in parenthesis immediately following the title.

4. DESCRIPTIVE NOTES: If appropriate, enter the type of report, e.g., interim, progress, summary, annual, or final. Give the inclusive dates when a specific reporting period is covered.

5. AUTHOR(S): Enter the name(s) of the author(s) in normal order, e.g., full first name, middle initial, last name. If military, show grade and branch of service. The name of the principal author is a minimum requirement.

6. REPORT DATE: Enter the date of the report as day, month, year; or month, year. If more than one date appears on the report, use date of publication.

7a. TOTAL NUMBER OF PAGES: The total page count should follow normal pagination procedures, i.e., enter the number of pages containing information.

7b. NUMBER OF REFERENCES: Enter the total number of references cited in the report.

8a. CONTRACT OR GRANT NUMBER: If appropriate, enter the applicable number of the contract or grant under which the report was written.

8b, 8c, and 8d. PROJECT NUMBER: Enter the appropriate military department identification, such as project number, task area number, systems numbers, work unit number, etc.

9a. ORIGINATOR'S REPORT NUMBER(S): Enter the official report number by which the document will be identified and controlled by the originating activity. This number must be unique to this report.

9b. OTHER REPORT NUMBER(S): If the report has been assigned any other report numbers *(either by the originator or by the sponsor)*, also enter this number(s).

10. DISTRIBUTION STATEMENT: Enter the one distribution statement pertaining to the report.

Contractor-Imposed Distribution Statement

The Armed Services Procurement Regulations *(ASPR), para 9-203* stipulates that each piece of data to which limited rights are to be asserted must be marked with the following legend:

> "Furnished under United States Government Contract No._____. Shall not be either released outside the Government, or used, duplicated, or disclosed in whole or in part for manufacture or procurement, without the written permission of _____, except for:
> (i) emergency repair or overhaul work by or for the Government, where the item or process concerned is not otherwise reasonably available to enable timely performance of the work; or (ii) release to a foreign government, as the interests of the United States may require; provided that in either case the release, use, duplication or disclosure hereof shall be subject to the foregoing limitations. This legend shall be marked on any reproduction hereof in whole or in part."

If the above statement is to be used on this form, enter the following abbreviated statement:

"Furnished under U. S. Government Contract No._____. Shall not be either released outside the Government, or used, duplicated, or disclosed in whole or in part for manufacture or procurement, without the written permission of_____, per ASPR 9-203."

DoD Imposed Distribution Statements *(reference DoD Directive 5200.20)* "Distribution Statements *(Other than Security)* on Technical Documents," March 29, 1965.

STATEMENT NO. 1 - Distribution of this document is unlimited.

STATEMENT NO. 2 (UNCLASSIFIED document) - This document is subject to special export controls and each transmittal to foreign governments or foreign nationals may be made only with prior approval of *(fill in controlling DoD office)*.

(CLASSIFIED document) - In addition to security requirements which must be met, this document is subject to special export controls and each transmittal to foreign governments or foreign nationals may be made only with prior approval *(fill in controlling DoD Office)*.

STATEMENT NO. 3 (UNCLASSIFIED document) - Each transmittal of this document outside the agencies of the U. S. Government must have prior approval of *(fill in controlling DoD Office)*.

(CLASSIFIED document) - In addition to security requirements which apply to this document and must be met, each transmittal outside the agencies of the U. S. Government must have prior approval of *(fill in controlling DoD Office)*.

STATEMENT NO. 4 (UNCLASSIFIED document) - Each transmittal of this document outside the Department of Defense must have prior approval of *(fill in controlling DoD Office)*.

(CLASSIFIED document) - In addition to security requirements which apply to this document and must be met, each transmittal outside the Department of Defense must have prior approval of *(fill in controlling DoD Office)*.

STATEMENT NO. 5 (UNCLASSIFIED document) - This document may be further distributed by any holder only with specific prior approval of *(fill in controlling DoD Office)*.

(CLASSIFIED document) - In addition to security requirements which apply to this document and must be met, it may be further distributed by the holder ONLY with specific prior approval of *(fill in controlling DoD Office)*.

11. SUPPLEMENTARY NOTES: Use for additional explanatory notes.

12. SPONSORING MILITARY ACTIVITY: Enter the name of the departmental project office or laboratory sponsoring *(paying for)* the research and development. Include address.

13. ABSTRACT: Enter an abstract giving a brief and factual summary of the document indicative of the report, even though it may also appear elsewhere in the body of the technical report. If additional space is required, a continuation sheet shall be attached.

It is highly desirable that the abstract of classified reports be unclassified. Each paragraph of the abstract shall end with an indication of the military security classification of the information in the paragraph, represented as *(TS)*, *(S)*, *(C)*, or *(U)*.

There is no limitation on the length of the abstract. However, the suggested length is from 150 to 225 words.

14. KEY WORDS: Key words are technically meaningful terms or short phrases that characterize a report and may be used as index entries for cataloging the report. Key words must be selected so that no security classification is required. Identifiers, such as equipment model designation, trade name, military project code name, geographic location, may be used as key words but will be followed by an indication of technical context. The assignment of links, roles, and weights is optional.

* U.S. GOVERNMENT PRINTING OFFICE : 1966 O—230-000

UNCLASSIFIED

Security Classification

DOCUMENT CONTROL DATA - R & D

(Security classification of title, body of abstract and indexing annotation must be entered when the overall report is classified)

1 ORIGINATING ACTIVITY *(Corporate author)*

Westinghouse Electric Corporation
Astronuclear Laboratory
P. O. Box 10864
Pittsburgh, Pennsylvania 15236

2a. REPORT SECURITY CLASSIFICATION: Unclassified

2b. GROUP:

3 REPORT TITLE

"Development of Columbium Base Alloys"

4 DESCRIPTIVE NOTES *(Type of report and inclusive dates)*

Final Report; Period 1 July 1965 to 31 December 1966.

5 AUTHOR(S) *(First name, middle initial, last name)*

R. T. Begley
J. A. Cornie
R. C. Goodspeed

6 REPORT DATE	7a. TOTAL NO. OF PAGES	7b. NO. OF REFS
	135	23

8a. CONTRACT OR GRANT NO	9a. ORIGINATOR'S REPORT NUMBER(S)
AF 33(615)-1728	
b. PROJECT NO: 7351	AFML-TR-67-116
c. Task No. 735101	9b. OTHER REPORT NO(S) *(Any other numbers that may be assigned this report)*
d.	

10 DISTRIBUTION STATEMENT This document is subject to special export controls and each transmittal to foreign governments or foreign nationals may be made only with the prior approval of the Metals and Ceramics Division, MAMP, Air Force Materials Laboratory, Wright-Patterson Air Force Base, Ohio.

11. SUPPLEMENTARY NOTES	12. SPONSORING MILITARY ACTIVITY
	Air Force Materials Laboratory Wright-Patterson AFB, Ohio 45433

13 ABSTRACT

A high strength columbium alloy, Cb-28W-2Hf-0.067C, was scaled up to 3 inch diameter ingots and processed to bar for evaluation as a potential gas-turbine bucket material. Recrystallization, grain growth and thermal-mechanical processing response were studied. To correlate structure with mechanical properties, carbide phase identity, stability and morphology were investigated. A metastable carbide phase was found, after 1700°C annealing, which transformed to a cubic (Cb;Hf) C_{1-x} phase with intermediate temperature aging. Mechanical properties were measured for several structural conditions. The best low temperature ductility-high temperature creep strength combination occurred upon a 1 hour, 1700°C anneal after extrusion and warm swaging. This material had a 100 hour rupture strength at 1315°C of 25,500 psi (strength-density ratio of 68,500 inches) and room temperature elongation of 11%. Electron microscopy indicated that the carbide phase may strengthen this alloy by stabilizing dislocation networks. A section of as extruded bar stock was precision forged into a turbine bucket shape. Limited study of the substitution of 1 atom % Zr for 1 atom % Hf revealed no creep strength change but the Hf alloy was more fabricable.

(This abstract is subject to special export controls and each transmittal to foreign governments or foreign nationals may be made only with the prior approval of the Metals and Ceramics Division, MAMP, Air Force Materials Laboratory, Wright-Patterson Air Force Base, Ohio 45433.)

DD FORM 1 NOV 65 1473

UNCLASSIFIED

Security Classification